Electronics, Pneumatics and Computer Vision for Advancing Droplet-based Microfluidic Automation

by

Md Mohibullah

A dissertation submitted to the Graduate Faculty of
Auburn University
in partial fulfillment of the
requirements for the Degree of
Doctor of Philosophy in Chemistry

Auburn, Alabama
August 3, 2024

Keywords:
Analysis, Automation, Droplet Microfluidics, Image Processing, Pneumatic Logic, 3D printing

Approved by

Christopher J. Easley, Chair, C. Dent Williams Professor, Dept. of Chemistry & Biochemistry
Byron H. Farnum, J. Milton Harris Associate Professor, Dept. of Chemistry & Biochemistry
Evangelos Miliordos, James E. Land Associate Professor, Dept. of Chemistry & Biochemistry
Christopher Grieco, Assistant Professor, Dept. of Chemistry & Biochemistry
Jean-Francois Louf, Assistant Professor, Department of Chemical Engineering

Abstract

This dissertation explores the subdomain of droplet-based microfluidics flow control, a field of study to precisely manipulate multiphase flow segmentation at the microscale. The focal point of this research is to advance the automation of droplet-based microfluidic systems through the synergistic integration of electronics, pneumatics, and computer vision. By addressing the limitations inherent in existing methodologies, this work lays the groundwork for the development of innovative applications.

Chapter 1 introduces droplet microfluidics, highlighting its development from stable emulsions to a versatile tool in scientific research. The chapter reviews key advancements in droplet manipulation and analysis, enabling high-throughput screening and precise control. It discusses passive and active droplet control and the integration of optical detection methods. Innovations in fluidic control and unique droplet junction designs have been addressed. Despite these advancements, challenges remain integrating solid-phase techniques and enhancing the accuracy and efficiency of droplet-based systems for broader use. Identifying the key challenges, this chapter provides the outline for the rest of the dissertation where different power-based control systems have been explored in the context of droplet microfluidics.

Chapter 2 focuses on the design and fabrication of microfluidic devices using direct 3D printing and polydimethylsiloxane (PDMS) with 3D-printed templates. The reproducibility of both methods has been validated through the development of various custom microenvironments. The chapter provides a detailed discussion on the curing chemistry of PDMS on 3D templates, followed by the development, characterization, and application of several microfluidic flow control systems for single and multiple, laminar, and segmented flows.

Chapter 3 explores the automation of microfluidic droplet generation and manipulation through computer programming, utilizing LabVIEW and Arduino to orchestrate a 'normally closed' valve system. A multi-step microfluidic automation has been proposed, designed, and validated on the system developed in the previous chapter. This chapter also introduces a serial communication-based valve control system capable of executing multiple operations simultaneously and a high-resolution pressure sensor for detecting rapid pressure changes, to be integrated for device functionality and control.

Chapter 4 transitions to a pneumatic automation approach, employing in-house designed, 3D-printed and assembled logic gates for droplet-based manipulation. Characterization of the fundamental pneumatic logic gates is followed by their applications in controlling single and multiple phase aqueous in oil droplet generation. After demonstrating how the entire droplet generation process can be completely automated without electronic power, the development of a pneumatic multiplexer illustrates a significant move towards minimizing electronic dependency, showcasing the feasibility of a fully pneumatic-controlled microfluidic system.

Chapter 5 introduces computer vision – integrated with serial communication - as a transformative tool for real-time feedback and control of droplet generation. By analyzing microscopic data through Python programming, the system dynamically adjusts valve actuation, optimizing droplet formation and demonstrating a leap towards precision and efficiency in microfluidic automation.

In **Chapter 6,** the dissertation concludes by contemplating future research directions, emphasizing the potential of these technologies to foster fully autonomous, electronic-less microfluidic devices for a wide array of applications.

Acknowledgments

Receiving the opportunity for advanced research in the Analytical division at Auburn University's Chemistry department was a significant milestone for me. As I write the conclusion to a journey that began seven years ago and took me over eight thousand miles from home, I am filled with gratitude and emotion. Overcoming the challenges of adapting to a new country, language, culture, and cuisine, my pursuit of discovery was made possible by the supportive and friendly environment on the Plains and the unfaltering assistance from the faculty, colleagues, staffs and students in the Chemistry department. Therefore, I begin my dissertation acknowledgment by expressing heartfelt gratitude to everyone in the Auburn University Chemistry and Biochemistry family.

At the forefront of my gratitude stands my supervisor, **Dr. Christopher J. Easley**, whose unwavering dedication and support have been instrumental throughout my PhD journey. His guidance, marked by a unique blend of kindness, patience, and intellectual rigor, has been a constant source of inspiration. During moments of slow progress and self-doubt, Dr. Easley's thoughtful discussions and encouraging words dispelled my worries, reigniting my determination. His humor and engaging lab meetings transformed even the most challenging days into enjoyable and productive experiences, making the arduous journey of a PhD both fulfilling and enriching.

I will always remember the days when he left his favorite family gathering during the weekend to help me build the solenoid control system. I also remember the trust and responsibilities you entrusted me with, many of which I may not have done justice to. For that, I apologize. Alongside gaining research skills, I had the fortune to serve on an administrative committee with Dr. Easley. Thanks to my DCB graduate students whose votes gave me the only elected responsibility I have held in my life.

I would like to express my gratitude to my esteemed committee members and the honorable reader for taking time out of their busy schedules to evaluate my research work. Having taken multiple courses with **Dr. Byron H. Farnum** since my first year as a graduate student, I developed a strong understanding and appreciation of his teaching and mentorship. His critical observations during the qualifying exam greatly helped shape this dissertation into a complete form. Working with **Dr. Evangelos Miliordos** as a teaching assistant was a great opportunity, as he accepted my various personal limitations without complaint and extended a helping hand to resolve them. It was memorable to work with such a brilliant yet down-to-earth professor over multiple semesters and to serve as a shadow instructor for one semester during my graduate student life.

Although my acquaintance with **Dr. Christopher Grieco** is not very long, I have been an admirer of his pioneering research since the beginning. I also thank him for his constructive advice during the qualifying exam. Although I do not have direct acquaintance with **Dr. Jean-Francois Louf**, I had the opportunity to collaborate on a project with his postdoctoral researcher, Dr. Shankar Kharal. The results of that project are awaiting publication soon. I also thank him for taking on the responsibility of being the external reader of this dissertation amidst his busy schedules.

I extend my gratitude to my senior, contemporary, and junior colleagues who have made my journey in Easley Lab truly memorable. **Dr. Mark Holtan**, **Dr. Subramaniam Somasundaram**, **Dr. Juan Hu**, **Dr. Niamat Khuda**, **Dr. Katerina Ford**, and **Dr. Nan Shi** created a welcoming environment during my initial days. The camaraderie was further enriched by our "Pandava Quintet": **Dr. Amanda Kurian**, **Dr. Asanka Nuwan**, **Dr. Yvette Kayirangwa**, **Dr. Md. Moniruzzaman**, and myself—the last one yet to earn the esteemed title. Their friendship, both inside and outside the lab, inspired me throughout the journey, encouraging me to persevere and strive for excellence. Among the junior lab members, **Joanne Seow**'s professional and friendly support

significantly eased the challenges of my PhD journey. I am particularly grateful for her leadership on the '3D-Printing' sub-project of the Easley Lab. Thanks to my former teacher and later lab-mate Mainul Mazumder, your patronage has been invaluable for me. I am also thankful to my former undergraduate mentee and future doctor, Jacob Sinopoli, for his relentless dedication and invaluable assistance in our research endeavors.

Outside the lab, I am grateful to Auburn's Bangladeshi community, whose warmth made my time abroad feel less lonely and more like home, creating a sense of belonging and cultural connection that greatly eased the challenges of living far from my homeland. My deepest gratitude goes to my wife, **Zahin Fairuza**, whose understanding, care, and empathy have been my greatest source of strength throughout this journey. I am also immensely thankful to my father, a retired organic chemist, and my mother, a retired schoolteacher, for their unconditional support and lifelong dedication to education and science. Their belief in my potential and their constant encouragement have been the foundation of my academic and personal achievements. I would like to extend my heartfelt thanks to my long-term friends and undergraduate research lab mates from Dhaka University, **Dr. Nadim Shahriar Russel**, a recent graduate from Temple University, and soon to be doctorates and my former roommates **Rezonaul Islam** from Dr. Farnum’s Lab and **Anjam Sadik** from the University of Kentucky. Their consistent support and check-ins during difficult times were invaluable, providing much-needed encouragement and friendship throughout my journey.

Lastly, I would like to acknowledge the assistance of various **GPT-4** models in different aspects of my dissertation. These advanced tools have played a significant role in writing complex programs for data acquisition, analysis and control while translating many of my thoughts from Bengali into English, significantly enhancing the efficiency, accuracy and clarity of this work.

Table of Contents

List of Tables

List of Figures

Chapter 1

Introduction

(*Portions of this chapter were adapted from our published review article: Active Flow and Dynamic Analysis in Droplet Microfluidics*[1]**)**

1.1 Developments in Droplet Microfluidics

The exploration of droplet microfluidics is relatively recent. Although fundamental research in microfluidics began in the 1970s and made significant progress by the end of the 20th century, the concept of droplet-based microreactors was first scientifically published only two decades ago - emerging from earlier research on stable monodisperse emulsions[2–4] – as Thorsen and colleagues were among the pioneers who recognized that the unique fluid dynamics in microfluidic channels could be harnessed to reliably create droplets from two immiscible fluids[5], such as water and oil. This realization paved the way for numerous studies demonstrating that droplet microfluidics could facilitate a variety of manipulations and innovative analytical applications for microscale synthesis, storage and delivery[1].

What is Microfluidics?

Study of the systems to manage tiny volumes of fluids, from microliters to picolitres, using channels that are tens to hundreds of micrometers in size. It involves precise fluid has various applications in fields like biology, chemistry, and medicine, including the development of lab-on-a-chip devices, point-of-care diagnostics, and high-throughput screening methods.

Several research groups played key roles in advancing this field. Advanced methods have been developed for manipulating and analyzing individual droplets, which act as tiny reactors, enabling precise control and high-throughput screening in various scientific applications. Ismagilov's team investigated rapid fluid dynamics[6], while the Whitesides and Stone labs focused on device-specific behaviors[7]. The Weitz group explored high-throughput analysis and multiple

emulsions[8], and the Mathies lab worked on integrating valve-based automation into droplet microfluidics[9]. Meanwhile, Chiu's research focused on precise droplet analysis using fluorescence correlation spectroscopy[10]. These and other studies showed that microfluidic devices could produce highly uniform droplets, which acted as individual microreactors of picolitre or nanoliter volumes[11], suitable for various downstream processes like delivery[12], merging[13], mixing[14], sorting[15], and analysis[16].

Most research in droplet microfluidics uses optical methods, especially fluorescence, because it is simple, works well with microchannels, and avoids interference from oils.

Using uniform droplet populations has proven to have several advantages. The extremely small volumes reduce reagent consumption and enable unique single-cell or single-molecule analyses[16]. The ability to generate nearly identical droplets at high frequencies allows researchers to investigate biological systems and produce large datasets efficiently. Droplet microfluidics has thus enabled numerous applications in biology and chemistry, including single-cell genome sequencing[17], enzyme activity studies[18], combinatorial synthesis[19], drug discovery[20], protein and nucleic acid quantification[21], and cellular secretion detection[22,23]. There are extensive review articles on droplet microfluidics[24] that cover a wide range of topics, such as recent advancements[25], analytical techniques[26], droplet dynamics[27], passive and active droplet formation[28], droplet tracking and barcoding, single-cell analysis, tissue engineering, synthetic biology, nucleic acid cytometry, and drug discovery within droplets.

Most research in droplet microfluidics has relied on optical methods to read droplet contents, primarily fluorescence, due to its simplicity and compatibility with microchannels, and because it avoids interference from carrier fluids like oils. Traditionally, passive fluidic features have been

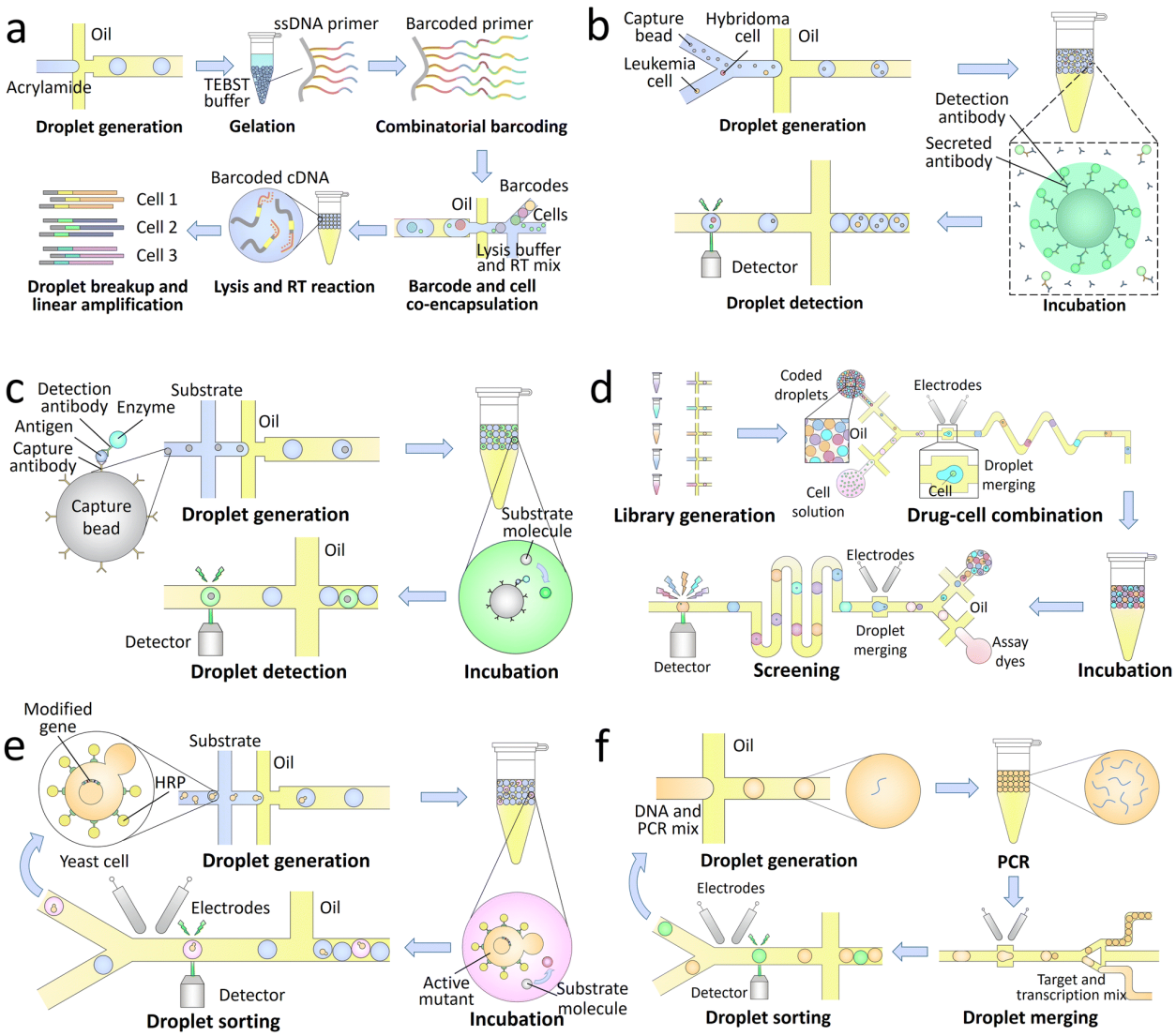

Figure 1.1 Droplet-based lab-on-a-chip applications in biotechnology. (a) Single-cell sequencing using barcoded hydrogels and droplet encapsulation. (b) Single-cell secretion analysis with capture beads and fluorescent detection antibodies. (c) Droplet digital ELISA for high-sensitivity antigen detection. (d) Drug screening using optically coded drugs and droplet fusion. (e) Directed evolution via yeast cell surface display and fluorescent substrate conversion. (f) Single-aptamer selection through PCR and transcription in droplets.

used in these studies. However, more recent efforts have focused on active droplet formation and control (see **figure 1.1**), incorporating elastomeric valves, and integrating additional analytical

steps like bead-based cleanup and mass spectrometry with droplet microfluidics. This chapter will highlight significant recent advancements in active or automated microfluidic flow control strategies for droplet creation and management, drawing connections to digital and analog electronic concepts and providing examples of channel designs and analytical applications.

1.1.1 Flow Control in Droplet Microfluidics

1.1.1.1 Passive Droplet Control

In microfluidic systems, two immiscible fluids, such as oil and water, can be directed to meet at a junction where they form droplets. The movement and formation of these droplets downstream are influenced by the viscous and interfacial forces acting on them. Passive mechanisms control these droplets by adjusting channel geometry, surface properties, hydrodynamic pressures, viscosities of the fluids, and interfacial tension between the phases. Surfactants are often used to modify droplet properties because of their effect on surface tension.

Various methods have been developed to generate droplets passively. The main types include crossflow, co-flow, and flow-focusing, each named based on how the fluid phases interact at the interfaces. These methods utilize different device designs to control the size and frequency of the droplets passively. For detailed insights, comprehensive reviews by experts in the field provide extensive information on passive droplet formation techniques.

1.1.1.2 Active Droplet Control

For many applications in droplet microfluidics, precise control over the size, volume, and frequency of droplet formation is crucial. While passive methods can achieve this without external inputs, active regulation offers greater precision and flexibility, although it usually operates at lower throughput and requires additional energy[1]. Active control mechanisms are essential in mitigating inconsistencies caused by device manufacturing variations, environmental conditions, and changes in surface chemistry. These mechanisms enable programmable droplet formation, which

allows precise control over droplet characteristics via computer interfaces. For instance, the use of acceleration-mode dip-coating can create gradient droplet arrays with tunable characteristics such as size and content[29]. Additionally, membrane displacement traps offer deterministic control over droplet operations, including generation, capture, and sorting[30]. Valve-based systems further enhance this precision, enabling the formation and manipulation of femtoliter-volume droplets[31]. Moreover, microfluidic droplet-storage arrays provide versatile handling for complex reactions[32], while platforms like DropLab facilitate high-controllability in droplet-based reactions[33].

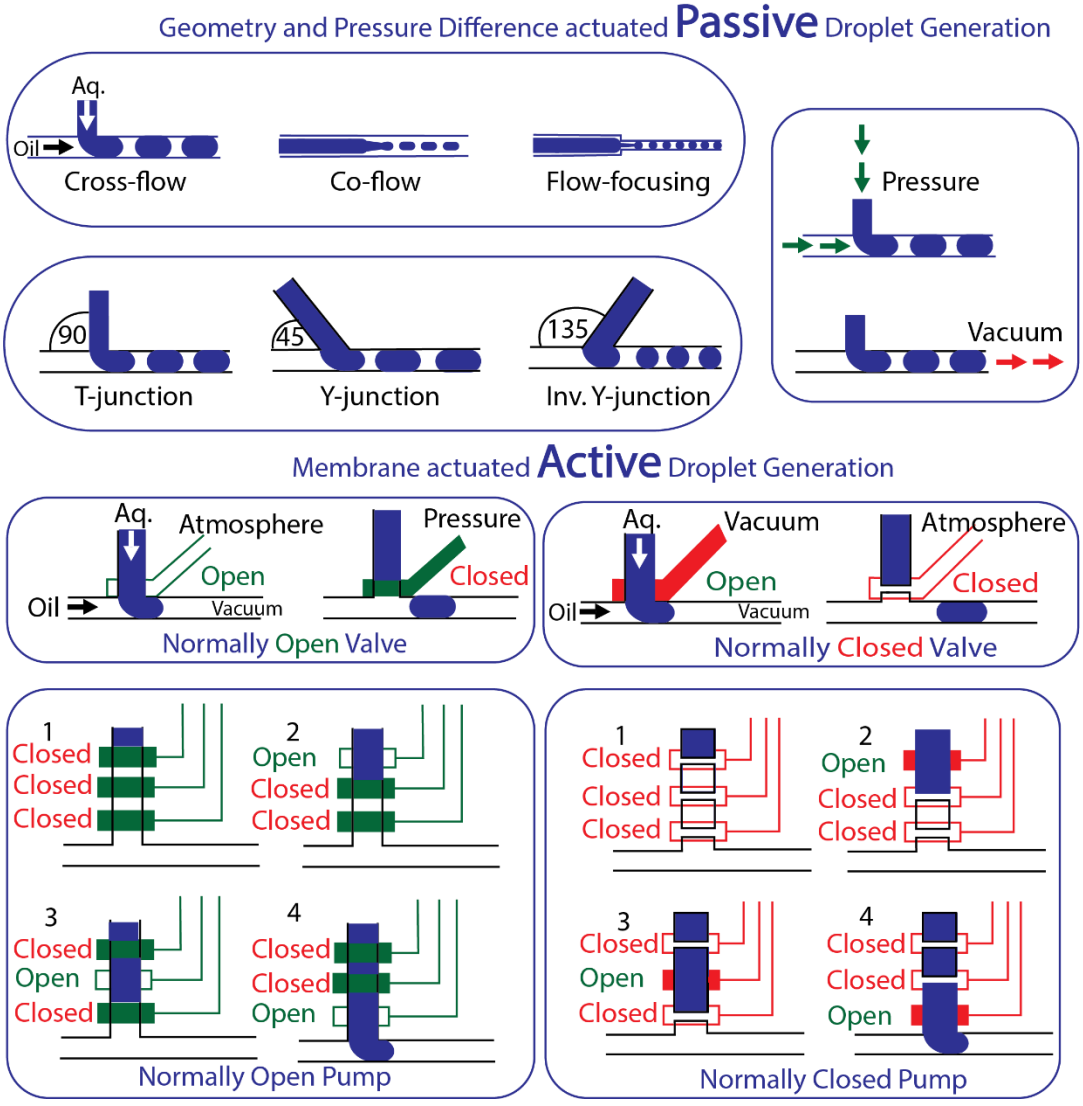

Figure 1.2 Schematic representation of passive and active droplet generation meth-

Active control methods use external forces to manipulate droplets, categorized by the type of energy applied: mechanical, electrical, thermal, or magnetic. Mechanical control often employs membrane valves[30,34], which can precisely regulate fluid flow and droplet formation. Recent advances in 3D printing technology have made it possible to produce these valves more quickly and affordably, enhancing their functionality and accessibility.

Electrical methods such as applying alternating current (AC) fields can destabilize fluid interfaces to facilitate droplet operations like formation, merging, and sorting. For example, AC fields are used in droplet microfluidics to control droplet formation and manipulation processes, enabling precise handling of fluids[35]. **Electrowetting** is another technique that uses electrical control to alter droplet dynamics on surfaces, known as digital microfluidics. This method allows for the precise movement and merging of droplets, critical in applications requiring fine droplet control[36]. Additionally, **magnetic** and **thermal approaches** further enhance droplet manipulation. Magnets can control ferromagnetic fluids, while heating elements can adjust fluid properties, providing fine-tuned control over droplet formation and manipulation[36].Although setting up active control systems can be complex due to the need for multiple external components, these methods provide high accuracy and precision, which are particularly valuable for experiments requiring exact volume control or extended operation times. For instance, phase-locked detection methods have significantly improved optical detection limits by generating sample and reference droplets in a controlled alternating pattern.

Figure 1.2. illustrates schematic representation of passive and active droplet generation methods. The top section illustrates geometry and pressure difference-actuated passive droplet generation, including T-junction, flow-focusing, and co-flow designs. The bottom section depicts

membrane-actuated active droplet generation with normally open and closed valves and pumps, demonstrating various states (open and closed) and their effect on fluid flow and droplet formation.

1.1.2 Advances in Fluidic Control and Interfacing

1.1.2.1 Active Systems Using Membrane Valves

The development of integrated membrane valving concepts in microfluidics has been significantly advanced by the work of the Quake[5] and Mathies[37] groups, among others. These innovations have opened the door to a variety of impactful microfluidic applications, though for many years, such valves were rarely used in droplet microfluidics due to the simplicity of forming droplets passively. Despite this, recent advancements have demonstrated the powerful capabilities of combining membrane structures for droplet formation and manipulation.

One notable advancement is by the DeVoe group, which demonstrated the programmable integration of droplet generators, traps, and mergers using membrane valves and strategically placed bypass channels[38]. This system enables various actions on demand, such as trapping droplets in a first-in-first-out manner, analysis, selective ejection, merging, and sorting. They applied this technology to single cell trapping and screening. Additionally, they developed a microfluidic multiplexer with a multi-depth droplet trap structure to allow random-access trapping and release of picolitre droplets or cells.

Our research group has also contributed to this field by demonstrating that precise control of droplet frequencies at narrow bandwidths can significantly reduce optical detector noise. This was achieved using a device we termed the μChopper[39–41]. By integrating this automated system with saltwater merging electrodes, we created a fully programmable device capable of combinatorial analysis and on-chip immunoassays[41]. While a drawback of these systems is their relatively

low droplet frequencies (approximately 0.1–10 Hz), their programmability offers exceptional consistency in regulating droplet frequency, size, merging ratios, and trapping and retrieval positions.

1.1.2.2 Unique Droplet Junctions with Active Control

Typical structures for droplet formation and handling in microfluidics are based on designs where two channels intersect at a junction, such as the common T-junction droplet generators. In 2017, Doonan & Bailey introduced a novel advancement termed the K-channel[42]. This innovative design involves multiple channels intersecting at a single node, which is connected to a nearby merging electrode and/or magnet. This setup allows cross-channel flow to interact with droplet flow at the intersection point, enabling multiple versatile operations with a single feature, including reagent injection, fluid extraction, droplet splitting, and magnetic bead capture. The K-channel requires a precisely balanced flow rate in a separate liquid stream, classifying it as an active structure. It operates successfully in the droplet frequency range of 200–500 Hz, making it suitable for various high-frequency applications. Despite the numerous benefits and potential applications of droplet microfluidics, a significant challenge has been the integration with solid-phase techniques.

To address this, the Bailey group developed another unique droplet junction known as the coalesce-attract-resegment wash (CAR-Wash) design[43]. This structure accepts three inputs with controlled flow: bead-containing droplets segmented in oil, a wash solution, and another oil stream for resegmenting. It uses two active on-chip structures, a saltwater electrode and a magnet, and outputs two streams containing both aqueous and oil components (waste and resegmented droplets with washed beads). The CAR-Wash design operates at droplet frequencies above 500 Hz, achieving 98% retention of beads and over 100-fold dilution in the final droplets. This system is particularly useful for integrating more sample preparation steps into on-chip droplet workflows and can be adapted for multistep, bead-based immunoassays in segmented flow streams.

Other unique junctions have also been developed recently. Shojaeian & Hardt applied a controllable direct current (DC) electric field within a channel adjacent to a standard T-junction droplet generator[44], enabling active control over droplet sizes and sequences. Similarly, Teo et al. enhanced the saltwater electrode design at the droplet junction, using alternating current (AC) electric fields for on-demand size control of droplets made from both Newtonian and non-Newtonian fluids[45]. Raveshi et al. used pressure-based control in an adjacent valve channel to achieve selective droplet splitting at a downstream junction, finding that the size of split droplets was strongly influenced by the pressure applied to the inlets and the valve[46]. The single-layer valve design also simplified device fabrication.

These examples demonstrate some of the creative adaptations and advancements in droplet control junctions in recent years, highlighting the ongoing innovation and potential of active droplet control in microfluidics.

1.1.3 Advanced Optical Interfacing

Optical detection methods, particularly fluorescence, are widely utilized to measure droplet contents in microfluidics. While absorbance detection is also used, it is often limited by the short optical path lengths inherent to microchannel dimensions. To overcome the challenges posed by weak optical signals, advanced optics or phase-locked detectors are required. Our group exploited the natural "chopping" action of droplet formation by developing the μChopper device[39,40,47], which functions similarly to an optical beam chopper. This innovation significantly enhanced absorbance detection limits by over 100-fold without the need for optical modifications. Furthermore, by employing continuous illumination and synchronizing the optical detector with the frequency and phase of droplet-forming valves, we achieved a more than 50-fold reduction in fluorescence detection noise. This system successfully quantified the uptake rate of free fatty acids in

single 3T3-L1 adipocyte cells and established a mass detection limit for insulin in in-droplet homogeneous immunoassays at 2×10^{-16} mol[39]. The precise frequency regulation provided by this system demonstrates the potential of integrating computer-controlled valves with droplet microfluidics to unlock new analytical capabilities.

Additionally, innovative optical interfaces have been developed, such as arrays of small lenses matched to droplet detection spots. The Baret group demonstrated the use of a micro-optical lens array for massively parallel droplet detection, achieving throughputs of approximately 2,000 droplets per second per lens, with over 625 measurement points[48]. The deMello group further validated this approach by analyzing 50,000 cells per second and later enhanced the system with a counter-propagating lens/mirror setup, which increased signal strength by two orders of magnitude while analyzing up to 40,000 droplets per second[49]. These microlens array systems are powerful and efficient, capable of being microfabricated to match the dimensions of microchannels, thereby advancing the capabilities of optical interfacing in droplet microfluidics.

Photoinitiated reactions within droplets have been effectively achieved using various light sources. For example, Choi et al. successfully demonstrated the on-chip photo-polymerization of monodisperse polyethylene glycol diacrylate (PEGDA) droplets with a UV light source positioned downstream of a crossflow droplet generator[50]. This process faced challenges due to the inhibition of PEGDA polymerization by oxygen molecules, which consume photoinitiated free radicals. To address this, Oakey's team introduced a nitrogen gas stream to purge the system, providing better control over the size and uniformity of the microspheres[51]. Di Carlo and coworkers improved scalability and throughput in microgel production by adjusting pH levels and using an oil-soluble organic base, and they also created "dropicles," which are uniform particles that form aqueous-in-oil compartments without the need for fluidic channels[52,53]. Another notable advancement came

from Paegel et al., who developed the hνSABR system[54]. This integrated an optical waveguide, mirror, droplet formation, and bead suspension hopper structures on-chip, enabling precise photochemical reaction dosing and facilitating dose-response screening in an HIV-1 protease activity assay.

1.1.4 Fluidic Analog-to-Digital Operations Using Droplets

In the context of analytical chemistry, droplet microfluidics can be compared to flow injection analysis (FIA) systems developed in the 1970s[1]. Droplet microfluidics offers distinct advantages over traditional Flow Injection Analysis (FIA) systems by effectively halting diffusion and dispersion between adjacent droplets, ensuring chemical isolation within each droplet segment. This is achieved by minimizing longitudinal dispersion after droplet segmentation, where mixing occurs only within each droplet through chaotic advection. This isolation is particularly beneficial for applications in analytical and bioanalytical chemistry, as it allows for precise control over chemical processes within each droplet. For example, microfluidic systems that utilize chaotic advection can achieve rapid mixing of reagents in droplets, which is crucial for chemical kinetics and biochemical assays that require low sample consumption and accurate description of fast reaction kinetics[55]. Additionally, controlling or minimizing oil partitioning during experiments further maintains the separation of droplet contents, enabling novel applications in fields where discrete and controlled reactions are essential[56].

In this regard, droplet segmentation plays a crucial role in the temporal analysis and control of fluidic streams and analyte signals. Devices that continuously sample a fluid stream and segment it into droplets function as microfluidic analog-to-digital converters (μADCs). Conversely, devices that begin with segmented flow and create well-controlled continuous flow patterns are referred to as microfluidic digital-to-analog converters (μDACs). These systems enable precise temporal

resolution and spatial separation of chemical and biochemical components, facilitating advanced analytical applications.

1.1.5 Microfluidic Analog-to-Digital Conversion

Early research in microfluidics highlighted the power of droplet-based segmentation to preserve the temporal dynamics of systems under study. One notable example is the chemistrode device[57], which uses segmented flow streams as both the input and output to external systems, such as cells on a glass surface. This pioneering work demonstrated that dynamically varying systems could be sampled fluidically at short timescales and then analyzed using immunoassays, fluorescence readouts, and mass spectrometry (MS).

For instance, Easley et al. showed that continuous droplet sampling could be employed to sample secretions from pancreatic islets with a resolution of 1.9 seconds, revealing two classes of oscillations in secreted zinc[58]. Similarly, Kennedy's group combined microdialysis sampling with droplet segmentation to maintain temporal resolution, coalescing droplets into a continuous stream for analysis by microchip electrophoresis, which was used to evaluate glutamate and aspartate release in the striatum of anesthetized rats[59].

These systems, introduced over a decade ago, can be viewed as microfluidic analog-to-digital converters (μADCs). They allow dynamic systems to be sampled with nanoliter or picoliter droplets, with aqueous-in-oil segmentation preventing diffusion and dispersion from compromising the temporal record within the fluid. The fluidic sampling resolution (Δt) defines the achievable measurement resolution downstream, especially when mixing with assay reagents is required prior to readout. By coupling μADC systems to actively controlled merging structures, researchers can maintain temporal resolution by mixing with assay reagent droplets downstream of the sampling

site[41]. This approach allows for numerous downstream operations on the droplets without detri-

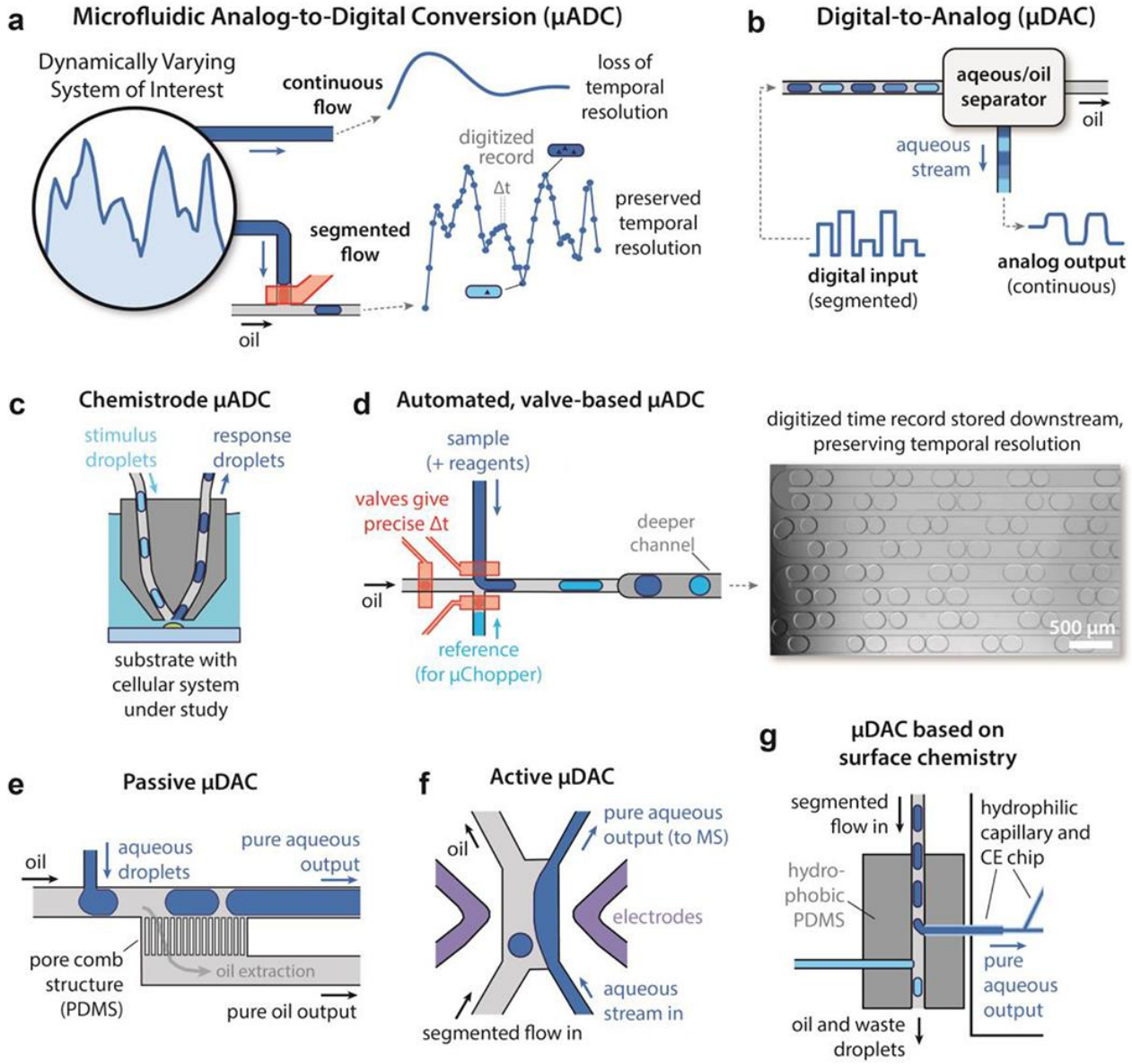

Figure 1.3 Microfluidic analog-to-digital (μADC) and digital-to-analog conversion (μDAC) designs using droplets. (a) μADC preserves dynamic information at high temporal resolution. (b) μDAC coalesces droplet trains into a continuous stream. (c) Chemistrode device as μADC. (d) Automated valves ensure consistent Δt for digital data storage. (e) Passive separator for μDAC. (f) Active μDAC using dielectrophoretic merging with mass spectrometry. (g) μDAC using surface wettabilities to separate streams. Adapted with permissions from various sources.

ment to Δt.

Treating each sampled droplet as a time-stamped snapshot of the chemical and biochemical information from the system of interest provides a fluidic system analogous to analog-to-digital

conversion circuitry. In contrast, continuous flow systems lose much of the temporal information due to diffusion and dispersion in the sampling channel, with subsequent operations further compromising the temporal resolution.

Two examples of μADC fluidic architectures are shown in **Figure 1.3**, namely the chemistrode (101) (**Figure 1.3c**) developed by the Ismagilov group and the valve-automated μADC device developed by our group for tissue secretion sampling and downstream quantitative analysis[60,61] (**Figure 1.3d**). As shown in **Figure 1.3d**, automated valve-controlled segmented flow allows the time difference between droplets (Δt) to be precisely regulated, and the fluidically digitized time record can be stored downstream in an incubation channel (Figure 1.3d, inset) akin to digital data storage on a hard disk.

1.1.5.1 Applications of μADCs

Microfluidic analog-to-digital converters (μADCs) have been instrumental in uncovering novel chemical and biochemical information, as illustrated in various studies. One notable example is a neural probe μADC system developed by Petit-Pierre and colleagues[62,63]. This system combined a microfluidic droplet generator with recording and stimulation electrodes, positioning the droplet generator within 170 μm of the sampling inlet to achieve a resolution (Δt) of only a few seconds. This engineered probe was validated for translating an analog stream into digital fluid segments with high temporal resolution and was later used to monitor neurochemical dynamics in rat brains with a 50-second resolution.

The Kennedy group also made significant strides in this area by integrating a microfabricated push-pull probe with droplet-based sampling[64]. The small size of the probe allowed for a 1,000-fold improvement in spatial resolution, and droplet-based segmentation close to the downstream site enabled 6-second temporal sampling resolution at low perfusion rates. They further

coupled the system to nanoelectrospray ionization–mass spectrometry (nESI-MS) to simultaneously measure glutamine, glutamate, γ-aminobutyric acid, and acetylcholine, revealing rapid neurochemical release times of 15 seconds in the brains of live rats following potassium stimulation.

Another impressive in vivo application was demonstrated by Nightingale et al., who developed a wearable μADC device for droplet sampling to quantify glucose and lactate directly in dermal tissue[65].

In our laboratory, an automated, valve-based μADC system has been employed for sampling and quantifying secretions from endocrine tissue explants. Building on earlier work with a passive sampler[58], automated μADC was applied to murine pancreatic islet tissue[60]. Small-volume, droplet-compatible homogeneous immunoassays for insulin were developed and mixed upstream of droplet formation using on-chip pumps[66]. Utilizing the μChopper concept[39–41], highly sensitive insulin quantification was achieved through simple optical measurements on-chip with a standard fluorescence microscope. This device revealed insulin secretion oscillations upon glucose stimulation, matching the timing of calcium oscillations, and allowed for the quantitative observation of rapid insulin bursts in the range of hundreds of attomoles.

Our μADC device was recently updated to include more assay reagent channels, incorporating a coupled enzyme assay for glycerol[61]. This system was used to study the differences between adipocyte spheroids and ex vivo adipose tissue from mice. High-resolution data showed rapid lipolytic oscillations in adipose tissue but not in cell spheroids, with oscillations occurring at frequencies of 0.2 to 2.0 min^{-1}. The application demonstrated that high-resolution, quantitative sampling with our μADC device enables the observation of unique biological information regarding cellular connectivity, providing an analytical framework suitable for studying dynamic oscillatory functions in various tissues.

1.1.6 Microfluidic Digital-to-Analog Conversion

Devices that perform the reverse operation, starting with a segmented flow stream (digital input) and then separating the aqueous and oil phases into individual streams (analog output), are known as microfluidic digital-to-analog converters (μDACs). These devices can effectively translate a dynamically varying signal into a segmented stream of nanoliter or picoliter droplets, resulting in an aqueous stream with precise temporal changes defined by the input droplets.

Many early studies on droplet mergers or aqueous/oil separators, though not explicitly described as such, fit the μDAC concept. For instance, Angelescu et al. demonstrated a passive aqueous/oil separator utilizing the native substrate (PDMS) surface chemistry and channel aspect ratios[67]. This design allowed the oil stream to flow downward through narrow channels while the aqueous stream moved forward, effectively performing μDAC operations. They also used oil-wet fluoropolymer membranes to retrieve the oil phase. Ostromohov et al. employed a similar oil-draining method to achieve the highest-resolution μDAC to date, with a temporal resolution (Δt) of 0.56 seconds.

Another approach by Fidalgo et al. used dielectrophoresis with high AC voltages applied to on-chip electrodes to coalesce segmented droplets with a continuous aqueous stream, which was then coupled to mass spectrometry (MS) analysis[68]. The Kennedy group utilized surface chemistry and wetting behavior to separate oil and aqueous solutions at a T-junction, converting segmented flow inputs into continuous streams[69]. This μDAC device was used to continuously inject samples into a microchip capillary electrophoresis (MCE) channel. They later modified the device to interface droplet inputs with both MCE and gel electrophoresis on-chip, enabling the study of protein-

protein interactions and enzyme samples at a rate of 10 seconds per sample, performing over 1,000 separations before reconditioning was needed[70].

1.1.6.1 Applications of μDACs

A variety of unique applications have been realized using microfluidic digital-to-analog converters (μDACs). One notable example, illustrated by Guetschow et al., involved sampling a library of potential enzyme activity modulators from multiwell plates[69]. These samples were segmented into 8-nL aqueous-in-oil droplets (representing digital information) and introduced into a microchip electrophoresis (MCE) device capable of subsecond separation times. This setup allowed the transformation of digital droplet input into a continuous analog output. Their μDAC device achieved a continuous stream of subsecond mobility shift assays for protein kinase A activity, analyzing 96 samples in just 12 minutes with minimal sample input.

Ostromohov et al. utilized a high-resolution μDAC device (with a temporal resolution of 0.56 seconds) to deliver sequential reagents with minimal dispersion to a surface[71]. Their device translated digitized segmented flow into a continuous aqueous stream using a wettability filter. This system was applied to modify the fluorescence emission of surface-immobilized green fluorescent protein (GFP) through rapid pH changes in the μDAC-delivered buffer.

The Inglis group developed a needle-like μDAC device to translate segmented flow through hydrophilic capillaries, resulting in a continuous solution stream to a surface with a chemical signal response time of approximately 3 seconds[72]. Their research on the dynamic transport of chemical signals using droplets is well-documented and provides complementary insights to this review.

One of the most powerful applications of droplet-based microfluidics is the mass-activated droplet sorting (MADS) device[73]. This device integrates multiple droplet-handling features, with

a μDAC component that reinjects a previously formed emulsion of droplet-encapsulated library components. The MADS device splits each droplet into two daughter droplets at a 4:1 volume ratio, directing the larger droplets to an exit leading to an electrospray ionization mass spectrometry (ESI-MS) interface. This part of the device acts as a μDAC because the ESI-MS requires continuous aqueous input. The smaller daughter droplets are fed into a delay line awaiting MS data and subsequently sorted based on the MS signal from their corresponding larger droplets.

The MADS technique enables the sorting of thousands of droplets at a rate of 0.7 samples per second (approximately 15,000 samples in 6 hours). It was used to detect a substrate of a transaminase for screening enzyme activity via in vitro expression within the droplets. This device represents a significant advancement in droplet microfluidics due to its label-free nature and the ability to sort droplets based on mass spectrometry data, greatly expanding the applicability of droplet sorting in future analytical applications.

1.2 Remaining Challenges in Droplet-Based Microfluidic Flow Control

As evident from the above discussion, droplet-based microfluidics has emerged as a powerful tool for precise manipulation and analysis of small volumes of fluids, offering numerous applications across various fields including biology, chemistry, and materials science. Despite its many advantages, several challenges remain in optimizing and expanding the capabilities of droplet-based systems.

High-Resolution Sampling and Stimulation: One primary consideration in droplet microfluidics is determining the appropriate resolution for sampling or stimulation. Oversampling can lead to wastage of valuable reagents, such as enzymes or biosensors, while undersampling can result in missed dynamic changes in the system. The concept is akin to electronic data acquisition, where

oversampling in an analog-to-digital converter (ADC) can be inefficient, and undersampling can cause aliasing[74]. It is crucial to align the droplet generation rate with the Nyquist rate to ensure accurate representation of the system's dynamics.Matching the scale of the system under observation with the microfluidic droplet generator is essential. For example, if biological samples like tissue explants are too large relative to the droplet size, critical dynamic information may be lost before droplets can form. Similarly, high-resolution chemical or biochemical patterns generated by a micro-digital-to-analog converter (μDAC) must be scaled appropriately to effectively stimulate the target system[75].

Oil Partitioning: The choice of carrier oil in droplet microfluidics significantly impacts the system's performance, as analytes, interacting partners, or optical labels may partition into the carrier oil, affecting experimental outcomes. Conducting partitioning studies within the microdevice is crucial due to the high surface area-to-volume ratios, which can influence results. If partitioning timescales are comparable to the experimental timescales, it may be necessary to switch to a different oil or surfactant to ensure accurate results. For example, certain oils might cause analytes to partition away from the aqueous phase, thus altering the observed chemical interactions[36].

Integration with analytical techniques presents another significant challenge in droplet microfluidics. While fluorescence-based optical readouts are commonly employed, there is a growing need for interfaces with rapid-readout spectrometers and other analytical tools. The coupling of droplet microfluidics with mass spectrometry (MS), as demonstrated by the new MADS technique, showcases the potential for enhancing the analytical capabilities of droplet microfluidics, making it a versatile tool for a wider range of applications[36]. This integration allows for the rapid analysis of

droplet contents, providing valuable insights in various fields, including chemical and biological research.

Active Versus Passive Control: Active control methods, although slower than passive techniques, offer precise regulation of droplet frequency and phase, which is critical for high-resolution applications. Active control allows for a narrow bandwidth operation, essential for tasks requiring high precision. However, the challenge lies in developing faster active control mechanisms while maintaining this precision. Advances in on-chip valve fabrication with more rigid materials or integrating continuous feedback systems for off-chip controls are potential solutions.

Future Directions: Looking ahead, there is a need for continued innovation in both the design and application of droplet-based microfluidic systems. This includes developing more robust and versatile droplet generators, improving the integration with analytical techniques, and refining control mechanisms to achieve higher precision and faster response times. Addressing these challenges will pave the way for broader adoption and more advanced applications of droplet microfluidics in scientific research and industry.

These challenges highlight the ongoing efforts and potential advancements needed to fully harness the capabilities of droplet-based microfluidics. By addressing these issues, the field can continue to evolve and provide more sophisticated tools for precise fluid manipulation and analysis.

1.3 Integration of Dissertation Content

The subsequent chapters of this dissertation are closely interwoven with the foundational concepts introduced in this chapter, focusing on the enhancement of droplet microfluidic systems through advanced control mechanisms and automation.

In **Chapter 2**, we delve deeper into the theoretical and practical aspects of control systems for droplet microfluidics, which were introduced here under passive and active control methods. This chapter provides a comprehensive exploration of various control strategies, setting the stage for the sophisticated automation techniques discussed in later chapters.

Chapter 3 moves from theory to practical application, detailing the development and implementation of electronically automated membrane-actuated microflow control systems. Building on the discussion of active control mechanisms, this chapter demonstrates how electronic systems such as LabVIEW and Arduino can be employed to achieve precise droplet control. The analysis includes a detailed examination of system performance metrics like response time and droplet volume consistency.

In **Chapter 4**, the focus shifts to pneumatic automation, emphasizing the development of pneumatic logic gates and their integration into droplet microfluidic systems. This chapter illustrates how pneumatic systems can automate droplet processes, providing an alternative to electronic controls. The experiments conducted highlight the potential for consistent droplet formation and manipulation using fully pneumatic setups, aligning with the future directions outlined earlier.

Chapter 5 synthesizes the advancements in both electronic and pneumatic automation, exploring their integration and potential applications across various scientific fields. This chapter ties back to the challenges and future directions identified in the introduction, showcasing practical applications in biological assays, chemical synthesis, and more.

This structured progression from foundational knowledge to practical applications and future innovations highlights the comprehensive scope of this dissertation. Each chapter builds upon the previous, demonstrating how advancements in control and automation can address current challenges and open new avenues in droplet microfluidics. This cohesive narrative underscores the

importance of precise, reliable, and scalable droplet manipulation in the continued development of microfluidic technologies.

1.4 Conclusions

This chapter has provided an overview of the developments and advancements in droplet microfluidics, emphasizing its relatively recent emergence and rapid evolution as a powerful tool for precise fluid manipulation and analysis. Beginning with the historical context, we traced the journey from early microfluidics research in the 1970s to the pioneering work on droplet-based microreactors in the early 2000s. These foundational studies have demonstrated the potential of droplet microfluidics for a wide range of applications in microscale synthesis, storage, and delivery.

We highlighted the contributions of key research groups in advancing droplet microfluidics. Their innovative approaches have enabled the manipulation and analysis of individual droplets as tiny reactors, facilitating high-throughput screening and precise control in various scientific fields. The advantages of using uniform droplet populations, such as reduced reagent consumption and the ability to conduct single-cell or single-molecule analyses, have been instrumental in enabling applications across biology and chemistry, including genome sequencing, enzyme activity studies, and drug discovery.

The chapter also explored the mechanisms of passive and active droplet control, each offering unique benefits for specific applications. Passive control methods rely on channel geometry and fluid properties to manipulate droplets, while active control methods employ external forces for greater precision and flexibility. Advances in both approaches have significantly enhanced the capabilities of droplet microfluidics, enabling more sophisticated and controlled fluid operations.

Furthermore, we discussed the integration of fluidic control systems with analytical techniques, such as fluorescence detection and mass spectrometry. These integrations have expanded the analytical capabilities of droplet microfluidics, allowing for more detailed and accurate measurements of droplet contents. The development of unique droplet junctions and advanced optical interfacing techniques has further improved the precision and efficiency of droplet-based analyses.

Finally, the chapter introduced the concept of fluidic analog-to-digital (μADC) and digital-to-analog (μDAC) converters, illustrating how droplet segmentation can preserve temporal dynamics and enable precise control of fluidic streams. These systems provide a framework for advanced analytical applications, where droplet-based microfluidics can offer unparalleled resolution and accuracy.

Despite these advancements, several challenges remain, including optimizing sampling and stimulation resolutions, addressing oil partitioning issues, and enhancing the integration with various analytical techniques. Continued innovation in droplet generator design, control mechanisms, and analytical interfacing will be crucial in overcoming these challenges and unlocking the full potential of droplet microfluidics.

In conclusion, the developments in droplet microfluidics represent a significant leap forward in the field of microfluidics. The ability to manipulate and analyze fluids at such a small scale with high precision opens up numerous possibilities for scientific research and industrial applications. As the field continues to evolve, addressing the remaining challenges will pave the way for even more sophisticated and impactful uses of droplet-based microfluidic systems.

Chapter 2

Development of Microfluidic Flow Control Systems

2.1 Background

2.1.1 Brief History of Electronics

The history of computing technology has seen several significant milestones that have transformed the field and paved the way for the advanced systems we have today. Almost eighty years ago, the invention of the world's first general-purpose electronic digital computer, the Electronic Numerical Integrator and Computer (ENIAC), set a monumental milestone in technological history. Developed by John Presper Eckert and John Mauchly at the University of Pennsylvania, the ENIAC comprised 19,000 vacuum tubes and occupied an entire room[76–78]. This revolutionary machine demonstrated the potential of electronic computing, followed by the invention of the transistor in 1947 marked a significant shift in computing technology. Developed by John Bardeen, Walter Brattain, and William Shockley at Bell Labs, the transistor replaced vacuum tubes, allowing for more reliable, smaller, and energy-efficient computers[79].

Moore's Law

An observation made by Gordon Moore, the co-founder of Intel, in 1965. His prediction on the number of transistors integrated circuit (IC) would double approximately every two years. This prediction has held remarkably true for several decades, leading to exponential growth in computing power.

This breakthrough enabled the development of more compact and efficient electronic devices, transforming the landscape of computing. The advent of integrated circuits in the late 1950s and early 1960s, pioneered by Jack Kilby at Texas Instruments and Robert Noyce at Fairchild Semiconductor, revolutionized electronics by drastically miniaturizing components[80–82]. Integrated circuits allowed for the creation of smaller, more powerful computers, fundamentally transforming technology and computing. This innovation laid the groundwork for the modern electronics industry and enabled the development of increasingly sophisticated computing devices.

The 1970s and 1980s saw the introduction of microprocessors and very large-scale integration (VLSI). Microprocessors, which are central processing units contained on a single chip, and VLSI technology, which exponentially increased the density of transistors on chips, played a crucial role in enhancing computing power[83,84]. These advances followed Moore's Law, which predicted the doubling of transistors on a chip approximately every two years, leading to significant improvements in computing performance and capabilities[85,86].

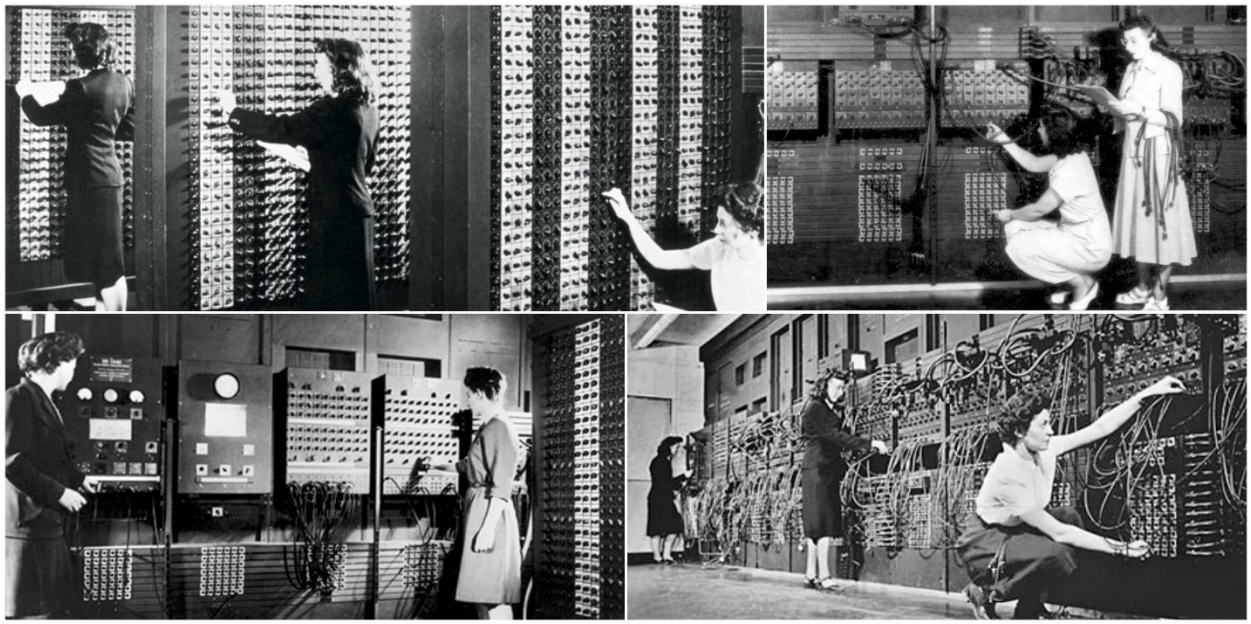

Figure 2.1 Top Left: Jennings, Wescoff, and Lichterman work on portable function tables connected to the main mechanism. (Credit: Corbis). Top Right: The ENIAC, the first electronic computer, at the University of Pennsylvania in 1946. (Credit: Apic/Getty Images, U.S. Army Photo). Bottom Left: Programmers Betty Jean Jennings Bartik and Fran Bilas Spence operate ENIAC's main control panel at the Moore School of Electrical Engineering. (Credit: U.S. Army/ARL Technical Library Archives). Bottom Right: Women program ENIAC by plugging and unplugging cables and adjusting switches. (Credit: Los Alamos, Corbis/Getty Images).

Advances in semiconductor technology continue to push the boundaries of miniaturization, researchers are now exploring molecular and quantum computing as future frontiers[87]. These emerging technologies promise to overcome the limitations of traditional silicon-based electronics and open new possibilities for the future of computing. Molecular computing involves the use of molecules to perform computational operations, while quantum computing leverages the principles of quantum mechanics to process information in fundamentally new ways. Both fields hold the

potential to revolutionize computing by offering unprecedented levels of performance and efficiency[77,88].

These milestones highlight the incredible journey of computing technology from large, room-sized machines to the highly compact and powerful devices we use today. The continuous innovation in this field underscores the dynamic and rapidly evolving nature of technology. Integrated circuits have enabled the development of microvalve arrays that allow for precise fluid flow control at a macroscopic level. These arrays achieve high precision by controlling the number of microvalves that are open, thus regulating the flow with remarkable accuracy[34].

Similarly, digital microfluidic chips have been developed to allow for precise control of liquid drops through the application of electric signals on the chip's electrodes, further advancing the capabilities of microfluidic systems[89]. However, achieving comparable success in fluidics at the microscale necessitates a level of precision and control that remains elusive. One significant challenge is the automation of sequential liquid control in microfluidic circuits. This has been addressed through the development of 3D slope valves, which facilitate precise control of fluid flow in a disk platform, allowing for more complex microfluidic operations. Additionally, smart flow control processes at the micro-scale have been enabled by integrated circuits, allowing for precise control of flow rates and distribution in microreactors and micro-mixers using components like micro-pumps, micro-channels, and micro-valves.

One significant challenge is the automation of sequential liquid control in microfluidic circuits.

The use of shape memory alloys in the design of microvalves has also contributed to advancements in fluidic control systems, enabling precise fluid regulation with high accuracy and rapid response times[90]. Moreover, closed-loop feedback control systems have been developed to manage microbubble diameter in flow-focusing microfluidic devices, demonstrating real-time measurement and control capabilities[91]. In lab-on-a-chip and organ-on-a-chip applications, precise

microflow control is crucial. Innovations such as the introduction of pressure-driven methods for microflow control have shown promise in achieving the necessary precision[92].

Furthermore, the development of digitally controlled hydraulic resistors at the microscale level reflects the advancements in integrated circuits, allowing for better control of fluid flow within lab-on-a-chip systems[93]. The generation of nanoliter droplets on demand at high frequencies has been made possible using precision micropumps with custom-designed piezoelectric valves, addressing the need for fast and precise fluid control at the microscale. These innovations highlight the ongoing efforts and advancements in achieving the precision and control necessary for the success of fluidics at the microscale[94].

For microfluidics to reach its full potential, the integration of electronic components is essential. Despite significant advancements in incorporating electronics into microfluidic systems over the past five decades, large-scale integration remains a formidable challenge. The intricacies involved in managing and manipulating fluids at the microscale are far more complex than those encountered in microelectronics. Consequently, the progress of microfluidics has been slower, and achieving the level of integration seen in microelectronics continues to be an ambitious goal. The integration of electronic components in microfluidics faces several challenges. For instance, the manufacturing efficiency and the need for seamless integration of microfluidics with electronics are critical issues. Efficient packaging techniques that accommodate both electrical and fluidic connections are essential to enhance device functionality and reliability[95].

One approach to addressing these challenges is the development of CMOS-compatible microfluidic systems, which enable the direct integration of electronic components such as sensors and actuators. This integration expands the functional applications of microfluidic systems, making them more versatile and capable of performing complex tasks[96]. However, material selection

remains a significant obstacle, as it affects the flow properties, absorptivity, biocompatibility, and overall functionality of the devices[97,98].

Another challenge is the complex arrangement of multiple electrodes with different electrical potentials within digital microfluidic platforms. This complexity necessitates innovative solutions to ensure accurate and reliable control of fluid movement within the microchannels. Additionally, the integration of soft electronic systems into microfluidics aims to enhance the mechanical performance of wearable electronics, increasing their flexibility, twistability, and stretchability[99].

The development of hybrid microfluidic devices, which combine polymer microfluidic chips with functional elements made from different materials such as metals, silicon, and organic semiconductors, has been a significant advancement[100]. These hybrid systems meet the demand for additional functionalities and improve the overall performance of microfluidic devices. Moreover, advancements in microfluidic liquid handling, including continuous-flow microfluidics and digital microfluidics, offer promising future perspectives[99].

Innovations such as the integration of Ionic Polymer-Metal Composite (IPMC) actuators into microfluidic channels demonstrate practical applications for point-of-care tests (POCTs), addressing some of the integration challenges[101]. Furthermore, the use of shape memory alloys for electronically activated microfluidic components assembled on printed circuit boards allows for high-density integration alongside standard opto-electronic components[102].

In summary, while the integration of electronic components into microfluidic systems presents numerous challenges, significant advancements have been made. These advancements include the development of CMOS-compatible systems, hybrid devices, and innovative materials

and fabrication techniques, all contributing to the gradual progress towards achieving large-scale integration[45,95,96,99,101,102].

2.1.2 Analogy between Electronic Circuits and Microfluidics

Microfluidics, the science of manipulating fluids in channels with dimensions of tens to hundreds of micrometers, shares several conceptual and functional similarities with electronic circuits[103]. Both fields involve the precise control and manipulation of entities within confined pathways to achieve desired outcomes. Understanding the analogy between these two domains can provide insights into the design and operation of microfluidic systems by drawing parallels with well-established principles in electronics[104].

Fluid Flow and Resistance: The fluid flow rate (Q) through a microfluidic resistor is analogous to the electric current (I) through an electrical resistor[104]. The hydraulic resistance (R_h) plays a similar role to electrical resistance (R): where ΔP is the pressure difference across the resistor. $Q = \frac{\Delta P}{R_h}$

Fluid Storage and Compliance: The fluid volume (V) stored in a microfluidic capacitor[105] under pressure (P) is analogous to the charge (Q) stored in an electrical capacitor under voltage (V). The compliance (C_h) is analogous to capacitance (C): $V = C_h \cdot \Delta P$

Table 1 Comparison of components and functions in electronics and microfluidics.

Component	Electronics	Microfluidics
Channels/Wires	Wires conduct electricity between components	Channels guide the flow of liquids between regions of the device
Valves/Switches	Switches control the flow of electrical current	Valves control the flow of liquids, actuated by mechanical, pneumatic, or electrokinetic methods

Pumps/Power Supplies	Power supplies provide necessary voltage and current	Pumps drive the movement of fluids through channels, can be external or on-chip
Sensors/Detectors	Sensors detect physical quantities (e.g., light, temperature)	Detectors sense the presence and concentration of substances within the fluid
Capacitors/Reservoirs	Capacitors store and release electrical energy	Reservoirs hold and release fluid within the system
Resistance	Electrical resistance opposes the flow of current (Ohm's law)	Fluidic resistance opposes the flow of liquid (Hagen-Poiseuille equation)
Capacitance	Ability to store charge	Ability of a chamber to store a volume of fluid, important for precise dosing and timing
Inductance	Ability to induce voltage based on changing current	Parallel to the inertia of fluid flow, where changes in flow rate induce pressure variations
Network Analysis	Analyzed using network theory and Kirchhoff's laws	Analyzed using similar principles, with counterparts for flow rates and pressures
Fluid Flow and Resistance	$I = V / R$	$Q = \Delta P / R_h$
Capacitance/Compliance	$Q = CV$	$V = C_h.\Delta P$

2.1.3 Introduction to 3D Printing

3D printing, also known as additive manufacturing, is a process of making three-dimensional solid objects from a digital file[106,107]. The creation of a 3D printed object is achieved using additive processes, where an object is created by laying down successive layers of material until the object is formed. Each of these layers can be seen as a thinly sliced horizontal cross-section of the eventual object. There are several types of 3D printing technologies, and some of the most

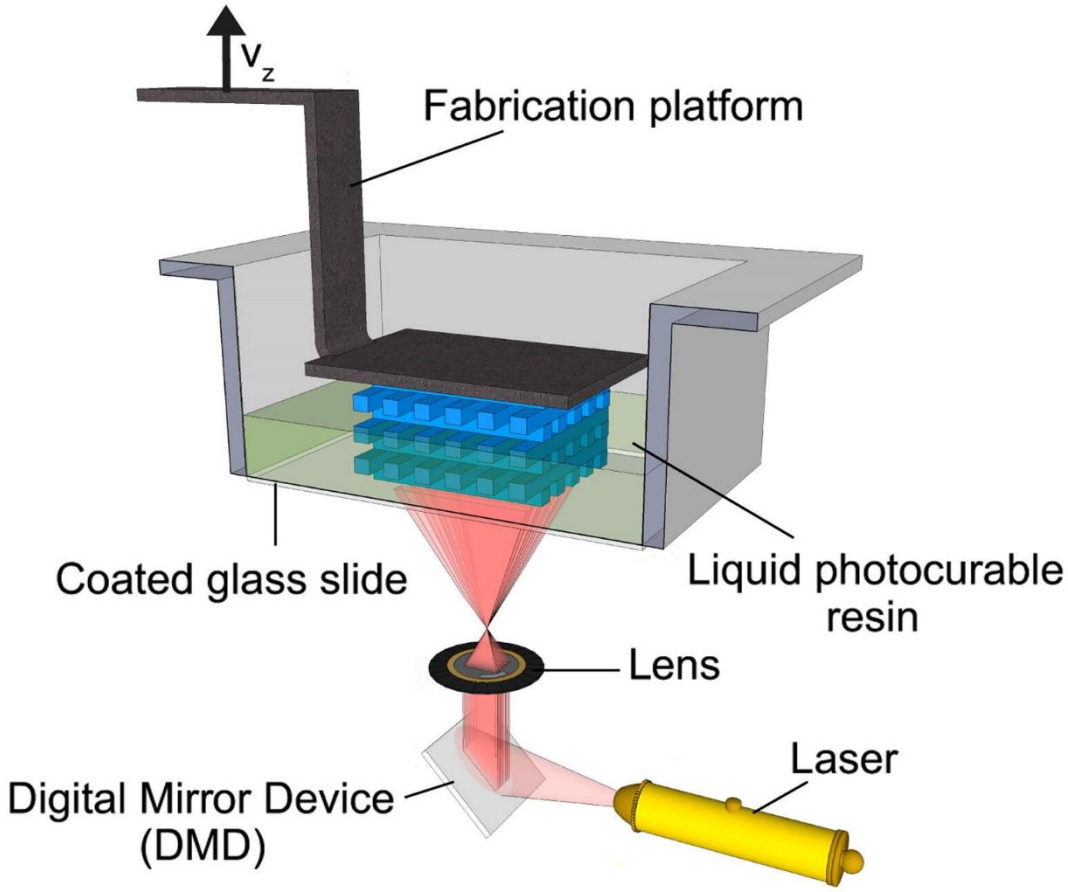

Figure 2.2 Illustration of a 3D printing process using Digital Light Processing (DLP). The setup includes a laser source, a lens system, and a Digital Mirror Device (DMD) to project the light pattern onto a coated glass slide immersed in liquid photocurable resin. Adapted with permission from reference #96.

common ones include Fused Deposition Modeling (FDM, Stereolithography (SLA), Digital Light Processing (DLP), Selective Laser Sintering (SLS) and Direct Metal Laser Sintering (DMLS).

The photopolymerization-based 3D printing methods, such as SLA and DLP, involve converting liquid resin into solid objects layer by layer using light, typically UV or visible light. This process hinges on the use of photoinitiators, which are chemicals that absorb light and initiate the polymerization reaction[106]. Phosphine oxide-based photoinitiators, such as diphenyl (2,4,6-trimethylbenzoyl) phosphine oxide (TPO) and phenylbis (2,4,6-trimethylbenzoyl) phosphine oxide (BAPO), are widely used in photopolymerization processes due to their ability to absorb visible and UV light and efficiently initiate polymerization[108]. The general mechanism of action for these photoinitiators can be described through a series of steps, starting with light absorption and leading to the initiation of polymerization. The detailed reaction mechanisms and equations are as follows:

i. **Light Absorption:** The process begins when the photoinitiator in the resin absorbs light. Upon exposure to the appropriate wavelength, the photoinitiator (PI) is promoted from the ground state (S_0) to an excited state (S_1) which can be represented as: $\mathbf{PI} + \boldsymbol{h\nu} \rightarrow \mathbf{PI^*}$, where PI^* represents the excited state of the photoinitiator.

ii. Intersystem Crossing (ISC): The excited photoinitiator undergoes intersystem crossing to form a triplet state (T_1), which is more reactive and longer-lived than the singlet excited state: $\mathbf{PI^* \rightarrow PI^{T1}}$

iii. Cleavage: In the triplet state, the phosphine oxide photoinitiator undergoes α-cleavage, breaking the C-Ph bond adjacent to the phosphine oxide group, leading to the formation of two radicals: a phosphinoyl radical and a benzoyl radical: $\mathbf{PI^{T1} \rightarrow \cdot POPh + \cdot C(O)Ph}$

iv. **Initiation of Polymerization:** The generated radicals, particularly the benzoyl radical (·C(O)Ph), can then initiate the polymerization of acrylate or methacrylate monomers (M) by adding to the double bond of the monomer: **·C(O)Ph + M→ C(O)Ph-M·**

v. **Propagation:** Once generated, radicals attack the double bonds of monomers (the building blocks of polymers) present in the resin. This reaction forms new radicals at the end of the attached monomer, which then react with other monomer molecules. This chain reaction, known as propagation, continues, with each step adding another monomer to the growing polymer chain: **M· + nM → Polymer.**

vi. **Termination:** The chain growth can terminate in several ways, such as when two radicals recombine, or when a radical is quenched by encountering an inhibitor. Termination stops the growth of the polymer chain.

vii. **Curing and Solidification:** As the polymer chains grow, the resin begins to solidify. In 3D printing, this process is precisely controlled and occurs layer by layer. The printer directs the light source (UV or visible light) to specific regions of the resin according to the digital design, causing those areas to cure and solidify. The build platform then moves, allowing a new layer of liquid resin to cover the solidified part, and the process repeats. This layer-by-layer curing builds up a three-dimensional object.

viii. **Post-Curing**: After printing, the object may undergo post-curing, an additional exposure to light, to ensure that the polymerization process is complete throughout the material. This step enhances the mechanical properties and stability of the printed object.

The advantages of photopolymerization in 3D printing include high resolution, the capability to produce complex geometries, and rapid prototyping. However, the process's success heavily depends on the type of photoinitiator used, the light source's wavelength and intensity, and the

resin composition. These factors collectively influence the efficiency of polymerization, the physical properties of the cured material, and the overall quality of the 3D printed object.

2.1.4 PDMS in Microfluidic Device Fabrication

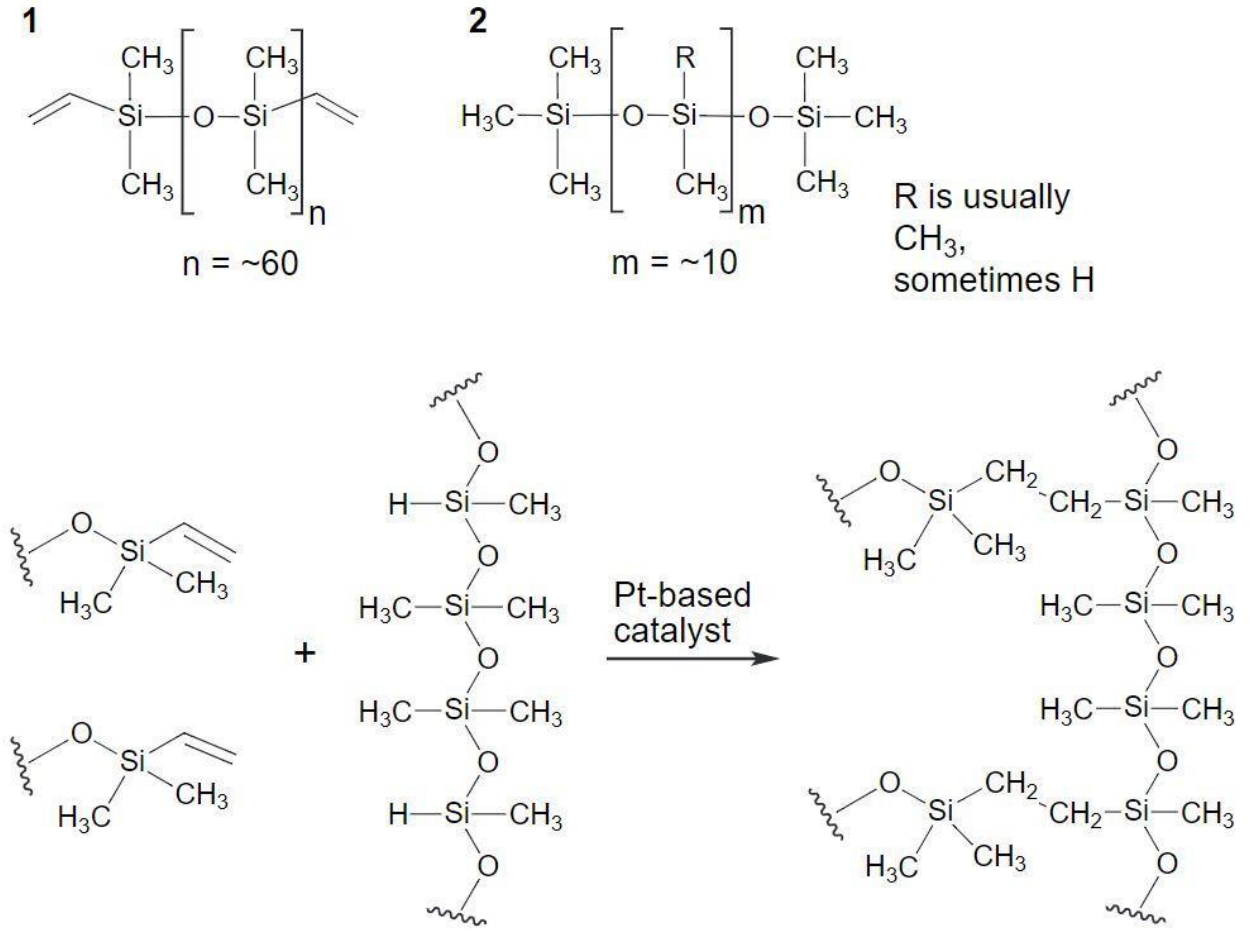

Figure 2.3 Polymerization reaction of dimethyl siloxane oligomers for PDMS.

Polydimethylsiloxane (PDMS) has been acclaimed for its biocompatibility, optical clarity, and gas permeability[109]. These attributes have made it an essential component in a wide range of applications, from chromatographic separations to integrated photonic devices[110]. PDMS's flexibility and transparency make it suitable as a gate dielectric in solution-processed organic field-effect transistors and in various biomedical applications, from implants to soft contact lenses, due to its biocompatibility and ease of manufacturing[111,112]. Its unique rheological properties allow

PDMS to be utilized in flexible electronics and even in the food and cosmetics industries. PDMS's properties meet different requirements in sustainable energy, such as in microfluidics and triboelectric nanogenerators. The optical, mechanical, and electrical properties of PDMS nanocomposite materials and nanostructures are beneficial in biomedical imaging, biosensing, and cellular bioengineering[113].

The history of using Polydimethylsiloxane (PDMS) in the development of microfluidic devices is rich and spans several decades. Though the field of microfluidics started gaining traction in the 1990s with the use of silicon and glass, the focus soon shifted to polymer substrates, particularly PDMS[114]. Duffy et al. pioneered a procedure that allowed for the design and fabrication of microfluidic systems in PDMS in less than 24 hours[115]. This development played a significant role in popularizing the use of PDMS in microfluidics, enabling rapid prototyping and easy fabrication of complex channel networks. McDonald and Whitesides summarized the techniques for fabricating microfluidic devices in PDMS, emphasizing its applications in biomedicine[116].

Advances in 3D printing technologies have enabled the creation of molds with complex geometries for PDMS casting. These molds allow for the fabrication of multi-level fluidic channels and integrated structures, providing a cost-effective and rapid prototyping method for LOC devices[117]. This approach circumvents the limitations of traditional photolithography and offers greater design flexibility. The quest for optimized integration of PDMS with SLA 3D printed templates continues to be an area of active research. Studies are focusing not only on the physical and chemical aspects of this integration but also on the biocompatibility and functional efficacy of the resulting devices in biomedical applications[118].

However, when PDMS is cast against these 3D printed molds, issues such as incomplete curing and surface irregularities can occur. This is partly attributed to the inhibitors in the 3D printing resins, such as phosphine oxide-based photoinitiators, which interfere with the platinum-catalyzed curing of PDMS[119]. The interaction of PDMS with uncured resin components from 3D printed devices can lead to incomplete curing and surface irregularities as illustrated in **figure 2.4**[120]. The curing process of PDMS itself is sensitive to various factors, including the storage conditions of its precursors[121] and Young's modulus of the material[122]. The inherent hydrophobicity and elastomeric nature of PDMS necessitate careful consideration of the surface properties of the 3D printed templates for successful integration[123]. Effective post-processing techniques such as UV curing and IPA washing have been explored to mitigate the leaching of inhibitory substances from the resin, which can significantly improve the quality of PDMS casting on these templates[124]. Additionally, the development of new resin formulations for SLA that mimic the

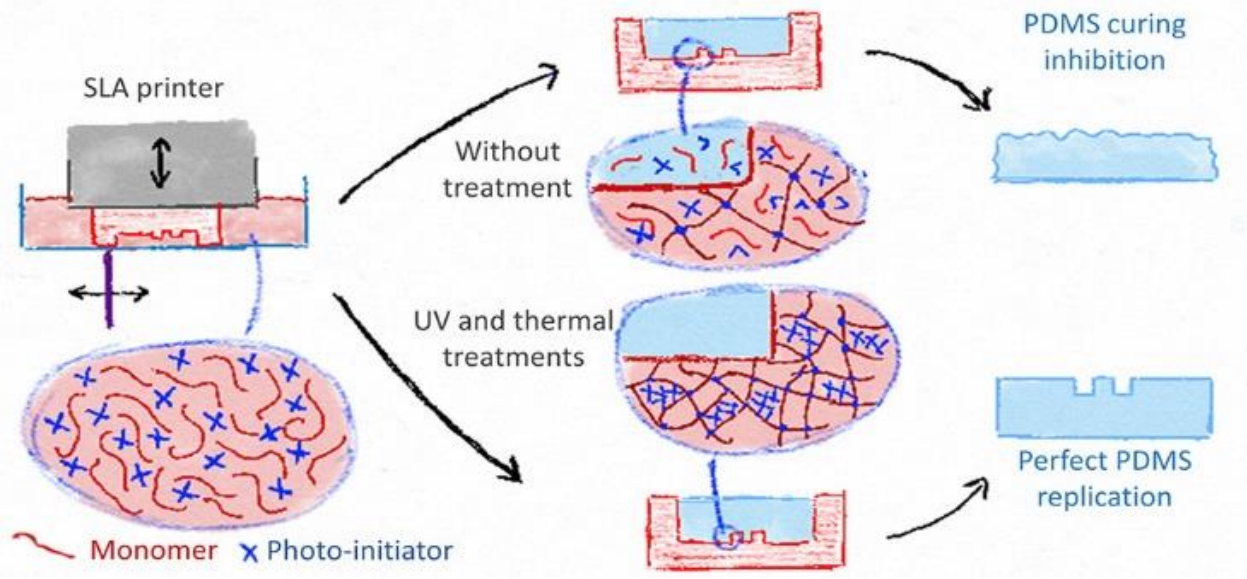

Figure 2.4 Illustration of the treatment process for SLA-printed molds to achieve perfect PDMS replication. The SLA printer creates a structure using monomers and photo-initiators. Without treatment, PDMS curing inhibition occurs, leading to imperfect replication. UV and thermal treatments cross-link the photo-initiators and monomers, eliminating inhibition and resulting in perfect PDMS replication. Adapted with permission from reference #109.

properties of PDMS opens avenues for more seamless integration of these two materials in device fabrication[125].

Despite its many advantages, PDMS faced challenges such as the absorption of small molecules and compatibility with certain solvents. Toepke and Beebe discussed PDMS absorption and its impact on microfluidic experiments, providing insights into the limitations of PDMS in certain applications[126]. In microfluidic applications, PDMS's intrinsic hydrophobicity can be problematic, especially when seeding cells on its surface, necessitating surface modification techniques[127].

This chapter aims to delve deep into the optimization of PDMS curing processes when interfacing with SLA 3D printed templates. We explore the chemical intricacies of PDMS and its interaction with 3D printing materials, along with proposed solutions to overcome the hurdles associated with this integration.

2.1.4.1 Chemistry of PDMS Curing

The PDMS curing process begins with the preparation of the PDMS mixture, typically involving a base polymer and a curing agent. The standard mixing ratio is often 10 parts of the base polymer to 1 part of the curing agent. This ratio can be varied to modify the mechanical properties of the final cured product. PDMS, or polydimethylsiloxane, is a polymer made up of repeating units of -$Si(CH_3)_2O$-. The base polymer is typically terminated with vinyl groups (-$CH=CH_2$), while the curing agent contains silicon-hydride (Si-H) groups. The curing process involves a hydrosilylation reaction, where the Si-H bonds in the curing agent add across the C=C double bonds of the vinyl groups in the base polymer. This cross-linking reaction is catalyzed by a platinum-based catalyst, and can be represented by the following chemical equation:

$$R_2SiH_2 + CH_2 = CHSiR_2 \rightarrow R_2SiHCH_2CH_2SiR_2$$

Where:

- R_2SiH_2 represents a silane with two Si-H bonds.

- $CH_2=CHSiR_2$ represents a vinyl-functionalized silane (a silane with a vinyl group).

- $R_2SiHCH_2CH_2SiR_2$ is the product, where the Si-H bond is added across the C=C double bond of the vinyl group, creating a longer chain with two silicon atoms linked by a -CH2-CH2- segment.

This reaction is catalyzed by platinum, which facilitates the addition of the Si-H bond across the C=C bond. As this reaction repeats across multiple molecules, it results in the formation of a cross-linked polymer network, which is the cured PDMS material. The "R" groups are typically methyl groups in PDMS but can vary depending on the specific PDMS formulation.

The curing of PDMS is influenced by several factors, including the ratio of base polymer to curing agent, curing temperature, and curing time. The curing temperature typically ranges from 60°C to 150°C, and the curing time can vary from a few minutes to several hours, depending on the desired properties and thickness of the PDMS. The final physical and mechanical properties of cured PDMS, such as elasticity, tensile strength, and thermal stability, are dependent on the degree of cross-linking achieved during the curing process. Higher cross-link density typically results in stiffer and less permeable PDMS. The properties of PDMS can be further modified by incorporating fillers, changing curing conditions, or surface treatments.

2.1.4.1.1 Role of Platinum in PDMS curing process

The platinum catalyst facilitates the hydrosilylation reaction in PDMS curing through a process called catalytic activation, which lowers the activation energy required for the reaction to occur. Here's a simplified overview of how platinum acts in this context:

I. **Activation of the Si-H Bond**: The platinum catalyst first interacts with the silane molecule (R_2SiH_2). It temporarily binds to the Si-H bond, increasing its reactivity. This activation makes the Si-H bond more susceptible to reaction with the vinyl group.

II. **Facilitation of the Addition Reaction**: Once the Si-H bond is activated, the platinum catalyst facilitates the addition of this bond across the carbon-carbon double bond (C=C) of the vinyl-functionalized silane (CH_2=$CHSiR_2$). This step is crucial and is where the catalytic power of platinum is most evident. The catalyst lowers the energy barrier for this addition, allowing the reaction to proceed at a practical rate and under milder conditions than would be possible without the catalyst.

III. **Formation of the Cross-Linked Structure**: The result of this addition reaction is a new Si-C bond, extending the polymer chain ($R_2SiHCH_2CH_2SiR_2$). As this reaction occurs repeatedly with multiple silane and vinyl-functionalized silane molecules, a cross-linked polymer network is formed, which is the cured PDMS.

IV. **Regeneration of the Catalyst**: After the reaction, the platinum catalyst is regenerated and can participate in another catalytic cycle. This regeneration is a key feature of catalysts, allowing a small amount of platinum to facilitate the reaction of a large quantity of reactants.

The specific mechanism by which platinum catalyzes the hydrosilylation reaction can involve complex organometallic intermediates and may vary slightly depending on the exact nature of the platinum catalyst (for example, whether it is a complex or a colloidal form of platinum). However, the fundamental process involves the activation of the Si-H bond and the facilitation of its addition across the C=C bond, leading to the formation of the cross-linked PDMS structure.

2.1.4.1.2 Inhibitors of PDMS curing on 3D-printed templates

Certain types of components present in the 3D-printing material, particularly those used in photopolymerization-based stereolithography (SLA) processes, are found to prevent successful PDMS curing on printed templates. These inhibitors can leach out of the 3D-printed structures and

poison the platinum-based catalyst in PDMS, impeding its curing process when cast against 3D-printed molds or templates.

For instance, phosphine oxide-based photo-initiators can coordinate the lone pair of electrons on phosphorus atom to the platinum center, potentially forming stable and catalytically inactive or less active platinum-phosphine oxide complexes.

This complex formation decreases the active platinum sites available for the curing reaction, leading to incomplete or inhibited curing of PDMS. The exact chemical structure of the [Pt-Photoinitiator Complex] depends on the specific photoinitiator used and the nature of its interaction with the platinum catalyst. For detailed mechanistic studies and specific reactions involving phosphine oxides and platinum catalysts, further research in organometallic chemistry and catalysis would be required.

Residual monomers or oligomers that have not fully polymerized during the 3D printing process can interfere with the PDMS curing. These components might remain on the surface or within the microstructure of the 3D-printed template, creating a barrier to effective curing[120]. Various substances used in the 3D printing resins, such as stabilizers, plasticizers, or other additives, could potentially migrate into the PDMS during curing[106]. These substances can alter the chemical environment, potentially hindering the PDMS curing process.

2.1.4.1.3 Prevention of PDMS curing inhibition on 3D-printed templates

To address the challenges of casting polydimethylsiloxane (PDMS) on 3D printed templates, molds, or masters without curing issues, several potential solutions have been explored. These solutions focus on ensuring smooth surface topology, preventing inhibition of the PDMS curing process, and improving the compatibility between PDMS and 3D printed structures. Methods such as UV and/or thermal post-curing of the 3D-printed templates can be employed. These

treatments can help to reduce the number of leachable photo-initiators and other inhibitory substances, enabling more reliable PDMS replication from 3D-printed molds.

Villegas et al. proposed a technique to produce smooth PDMS channels from low-resolution 3D printed molds using an omniphobic lubricant-infused coating[128]. This method involves coating the 3D printed mold with a fluorinated silane to produce a high affinity for the lubricant, which tethers it to the mold, resulting in significantly smoother topology for PDMS casting. Comina, Suska, and Filippini demonstrated the use of 3D printed templates for fabricating conventional PDMS on glass lab-on-a-chip (LOC) devices. These templates, which are cost-effective and reusable, can accommodate multiple thicknesses and are smooth enough for direct transfer and sealing to glass substrates.

Choudhury, Dutta, and Chatterjee explored using 3D printing resin for template fabrication followed by PDMS device development[129]. This approach reduces cost and enhances ease of template generation while retaining the advantages of PDMS devices. Bhattacharjee et al. reported the formulation and stereolithography (SL) application of a 3D-printable PDMS resin[130]. This method enables the creation of optically transparent submillimeter structures and microfluidic channels, offering a potential solution for seamless integration of PDMS in device[130]. Mazzeo and Hardt described a method for centrifugal casting and fast curing of PDMS-based components with microfeatures, which allows simultaneous patterning of multiple sides of a component and control of the part thickness without bubble entrapment[131].

Venzac et al. discovered that the inhibition of PDMS curing on 3D-printed molds, particularly those made using stereolithography (SLA), is primarily caused by phosphine oxide-based photo-initiators leaching from the SLA resins. These initiators poison the platinum-based catalyst

used in PDMS curing. The research identified UV and/or thermal post-curing as effective treatments to mitigate this issue[119].

2.1.5 Passive and Active Microfluidic Flow Control

Passive microfluidic flow control leverages the inherent properties of microscale fluid dynamics and device architecture to manipulate fluid flow without external energy sources. This approach is highly beneficial for simplifying device operation, reducing cost, and enhancing portability, making it especially suitable for point-of-care testing, drug delivery systems, and lab-on-a-chip applications. Xu et al. reviewed passive micropumping techniques suitable for point-of-care testing, highlighting the balance between the need for control and simplicity[132]. The review discusses capillary force and air transfer passive pumping methods as promising solutions for POCT applications, emphasizing their low cost and ease of use Kim et al. demonstrated system-level sequential and parallel microfluidic flow processing using fully passive capillarity-driven control[133]. By preprogramming inlet-well meniscus pressure and channel fluidic conductance, the study achieved preprogrammed flow control of 10 solutions, showcasing capillarity as a viable method for sophisticated microfluidic processing without active valves and pumps.

Jeong et al. developed a siphon-driven microfluidic passive pump with a yarn flow resistance controller[134], enabling adjustable and continuous media delivery to cell cultures over long periods. This innovation combines the simplicity of passive systems with the precision of active pumping methods. Zhang and Oseyemi introduced a microfluidic passive valve that operates under ultra-low threshold pressure for high-throughput liquid delivery[135]. This valve design, utilizing a novel combination of a liquid chamber, an elastic membrane, and an ellipsoidal control chamber, showcases the ability to stabilize flow rates under varying pressures, suitable for portable microfluidic devices. Zhang et al. presented a passive flow regulatory device with integrated check

valves for improved flow control[136]. The device maintains stable flow rates over a threshold pressure and enables accurate forward flow without backward leakage, demonstrating potential for Lab-on-a-Chip applications.

Active microfluidic flow control utilizes external energy sources to precisely manipulate fluid flow within microfluidic devices, enabling a wide range of applications from biomedical assays to chemical synthesis. Hardoüin et al. explored the control of directional flows and autonomous transport in a microfluidic network of connected annular channels containing a tubulin-kinesin active nematic[137]. This study demonstrates the ability to manipulate active flows in complex topologies, offering insights into synchronization, anti-correlation, and stabilization of high topological singularities in both flow and orientational fields.

Pan and Wang explored the flow characteristics of an active controlled microfluidic valve driven by a circular piezoelectric unimorph actuator[138]. This work demonstrated the valve's capability for on/off switching and continuous fluid control, providing a simple and easily fabricable solution for active flow control in microfluidic devices.

Takasaki and Takamizawa introduced a microfluidic device that utilizes stress-induced martensitic transition in a microporous molecular crystal for active fluidic control. This innovation enables spatiotemporal molecular flow controllability through mechanical reorientation of subnanometre channels, marking a significant step towards microfluidic devices capable of molecular-level control[139]. Saren et al. reported on an integratable micropump made from magnetic shape memory alloy Ni–Mn–Ga, which is actuated by an external magnetic field to drive fluid flow[140]. This technology allows for wireless, precise fluid delivery without the need for mechanical parts, offering a novel approach to active microfluidic flow control.

Iakovlev et al. provided a comprehensive review of active and passive microfluidic flow control methods, highlighting the precision and multitasking capabilities of mechanical systems in microfluidics[141]. This review emphasizes the importance of integrating microfluidic systems with smartphones or single-board computers for data processing and control, pointing towards future trends in microfluidic technology development.

2.1.5.1 Normally closed active flow control

Normally closed microfluidic valves are essential components in the design and function of microfluidic devices, enabling precise control over fluid flow. These valves are particularly advantageous in applications requiring the default state of the valve to be closed to prevent fluid flow until an actuation force is applied. Recent advancements have focused on various actuation mechanisms and fabrication techniques to improve performance, miniaturization, and integration capabilities. Xiang et al. introduced a novel pinch-type valving technology for centrifugal microfluidic systems, achieving both normally closed and normally-open valves[142]. This approach uses a sliding wedge to transduce centrifugal force, offering simpler actuation and less contamination risk compared to other techniques.

Mohan et al. detailed the design and fabrication of elastomeric normally closed microvalves, highlighting the influence of geometrical parameters on actuation pressures and reliability[143]. Their findings support the development of portable microfluidic devices for on-chip analysis and long-duration biological or chemical studies. Li et al. explored thermoplastic elastomer-based normally closed microvalves with microstructured valve seats, presenting a solution for the industrial manufacturing of microfluidic devices integrated with microvalves, addressing previous challenges in valve bonding during device assembly[144]. Takehara et al. developed microfluidic valves using the shape memory effect of poly(ε-caprolactone) for both normally open and closed

configurations, demonstrating fast actuation, low power requirements, and high withstanding pressure, suitable for disposable polymer chips[145].

These studies collectively highlight the ongoing innovation in microfluidic valve technology, particularly in achieving efficient, reliable, and easy-to-integrate normally closed valves for diverse applications in lab-on-a-chip devices, diagnostics, and biomedical research.

2.1.6 Lock-in Detection

Droplet-based lock-in detection is an advanced analytical method that integrates the advantages of droplet-based microfluidics with lock-in amplification, enhancing the sensitivity and selectivity for detecting analytes within complex biological matrices. In this approach, droplets containing the sample are produced and manipulated within a microfluidic channel, with precise control over the droplet frequency and phase, enabling effective analysis via lock-in detection[41].

Lock-in detection, a technique widely utilized in signal processing, facilitates the identification of weak signals amidst significant noise. This method involves modulating the signal of interest at a specific frequency and phase, and subsequently measuring the response at that same frequency and phase. By filtering out signals at other frequencies, lock-in detection can isolate and amplify the desired weak signal from the noisy background. In the context of droplet-based lock-in detection, sample droplets are generated at a predetermined frequency and transported through a microfluidic channel. The channel design induces a specific flow pattern that causes the droplets to oscillate at a designated frequency. These oscillating droplets are then analyzed using lock-in detection, where the modulation frequency matches the droplet oscillation frequency. By aligning the detection system to this frequency, the signal is amplified, and background noise is filtered out, enabling highly sensitive and selective analyte detection within the sample (see **Figure 2.5**).

As discussed already, in our laboratory, we have developed a technique termed "μChopper" for droplet-based lock-in detection[41,146]. This method involves segmenting the sample into droplets within microfluidic devices. The technique offers numerous advantages over conventional detection methods, such as enhanced sensitivity, increased specificity, and the capability to analyze minute sample volumes. Droplet-based lock-in detection holds significant promise for advancing the field of microfluidics and expanding its applications in biological and chemical analysis.

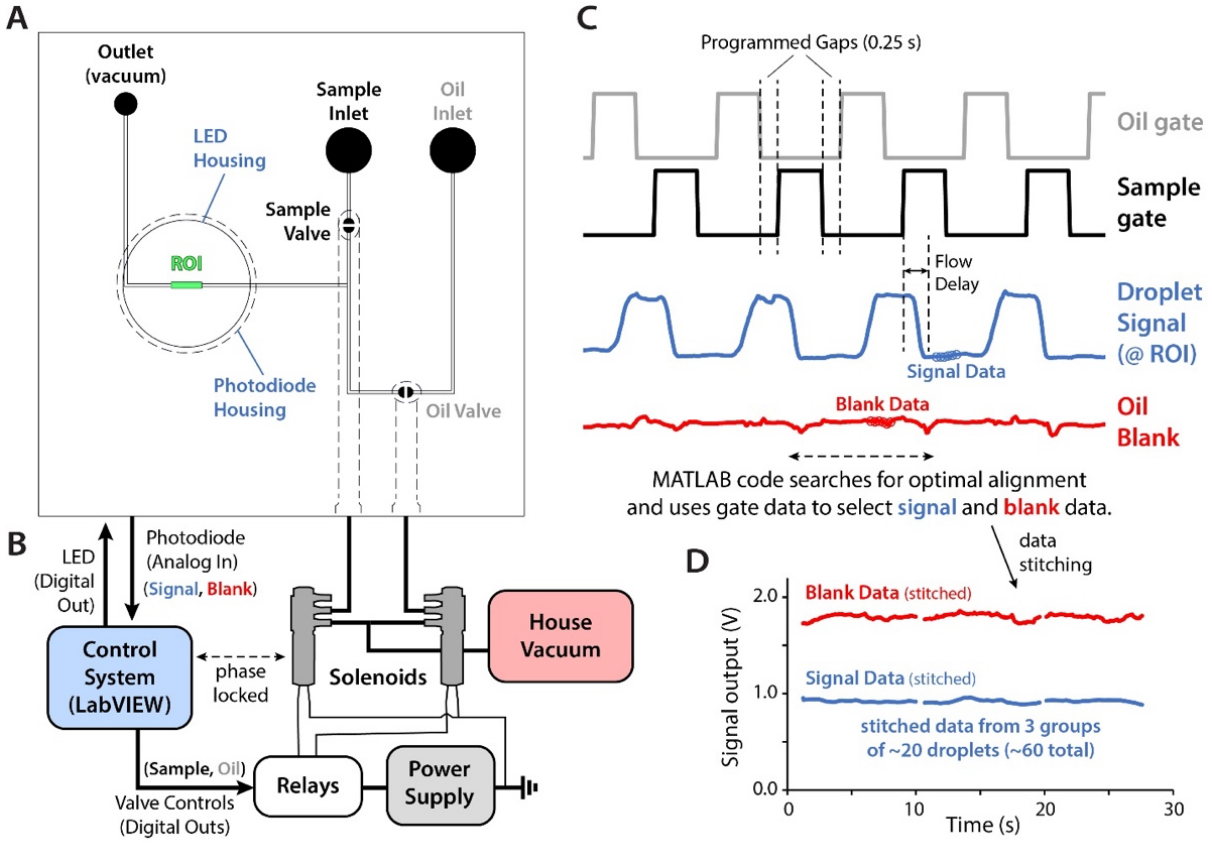

Figure 2.5 Lock-in operation of the μChopper device and low-cost instrumentation. (A) Schematic of the microdevice with 3D-printed photodiode (PD) and LED housing, featuring sample and oil inputs, a vacuum output, and pneumatic control lines. (B) Interfacing setup with control system, PD, LED, and solenoids for valve control. (C) Example data showing gate control and PD analogue input, realigned to correct flow delay using MATLAB. (D) Stitched droplet signal data demonstrating aligned and processed results. Adapted with permission from reference #138.

2.2 Objective

Polydimethylsiloxane (PDMS) is the most common substrate in microfluidic device fabrications due to its chemical inertness, non-toxicity, non-flammability as analyte container, and for

possessing the transparency required for unimpaired optical detections[8, 16]. Nevertheless, incorporation of microchannel into PDMS can be a complex, time-consuming, and laborious process that may require dedicated clean room facilities along with skilled technicians, especially in conventional photolithographic processes. With rapidly evolving high resolution 3D printing technologies, we can now directly print microfluidic features at tens of micrometer resolution. However, due to questionable biocompatibility and apparent opacity of the printed devices, bioanalytical systems still may prefer PDMS as the fluidic carrier material.

To date, casting PDMS on 3D-printed templates is complicated, multi-step process since uncured monomers present on a printed surface interfere with PDMS curing, resulting in uneven surface roughness [18, 28, 29]. Therefore, printed pieces have to undergo variety of surface coating, salinization and/or long term curing to get rid of the monomeric residues from the surfaces to be molded, often sacrificing the chemical compatibility and resolution of the final devices [18, 19, 30]. The key objective of this chapter is to develop a **simple and easy-to-reproduce process of making microfluidic devices from 3D-printed masters** (**Figure 2.6**) with and without integrated valves in direct 3D-printed substrates while also ensuring appropriate surface chemistry of the PDMS for uninterrupted production and automation of aqueous-in-oil droplets.

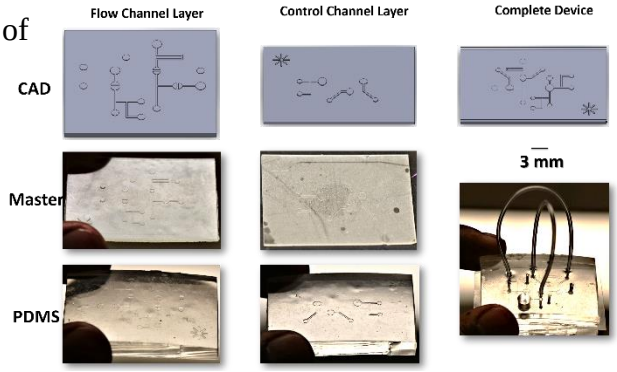

Figure 2.6. Microfluidic devices design and images of CAD layouts, 3D-printed masters and casted PDMS devices developed by the method proposed herein.

2.3 Materials and Methods

2.3.1 Computer-aided Design (CAD)

When designing microfluidic devices, choosing the right CAD software is crucial for precision and functionality. SOLIDWORKS is a powerful CAD software widely used for designing detailed and complex models across various engineering fields, including microfluidics. Its intuitive interface makes it accessible for both beginners and experienced designers, providing a wide range of tools and features that facilitate the creation of intricate designs. This ease of use is particularly beneficial in the precise and demanding field of microfluidics, where minute details and exact dimensions are crucial.

One of the key strengths of SOLIDWORKS is its capability for precision modeling. The software allows for exact control over dimensions, which is essential for designing microfluidic devices with features at the micrometer scale. Designers can create detailed 3D models that include all necessary components, such as channels, chambers, resistors, and valves, ensuring that every aspect of the device is accurately represented.

In addition to its modeling capabilities, SOLIDWORKS includes robust simulation tools that allow users to test fluid dynamics and other physical properties within the designed microfluidic device. These simulations are invaluable for optimizing the design before moving to the prototyping stage, as they help identify potential issues and refine the functionality of the device.

The software also supports parametric design, enabling designers to make easy modifications and iterations by adjusting parameters rather than starting from scratch. This flexibility is crucial in the iterative design process, allowing for quick adjustments and improvements.

2.3.1.1 Key SOLIDWORKS Features for Microfluidic Device Design

1. **Extrude Boss**: This feature is used to create the basic 3D structure of microfluidic channels by extruding a 2D sketch into a 3D form. It is essential for forming channel templates for PDMS molding, allowing for precise control over the height and shape of the channels.
2. **Extrude Cut**: This tool is critical for creating internal channels within a substrate. By cutting through a 3D model, designers can create complex internal fluid pathways, ensuring that channels are accurately placed and sized according to design specifications.
3. **Measurement Tools**: SOLIDWORKS offers a variety of measurement tools that allow designers to precisely measure and adjust the dimensions of channels and chambers. These tools ensure that all parts of the microfluidic device meet the required specifications and tolerances, which is crucial for device functionality.
4. **Assembly Feature**: This feature enables designers to assemble multiple layers of a microfluidic device virtually. It ensures proper alignment and fit between different layers, which is crucial when designing complex devices that consist of multiple assembled parts.
5. **Export Options**: SOLIDWORKS supports exporting designs in various formats, such as STL (Stereolithography) for 3D printing, converting the 3D model into a file readable by 3D printers, and AI (Adobe Illustrator) for creating detailed diagrams and graphics for documentation and presentations. These export options, among many others, facilitate both manufacturing and graphic documentation.

2.3.2 Fabrication of Pneumatic Control Layer

2.3.3 Development of Fluidic Flow Layer

All 3D structures discussed herein are designed using SOLIDWORKS. Fluidic circuit templates (**Figure 2.6**) are realized with extruded features of required height (~20-200 μm), width

(~50-500 μm), and length (~3-100 mm) on a thin (~1-2 mm) substrate. The complete design is converted and sliced into layers of desired thickness (layer-by-layer printing) to exploit the maximum additive resolution. As a standard protocol, we keep the printing layer thickness to half of the shallowest channel to be printed, i.e., 50 μm layers for a circuit containing 100 μm as the slightest depth. A digital light processing (DLP) 3D printer - Tiger XHD (Romanoff International, NY) or Photon Mono X (Anycubic, Shenzhen, China) - is used to photo-cure the entire design layer by layer. Depending on the number of layers to be printed, a template can be printed in ~5-15 minutes. The printed pieces are washed with isopropyl alcohol (IPA) for ~3-5 minutes, then air-dried and post-cured (405 nm) for 5 minutes to minimize uncured monomer residues and degrade excess curing agents, following the manufacturers' protocols.

2.3.3.1 3D-Printing Molds

2.3.3.2 Solvent Extraction

Cubic molds, 1 cm^3 in size, featuring channels of varying widths (100 μm, 250 μm, 500 μm) and depths (100 μm and 500 μm) were 3D printed and subjected to various solvent treatments, including methanol, ethanol, isopropanol, water, acetone, dimethylformamide (DMF), and a specialized acetone solution containing 1% Irgacure 819. Post-treatment, the molds were cast in PDMS and cured to assess the effectiveness of each solvent in facilitating successful PDMS curing.

2.3.3.3 PDMS Casting

Post printing, the molds were thoroughly rinsed with isopropyl alcohol (IPA), UV cured for five minutes, and then oven-baked for an hour to eliminate uncured monomers, as highlighted in Figure 4(a). The PDMS mixture, prepared from RTV 615 elastomer base and curing agent in a 10:1 ratio, was mixed, degassed, and poured onto the molds. The assembly was then oven-baked at 60°C for 60 minutes, ensuring complete curing. The final PDMS structures, incorporating precise channel designs, were then plasma-bonded to glass substrates for single-layer devices or to

each other for multilayer configurations, with the intricate channel details visible in **Figure 2.7**. This optimized process, supported by studies like those of Isiksacan et al. (2016) and Villegas et al. (2018), effectively overcomes PDMS curing challenges, facilitating the fabrication of high-fidelity microfluidic devices from 3D printed molds.

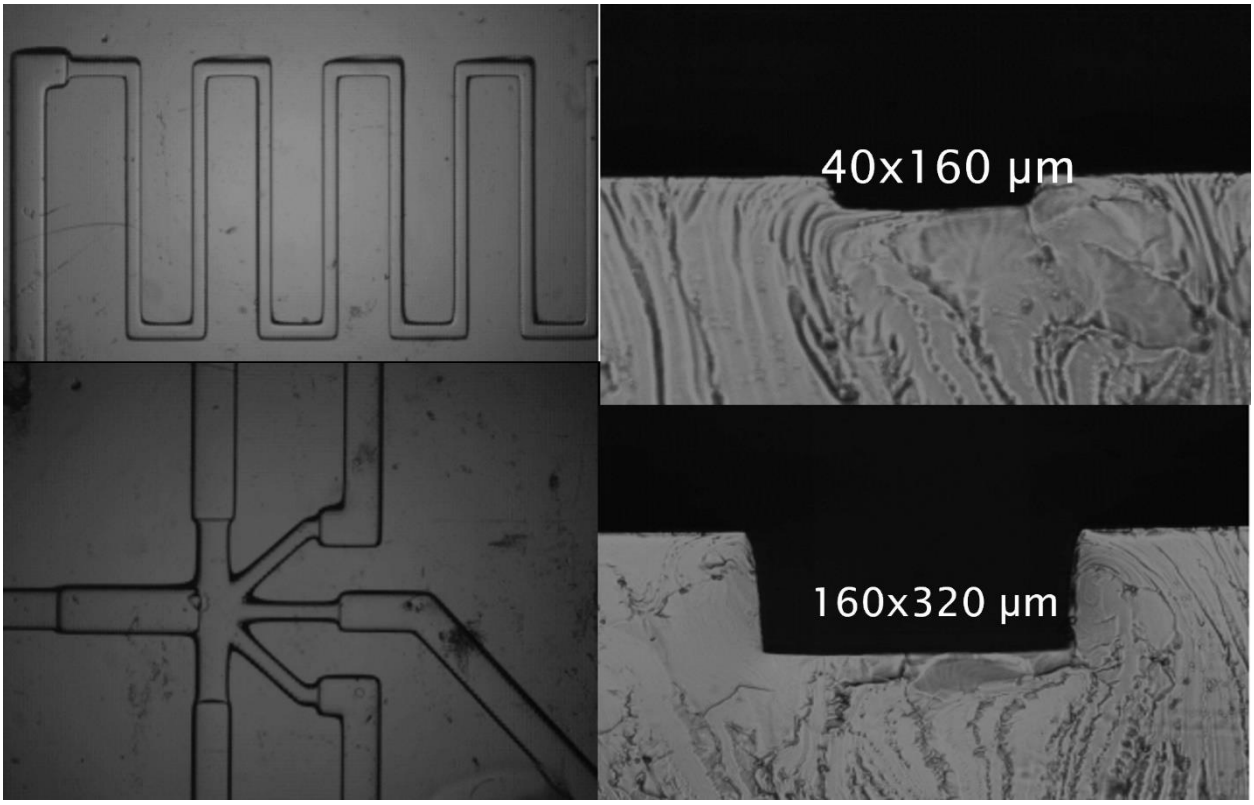

Figure 2.7 PDMS Microfluidic Structures from 3D-printed Templates

2.3.4 Computer Vision Techniques for Data Analysis

2.3.4.1 Surface Roughness Analysis Using Gaussian Filter and Sobel Edge Detection

The Sobel operator is a widely used edge detection method in image processing and computer vision. It is a discrete differentiation operator that computes an approximation of the gradient of the image intensity function. The operator consists of a pair of 3x3 convolution kernels, one for detecting changes in the horizontal direction (Sobel X) and one for detecting changes in the vertical direction (Sobel Y).

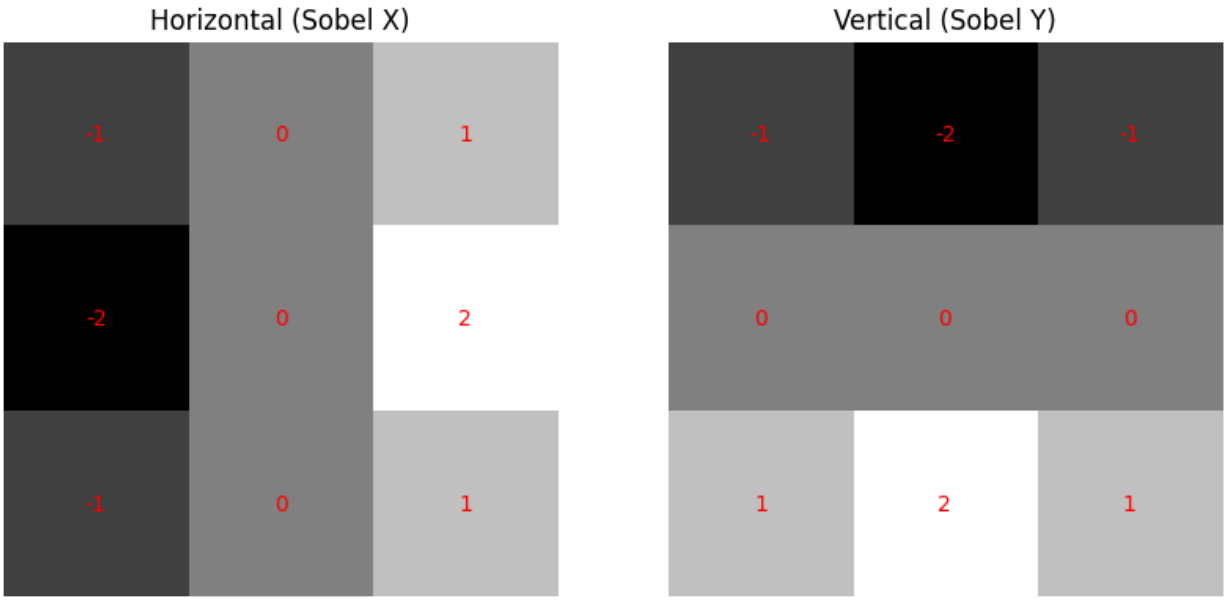

Figure 2.7 Visual representation of Sobel operators. The horizontal (Sobel X) operator detects horizontal edges by emphasizing changes in intensity along the horizontal axis, with kernel values ranging from -2 to 2. The vertical (Sobel Y) operator detects vertical edges by emphasizing changes in intensity along the vertical axis, also with kernel values ranging from -2 to 2.

Gaussian Filter Integration

To enhance the performance of the Sobel operator in detecting surface roughness, a Gaussian filter is applied to the image prior to the Sobel operation. The Gaussian filter smooths the image, reducing noise and minor variations that can create false edges. This preprocessing step helps to focus on significant edges and features in the image, leading to cleaner and more defined edge detection.

Sobel X Kernel

The Sobel X kernel emphasizes changes in intensity in the horizontal direction. The middle column (with zeros) means that the kernel does not change the central pixel's value directly but considers the differences in the adjacent pixels. The left and right columns (with -1 and 1) detect horizontal edges by subtracting the intensity values of the pixels on the left from those on the right. Additionally, the top and bottom rows have smaller weights (-1 and 1) compared to the middle row (-2 and 2) to give more weight to the central pixel's neighbors, which helps in better edge detection.

Sobel Y Kernel

The Sobel Y kernel emphasizes changes in intensity in the vertical direction. The middle row (with zeros) means that the kernel does not change the central pixel's value directly but considers the differences in the pixels above and below. The top and bottom rows (with -1 and 1) detect vertical edges by subtracting the intensity values of the pixels above from those below. The left and right columns have smaller weights (-1 and 1) compared to the middle column (-2 and 2) to give more weight to the central pixel's neighbors, which helps in better edge detection.

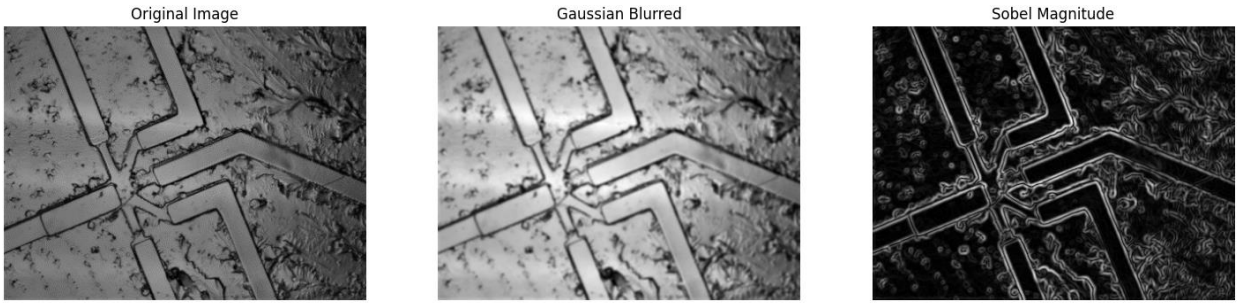

Figure 2.8 Surface roughness analysis of a microfluidic device image. The original image (left) is shown alongside a Gaussian-blurred version (middle), which reduces noise and minor variations. The Sobel magnitude image (right) highlights the edges detected after applying the Sobel operator, providing a clear view of surface roughness features.

Steps used for Edge Detection in Device Images

1. **Apply Gaussian Filter**: The image is first smoothed using a Gaussian filter to reduce noise and minor variations.
2. **Convolution with Sobel Kernels**: Each Sobel kernel (X and Y) is convolved with the smoothed image to produce two gradient images (G_x and G_y), which measure the rate of change of intensity in the horizontal and vertical directions, respectively.
3. **Calculate Gradient Magnitude**: The gradient magnitude at each pixel can be calculated using the formula:

$$G = \sqrt{Gx^2 + Gy^2}$$

Alternatively, an approximate magnitude can be computed as:

$$G \approx |Gx| + |Gy|$$

4. **Determine Gradient Direction**: The direction of the gradient can be calculated using:

$$\theta = \tan^{-1}\left(\frac{Gy}{Gx}\right)$$

2.3.4.2 Python Script for Flow Segment Detection using Computer Vision

This script provides an interactive way to define an ROI on a video, processes the frames within this ROI to detect droplets, measures their areas, and displays the results. The script loads a video file, allows the user to define a region of interest (ROI) interactively using the mouse, and then processes the frames within this ROI to detect and measure the area of droplets. The detected droplet areas are stored for further analysis.

Script Breakdown

Importing Libraries

```
1 import cv2
2 import numpy as np
```

The script imports the cv2 module for computer vision operations and the numpy module for numerical operations.

Loading the Video

```
video_path = 'path to you video file'
cap = cv2.VideoCapture(video_path)
```

The video file is loaded using cv2.VideoCapture, where video_path should be replaced with the actual path to your video file.

Initializing Variables

```
detected_droplets = []
roi_defined = False
roi = (0, 0, 0, 0)
drawing = False
```

The script initializes:

- detected_droplets: A list to store the areas of detected droplets.
- roi_defined: A boolean flag to indicate if the ROI has been defined.
- roi: A tuple to store the coordinates of the ROI.
- drawing: A boolean flag to indicate if the user is currently drawing the ROI.

Defining Mouse Callback for Drawing ROI

```
def detect_and_measure_droplet(roi_frame):
    gray = cv2.cvtColor(roi_frame, cv2.COLOR_BGR2GRAY)
    blurred = cv2.GaussianBlur(gray, (5, 5), 0)
    _, threshold = cv2.threshold(blurred, 127, 255, cv2.THRESH_BINARY_INV)

    # Morphological operations to remove small lines and noise
    kernel = cv2.getStructuringElement(cv2.MORPH_ELLIPSE, (5, 5))
    morphed = cv2.morphologyEx(threshold, cv2.MORPH_CLOSE, kernel)

    contours, _ = cv2.findContours(morphed, cv2.RETR_EXTERNAL, cv2.CHAIN_APPROX_SIMPLE)

    cv2.imshow('Threshold', threshold)  # Show thresholded image for debugging
    cv2.imshow('Morphed', morphed)  # Show morphed image for debugging

    if contours:
        for contour in contours:
            area = cv2.contourArea(contour)
            print(f"Detected contour with area: {area}")
            if area > 100:  # Minimum area to consider as a droplet
                return area, contour
    return None, None
```

```python
def draw_roi(event, x, y, flags, param):
    global roi, drawing, roi_defined

    if event == cv2.EVENT_LBUTTONDOWN:
        drawing = True
        roi = (x, y, x, y)

    elif event == cv2.EVENT_MOUSEMOVE:
        if drawing:
            roi = (roi[0], roi[1], x, y)

    elif event == cv2.EVENT_LBUTTONUP:
        drawing = False
        roi = (roi[0], roi[1], x, y)
        roi_defined = True
```

This function allows the user to draw a rectangular ROI on the video frame using the mouse:

- On left mouse button down (EVENT_LBUTTONDOWN), start drawing the ROI.
- On mouse move (EVENT_MOUSE-MOVE), update the ROI coordinates.
- On left mouse button up (EVENT_LBUTTONUP), finalize the ROI and set roi_defined to True.

Setting Up the Video Window and Mouse Callback

```python
cv2.namedWindow('Video')
cv2.setMouseCallback('Video', draw_roi)
```

Create a window named 'Video' and set the mouse callback to draw_roi.

Function to Detect and Measure Droplets

This function processes the ROI frame to detect and measure droplets:

- Converts the frame to grayscale and applies Gaussian blur.
- Applies binary thresholding to create a binary image.
- Uses morphological operations to remove noise.
- Finds contours in the processed image.
- Returns the area and contour of the detected droplet if its area is greater than 100 pixels.

Processing Video Frames

```
while cap.isOpened():
    ret, frame = cap.read()
    if not ret:
        break

    # Draw the ROI rectangle on the frame
    if drawing:
        cv2.rectangle(frame, (roi[0], roi[1]), (roi[2], roi[3]), (255, 0, 0), 2)
    elif roi_defined:
        cv2.rectangle(frame, (roi[0], roi[1]), (roi[2], roi[3]), (0, 255, 0), 2)
        roi_frame = frame[roi[1]:roi[3], roi[0]:roi[2]]

        # Detect and measure droplet
        area, contour = detect_and_measure_droplet(roi_frame)
        if area:
            detected_droplets.append(area)

            # Draw the contour and area on the frame
            cv2.drawContours(roi_frame, [contour], -1, (0, 255, 0), 2)
            cv2.putText(frame, f'Area: {area:.2f}', (roi[0], roi[1] - 10), cv2.FONT_HERSHEY_SIMPLEX, 0.5, (0, 255, 0), 2)

            # Show the frame with detected droplet
            cv2.imshow('Droplet Detection', frame)
            cv2.waitKey(0)  # Pause until a key is pressed to continue

    # Show the frame
    cv2.imshow('Video', frame)

    # Handle keyboard inputs for quitting
    key = cv2.waitKey(1) & 0xFF
    if key == ord('q'):
        break

cap.release()
cv2.destroyAllWindows()
```

This loop processes each frame of the video:

- Reads a frame from the video.
- Draws the ROI rectangle on the frame (blue while drawing, green when defined).
- If the ROI is defined, processes the ROI frame to detect and measure droplets.
- If a droplet is detected, draws the contour and area on the frame.
- Displays the frames and handles the 'q' key to quit the loop.

Outputting the Detected Droplet Areas

```
print("Detected droplet areas:", detected_droplets)
```

After the video processing is complete, the script prints the detected droplet areas.

(Special acknowledgement: *The author would like to extend heartfelt thanks to ChatGPT for the invaluable support provided throughout the development of Chapter 2. The assistance in translating complex thoughts into coherent and precise text was instrumental in clearly conveying the complex ideas and concepts discussed in this chapter.*

Furthermore, ChatGPT's help in writing and refining data analysis codes in Python greatly enhanced the efficiency and accuracy of the analyses conducted. The ability to quickly generate and troubleshoot code was essential for the successful completion of this chapter.

The author acknowledges ChatGPT for its indispensable support and contributions, which have been crucial in the successful completion of this project.)

2.3.5 Fabrication of normally closed (NC) valves

Both the top and bottom layers of the device are molded into PDMS from 3D printed templates. The bottom layer is designed to contain valve chambers and control channels, while the top layer comprises the flow channels. Each PDMS surface to be bonded is subjected to plasma oxidation, necessary for achieving a strong and permanent bond between the layers. However, it is essential to prevent plasma exposure to the closure regions of the flow channels. These areas must remain non-oxidized to allow the deflection of the thin membrane when a vacuum is applied to the control chamber beneath. To effectively shield these closure regions during plasma treatment, regions, thus blocking plasma exposure during the oxidation process.

Once all the PDMS layers are plasma bonded, the final device is placed in the oven for a specific period to ensure better sealing and to restore hydrophobicity, as described in Section C1.3.6. However, this additional baking step can cause the protected portions to stick together, resulting in the permanent closure of the valves. To prevent this, a thin PDMS layer undergoes a necessary washing and drying process. This in-house developed method involves sonication in 95% acetone for 15 minutes, followed by drying at 60°C for another 15 minutes. This process is repeated 3-4 times before the plasma oxidation step. This extraction aims to remove excess monomers from the thin

layer's surface, thereby minimizing the risk of plasma-inhibited portions sealing together during baking.

Following the fabrication process, a post-treatment step is implemented to modify the surface properties of the microfluidic device. The plasma oxidation technique initially used in the fabrication process imparts hydrophilicity to the PDMS surfaces. However, for applications

involving aqueous-in-oil droplet formation, it is imperative to revert these surfaces to a hydrophobic state. To achieve this, Aquapel, a fluorinated compound typically employed for rain repellent treatments on glass, is utilized. This compound effectively treats hydrophobic PDMS surfaces, presumably forming a chemical bond with the surface molecules and/or the excess oxide

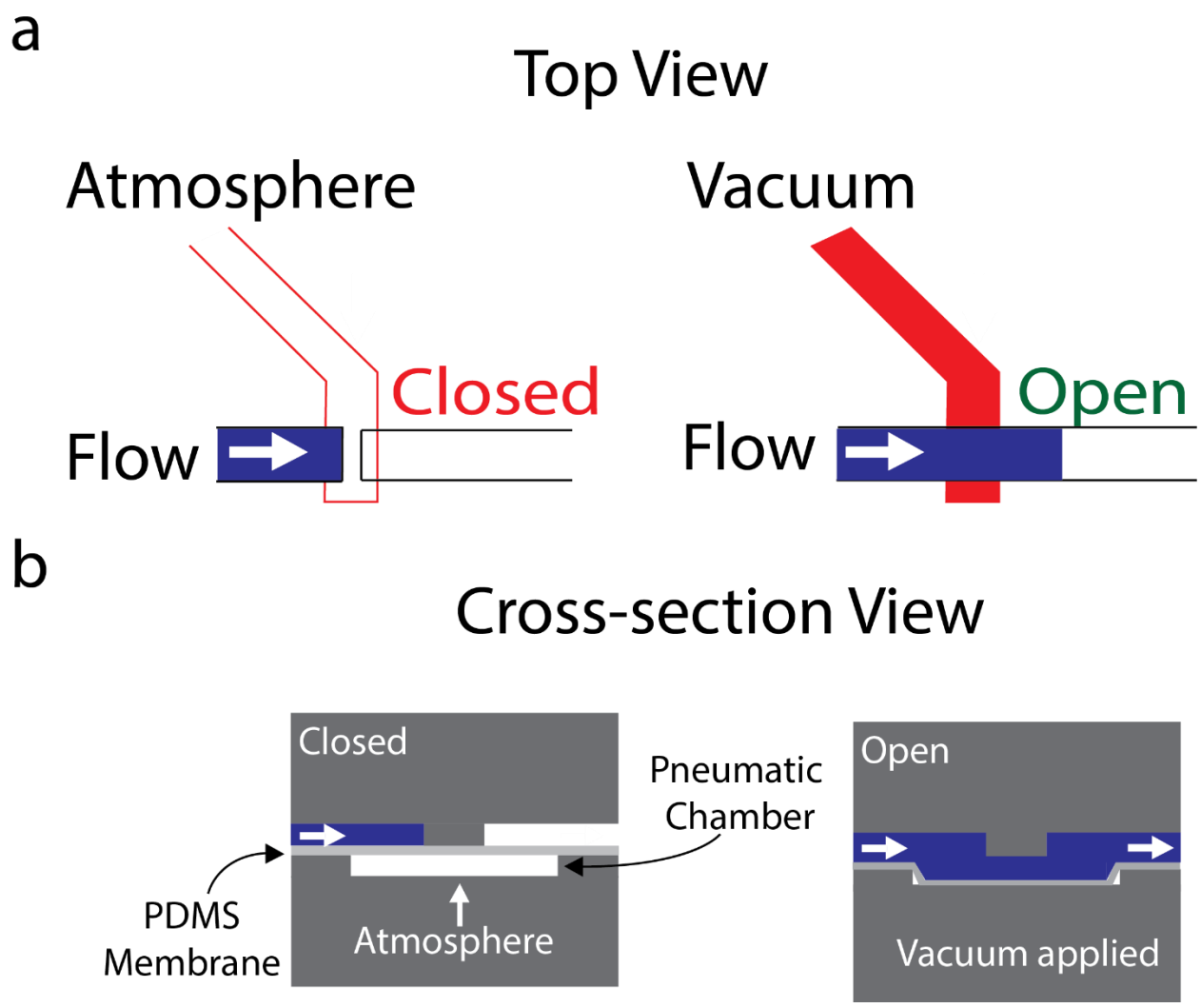

Figure 2.9 Schematic of normally closed membrane valve operation. (a) Top view: Valve is closed under atmospheric pressure and open under vacuum. (b) Cross-sectional view: The PDMS membrane blocks flow when closed and allows flow when vacuum pulls the membrane into the pneumatic chamber.

ions. The result is a surface that repels aqueous flows, thereby facilitating the formation of well-defined droplets.

The solution is first introduced into the oil reservoir. Subsequently, the oil valve is opened while ensuring that the aqueous valves remain closed. As the outlet vacuum is applied, the Aquapel flows exclusively through the oil channel. This selective passage ensures that only the necessary regions of the device retrieve their hydrophobic properties. This strategic application of Aquapel is pivotal in restoring the hydrophobicity of the PDMS surfaces, a key factor in the successful operation of microfluidic devices designed for droplet-based applications.

2.4 Results and Discussion

2.4.1 3D-Printing Parameters

Two different brands of 3D printers have been used throughout the course of this dissertation, Tiger XHD from Romanoff international and multiple versions (4K, 6K and 8K resolution) of Anycubic Photon and Primo series from Anycubic China. The initial PDMS curing on 3D templates project started with the Tiger XHD printer which had a maximum z resolution of 10 micrometer and xy resolution of 30 micrometers.

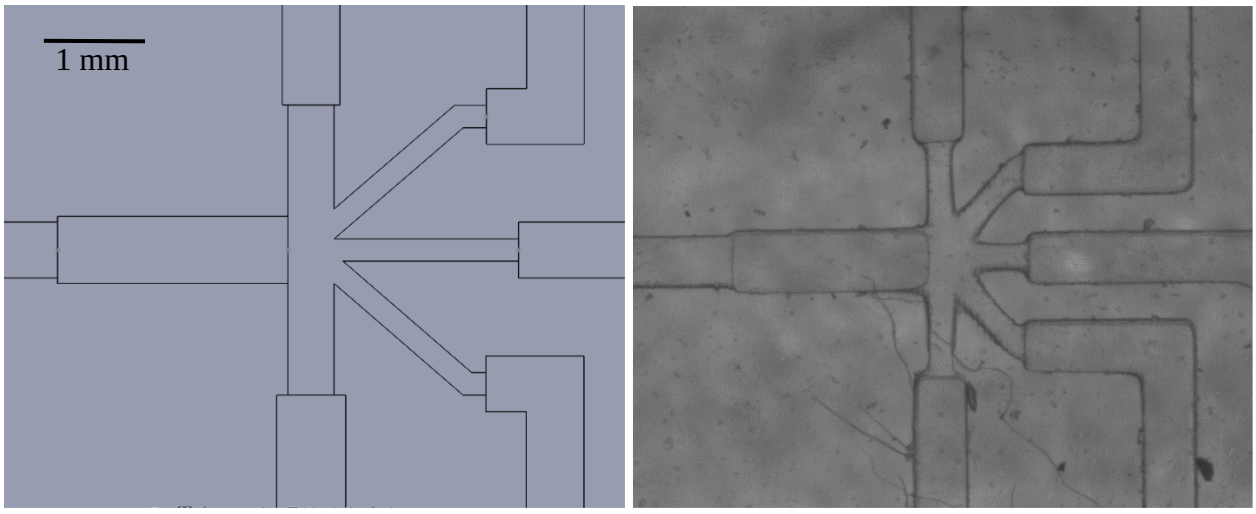

Figure 2.10 CAD schematic (a) and microscopic image (b) of a printed master microstructure. The depicted microfluidic circuit features channels with varying heights and widths, ranging from 20 µm to 200 µm.

2.4.2 Post-Print Solvent Extraction

The experiment assessing the effectiveness of various solvents (isopropyl alcohol, IPA; acetone; and ethanol) for cleaning 3D printed templates for PDMS casting showed distinct outcomes. IPA-treated templates resulted in the smoothest PDMS castings when acetone and ethanol treatments led to distorted channels in the PDMS castings, as evidenced in Figure X. IPA, with a dielectric constant of about 18 and a dipole moment of 1.66 Debye units, is classified as a medium-polarity solvent. This moderate polarity suggests a less aggressive interaction with the polymer network of resins, likely contributing to its effectiveness in cleaning without significant disruption to the resin structure. This is in line with the smooth PDMS castings observed from IPA-treated templates. In contrast, acetone (dielectric constant around 20.7) and ethanol (dielectric constant around 24) are more polar than IPA. This higher polarity can lead to more aggressive interactions with resin components, potentially causing swelling, partial dissolution, or structural alterations. Such interactions likely contributed to the distortions in PDMS castings seen with these solvents.

Given the known effects of solvents on various materials, the stronger solvency power and

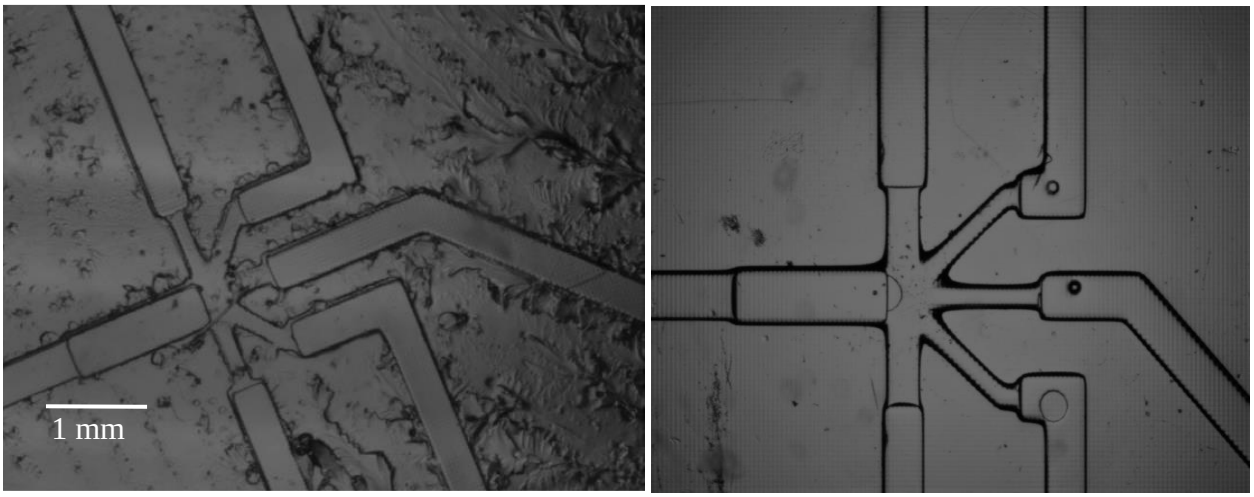

Figure 2.11 Microscopic images of PDMS surfaces cast on (a) an incompletely cured 3D-printed master and (b) a completely cured 3D-printed master.

higher volatility of acetone, and to a lesser extent, ethanol, can result

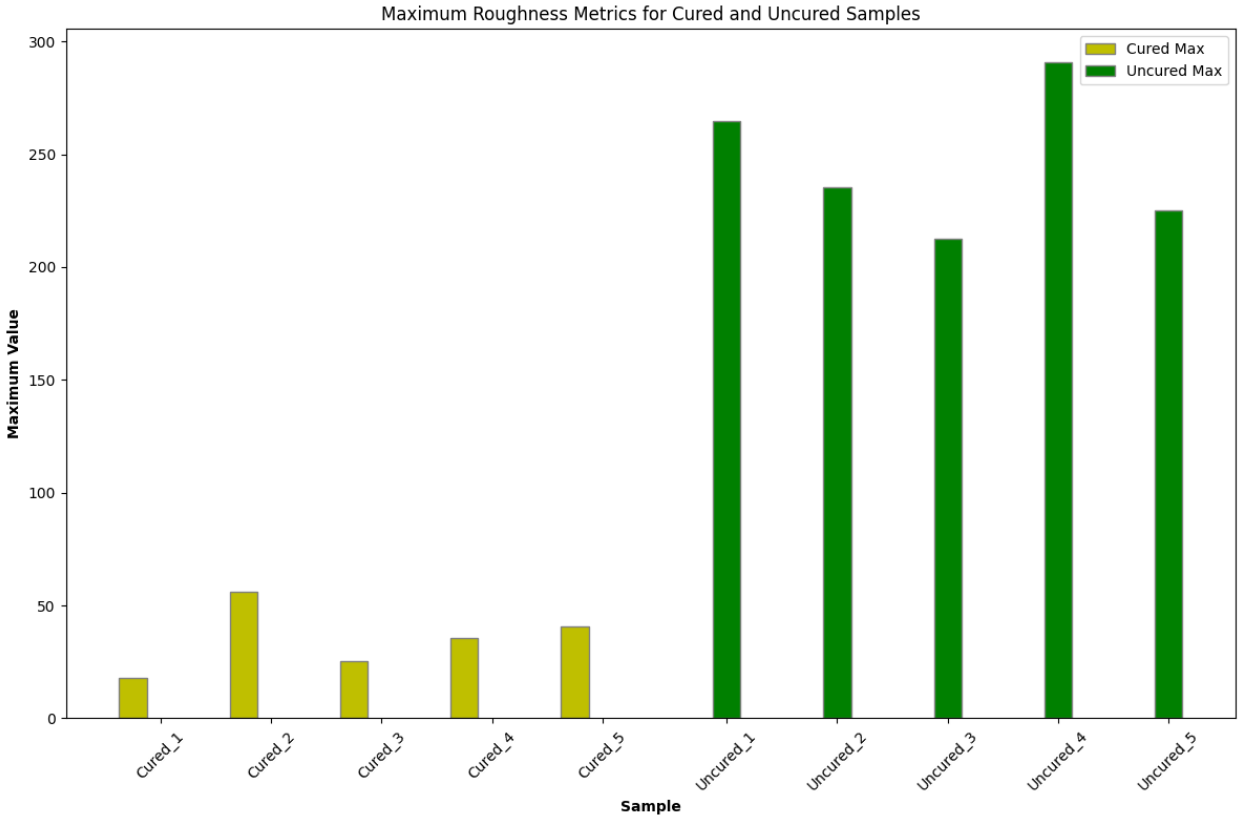

Figure 2.12 Maximum Roughness Metrics for Cured and Uncured Samples

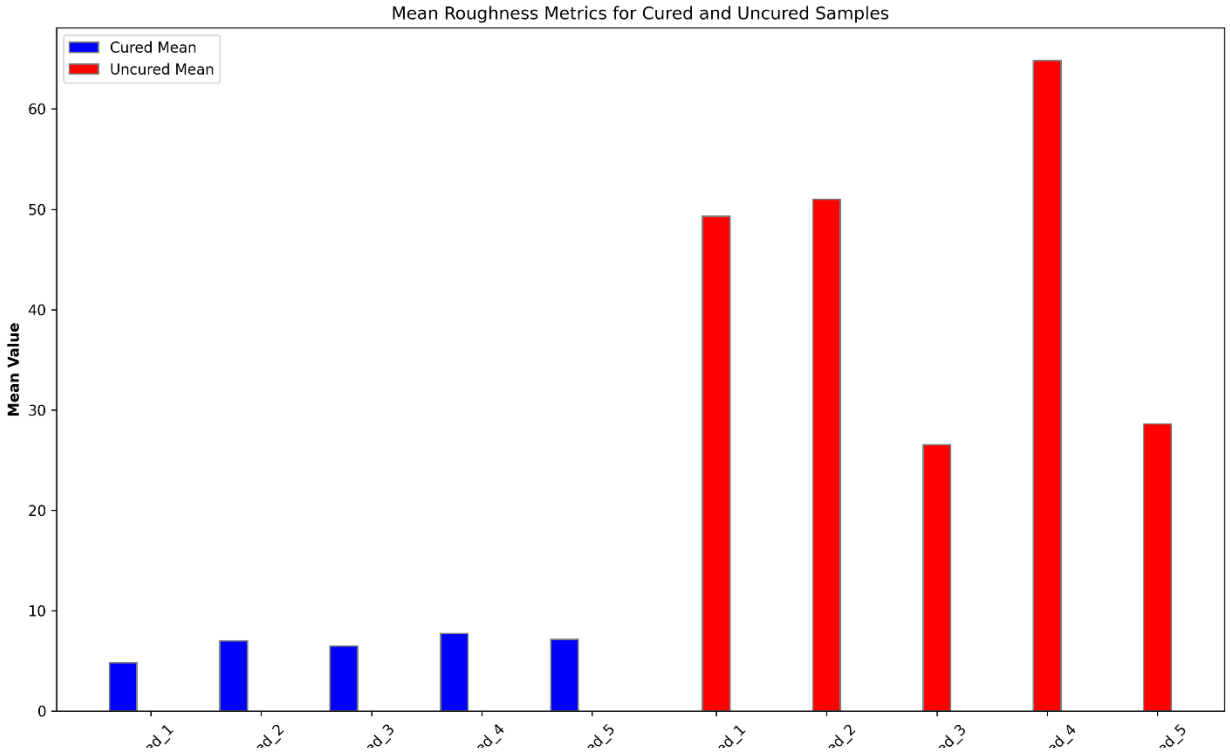

Figure 2.13 Mean Roughness Metrics for Cured and Uncured Samples

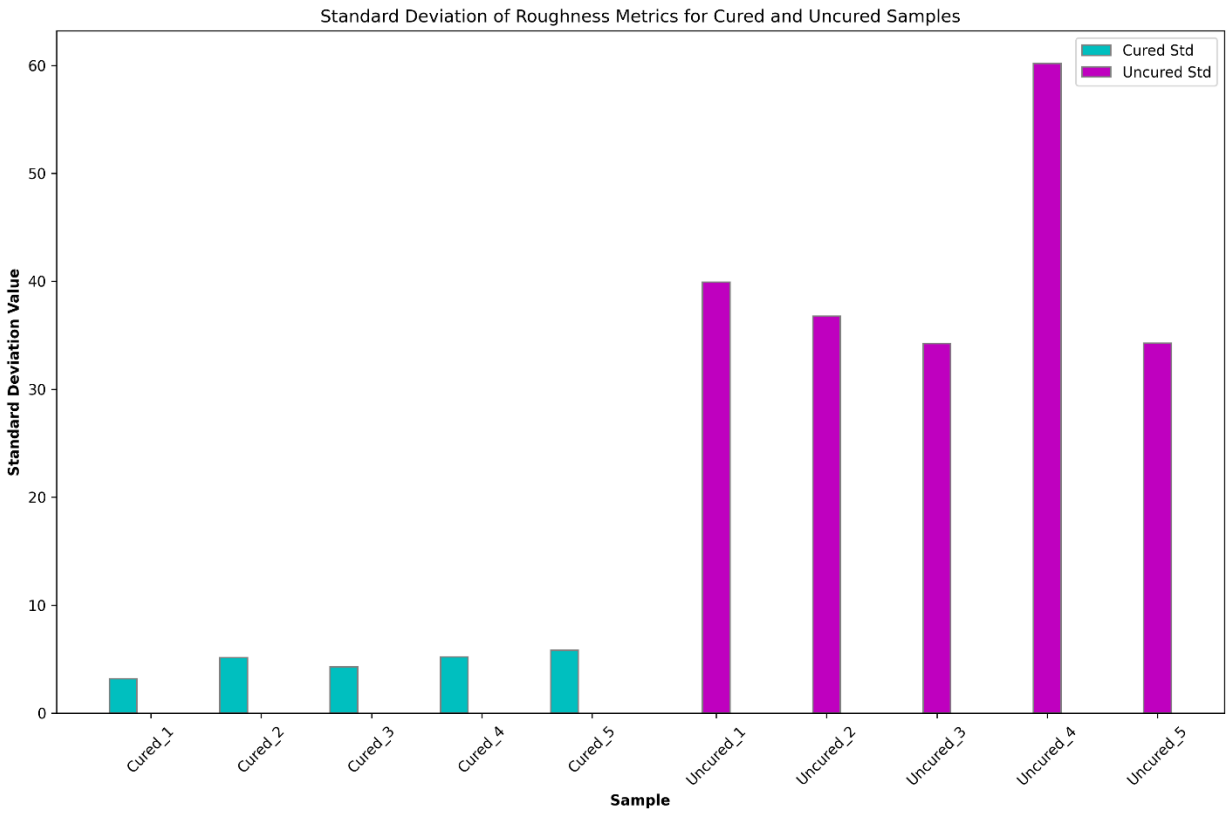

2.14 Standard Deviation Metrics for Cured and Uncured Samples

in more pronounced changes in resin properties. This is evidenced by the negative impact on the integrity of fine features in the 3D printed templates. IPA's balanced volatility and moderate solvent strength minimize the risk of uneven drying, residue formation, and excessive interaction with resin materials, crucial for preserving detailed features in the templates.

The bar charts on **Figure 2.12-2.14** compares the maximum, mean and standard roughness values for cured and uncured PDMS surfaces. The cured samples exhibit significantly lower roughness values compared to the uncured samples for all three data types, highlighting the effectiveness of the curing process in reducing surface roughness. This distinction between cured and uncured samples is evident, with cured samples showing maximum roughness values well below 60, whereas uncured samples have values exceeding 200.

2.4.3 PDMS Curing on 3D prints

Throughout the series of experiments, various outcomes were observed in the quality of PDMS casting from the 3D printed templates. In the initial attempts, the PDMS surface exhibited roughness near many channels, potentially impacting the fluid flow within these channels. Despite redesigning the device and altering post-processing conditions, the roughness persisted, although it was reduced. A significant improvement was noted when the washing with IPA was extended to 2 minutes and UV curing was increased to 600 seconds. The PDMS surface achieved near-perfect smoothness, indicating a successful resolution of the initial issues. Repeated use of the device showed consistent quality in PDMS surfaces. Interestingly, similar results were obtained even without the IPA treatment in repeat experiments. When the device was placed under the PDMS, following extended IPA treatment and longer UV curing, there was a slight unevenness at some points, but the overall result was successful. The adjustment of layer thickness and curing time was crucial for accurate printing of detailed structures like microchannels. The initial issues with horizontal channels indicated a balance needed between resolution and structural integrity, which was achieved with the optimal curing time.

The initial roughness of the PDMS casts suggested that the standard cleaning and curing procedures were insufficient, particularly for intricate designs. Extending the IPA wash and UV curing time significantly improved the surface quality, suggesting that residual uncured resin or insufficient curing was a major contributor to the initial problems. The sonication step in IPA likely aided in more thoroughly cleaning the intricate channels and surfaces of the printed device.

The ability to use the device multiple times without significant degradation in quality underscores the robustness of the optimized process. The similarity in results with and without IPA treatment in repeated uses suggests that initial thorough cleaning and curing might have long-lasting effects on the template's surface quality.

The experiments with different placements of the device in relation to the PDMS layer indicate that oxygen exposure, as hypothesized, might play a role in the curing process and the interaction between the resin and PDMS. However, this aspect requires further investigation to understand the underlying mechanisms.

Overall, the experiments demonstrated that fine-tuning both the 3D printing parameters and the post-processing techniques is essential for achieving high-quality PDMS casts. The results also open avenues for further research, particularly in understanding the chemistry of resin-PDMS interactions and the role of oxygen in the curing process.

2.4.3.1 Curing Behaviors of RTV 615 and Sylgard 184 PDMS

Two of the most used commercially available PDMS precursors in the development of microelectromechanical systems (MEMS), RTV 615 from Momentive Chemical and Sylgard 184 from Dow Corning, were tested for curing on 3D-printed templates.

Our experiments, alongside previous studies, suggest a faster curing time for RTV 615 compared to Sylgard 184. Our observations indicated that RTV 615 achieved satisfactory curing within 30 minutes to 1 hour, while Sylgard 184 required significantly longer curing times. The extended curing time for Sylgard 184 often resulted in uneven edges, attributed to interruptions from the 3D-printing materials, which posed challenges for achieving complete fluid sealing.

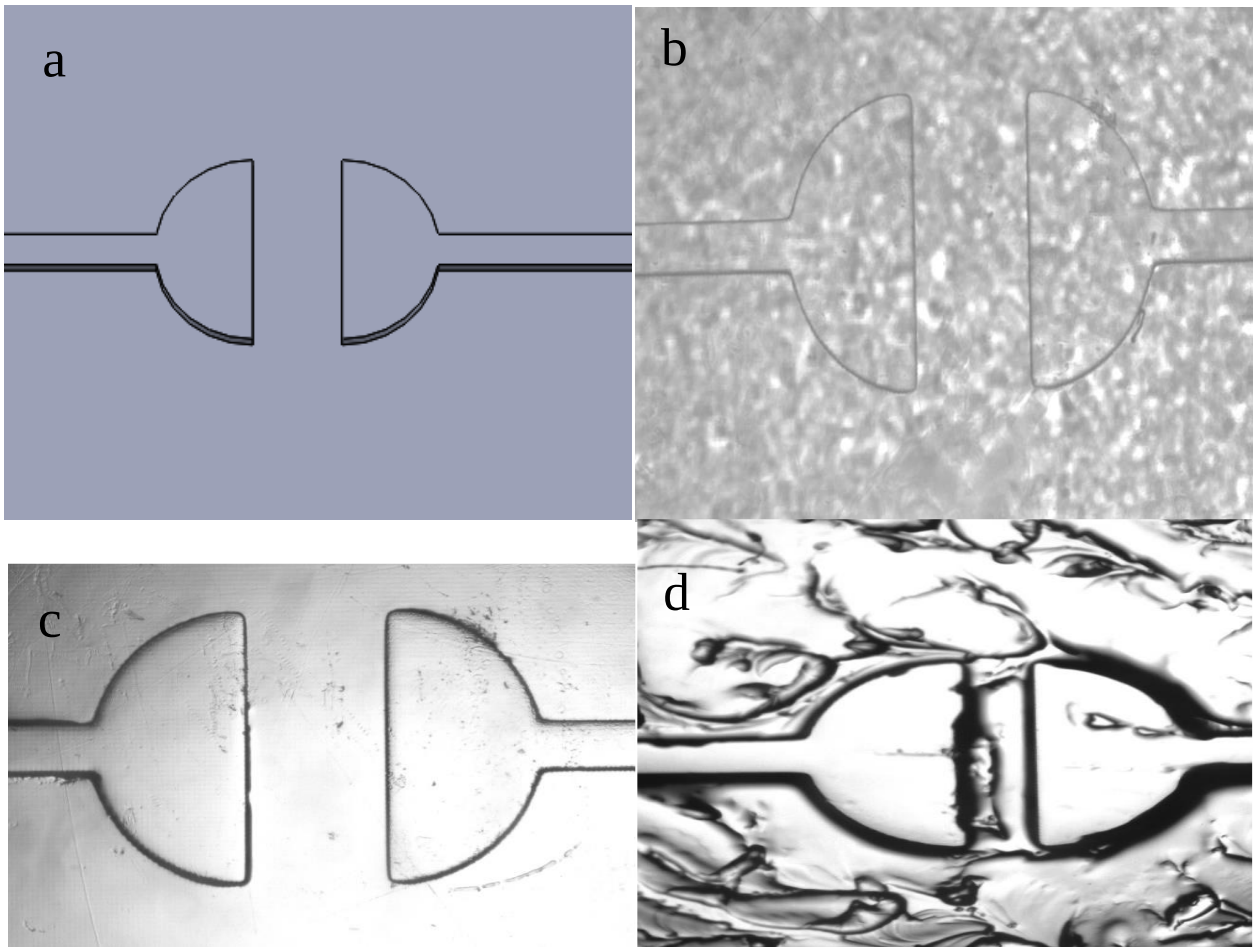

Figure 2.15 (a) CAD file of a microstructure with a height of 100 µm and a width of 300 µm. (b) Microscopic image of the 3D printed master. (c) Well-cured PDMS surface peeled off the master molded with RTV 615. (d) Premature PDMS surface peeled off the master molded with Sylgard 184.

As depicted in Figure 4, the differences in surface quality between the two PDMS types are evident. The CAD file (Figure 2.15a) of the microstructure designed with a height of 100 µm and a width of 300 µm serves as a reference. The microscopic image of the 3D printed master (Figure 2.15b) demonstrates the template used for PDMS curing. The cured PDMS surface using RTV 615 (Figure 2.15c) showed a smooth and uniform texture, indicating effective curing and minimal interference from the 3D-printed materials. In contrast, the PDMS surface cured using Sylgard 184 (Figure 2.15d) exhibited roughness and irregularities, confirming the challenges associated with its longer curing time and higher susceptibility to curing interruptions.

This observation aligns with the findings reported by Schneider et al. (2008), who noted that higher temperatures and extended curing times impact Sylgard 184 more significantly than RTV 615. Despite RTV 615's higher viscosity (4300 mPa·s) compared to Sylgard 184 (3900 mPa·s), which would theoretically suggest slower curing for RTV 615, the actual results contradicted this assumption. The elastic modulus of Sylgard 184 increased by 31% with prolonged and high-temperature curing, compared to only a 14% increase for RTV 615. This indicates that RTV 615 is better optimized for faster and lower temperature curing processes.

2.4.4 Passive microfluidic flow control

2.4.4.1 Microfluidic Circuit Design and Testing

To evaluate the feasibility of microfluidic circuits created with our 3D-printing capabilities, we designed five distinct microfluidic circuits, each with varying dimensions. These designs were theoretically predicted to exhibit a sevenfold increase in resistance for each subsequent variation, as detailed in Table 2. The aim was to systematically investigate how the dimensional changes impact the resistance and flow rate within the microfluidic channels.

Following the flow rate measurements, we applied the corresponding theoretical formulas to compute the actual resistance of each microfluidic device. These calculations allowed us to compare the experimental resistance values with the theoretical predictions.

Table 2 Dimensions and performance metrics of 3D-printed microfluidic circuits.

Circuit ID	Width (mm)	Height (mm)	Length (mm)	Resistance/R (kPa.s/mm^3)	Flow rate, Q (mm^3/s^1)	Ratio
191031_1	0.1	0.02	20.5	355.35	0.20	
191031_2	0.1	0.04	20	50.63	1.38	7.018
191031_3	0.1	0.06	8	7.22	9.70	7.016
191031_4	0.2	0.08	6.5	1.02	68.06	7.017
191031_5	0.2	0.1	1.65	0.14	479.55	7.046

2.4.5 Active microfluidic flow control

In this section, we discuss the experimental outcomes of implementing active microfluidic flow control using normally closed valves (NCVs). Our investigation focuses on how these valves can precisely regulate single-phase and multi-phase flows within microfluidic systems. The data presented showcases the performance and capabilities of these valves in achieving controlled fluid manipulation, essential for applications such as chemical synthesis, biomedical diagnostics, and analytical chemistry.

The experiments highlight the ability of NCVs to modulate flow rates and droplet volumes with high precision. By controlling the valve actuation time, we achieved variable droplet sizes, demonstrating the system's versatility in applications requiring precise dosing and mixing of reagents. The results underscore the importance of valve actuation timing in determining droplet characteristics, with shorter actuation times yielding smaller droplets and longer times producing larger droplets.

Additionally, the data reveal the dynamic response of the NCVs to external control signals, enabling real-time adjustments in fluid flow. This responsiveness is critical for applications that require rapid changes in flow conditions, such as in lab-on-a-chip devices used for diagnostic assays. The ability to swiftly open and close the valves allows for the precise control of fluid segmentation, which is particularly useful in the creation of segmented flow systems where multiple phases need to be carefully separated or mixed.

The findings also demonstrate the effective integration of NCVs in controlling complex flow patterns, such as multi-phase flows, where different fluids need to be managed simultaneously without cross-contamination. The NCVs' role in preventing backflow and maintaining the integrity of each fluid segment is crucial for the accuracy and reliability of the system.

In summary, the results presented in this section confirm the efficacy of NCVs in active microfluidic flow control, providing a robust solution for various high-precision applications. The successful implementation of these valves in our experiments paves the way for further advancements in microfluidic device design and functionality, particularly in areas requiring meticulous fluid handling and control.

2.4.5.1 Microfluidic normally closed valve (NCV)

Figure 2.17 presents two key plots highlighting the relationship between fluidic parameters in a microfluidic system controlled by a Normally Closed Valve (NCV). The first plot illustrates the correlation between frequency (Hz) and flow rate (nL/s), showing a positive linear relationship. As the frequency increases, the flow rate also rises linearly, indicating that the NCV can precisely control the flow rate by modulating the frequency. This relationship is crucial for applications requiring consistent and adjustable flow rates.

The second plot demonstrates the relationship between 1/frequency (Time in seconds) and volume per pulse (nL). This plot also exhibits a strong linear correlation, indicating that the volume of fluid dispensed per pulse can be accurately controlled by adjusting the frequency. The linear fit and corresponding R^2 values in both plots confirm the robustness of these relationships, showcasing the NCV's effectiveness in delivering precise fluid control.

These findings are significant for applications that demand fine-tuned fluid management, such as in chemical synthesis or biological assays. The ability to control flow rate and volume per pulse with high accuracy makes NCVs an invaluable component in the design of advanced microfluidic systems, where precise fluid handling is critical. The linearity observed in both relationships underscores the reliability and consistency of NCV-based flow control in microfluidic devices.

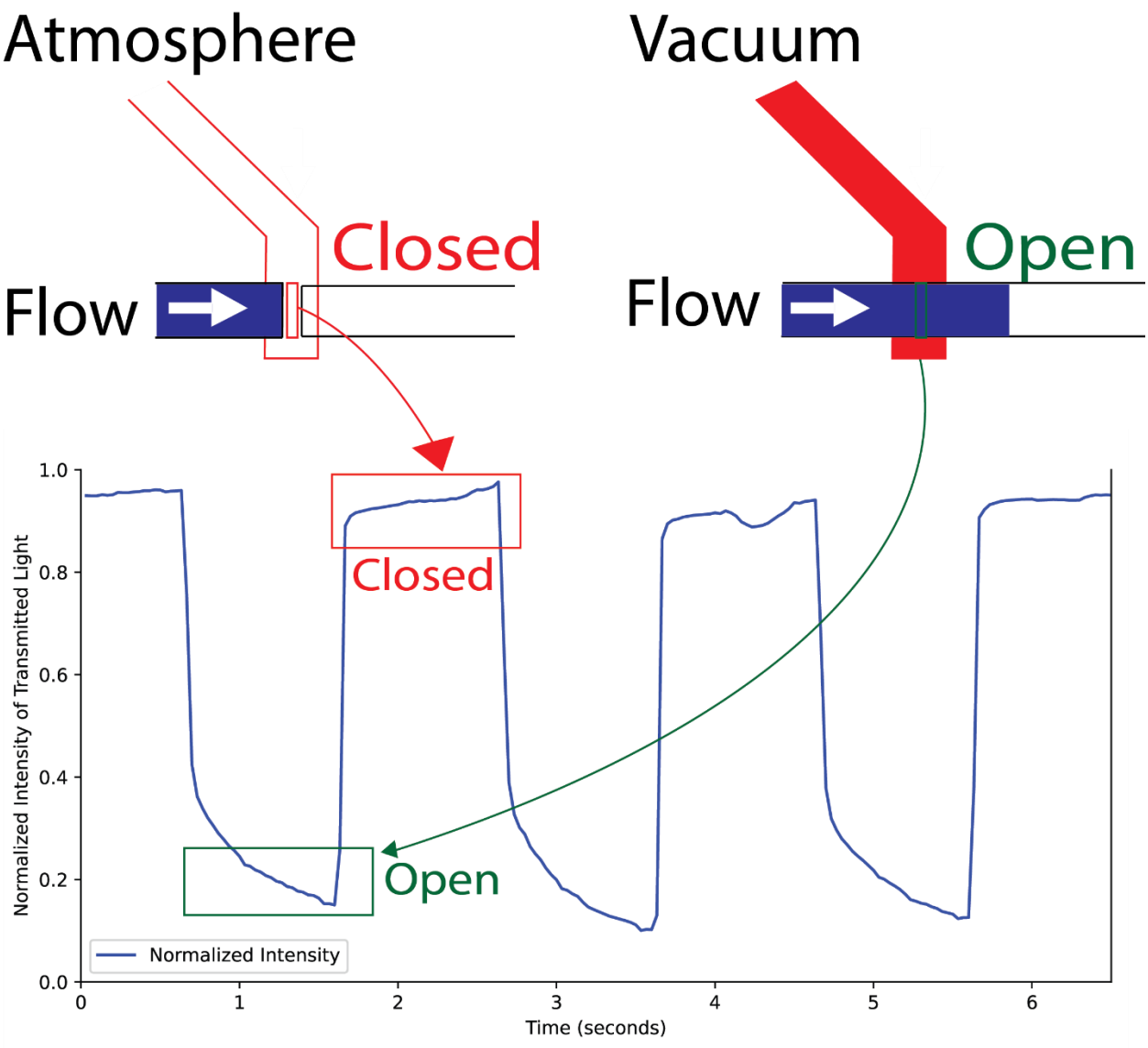

Figure 2.16 Time-lapsed actuation of a normally closed valve. The upper diagrams illustrate the valve's closed (red) and open (green) states. The lower graph shows the normalized intensity of transmitted light over time, correlating with the valve's open and closed states. The intensity is high when the valve is closed and low when the valve is open.

2.4.5.1.1 NCV-controlled single-phase flow

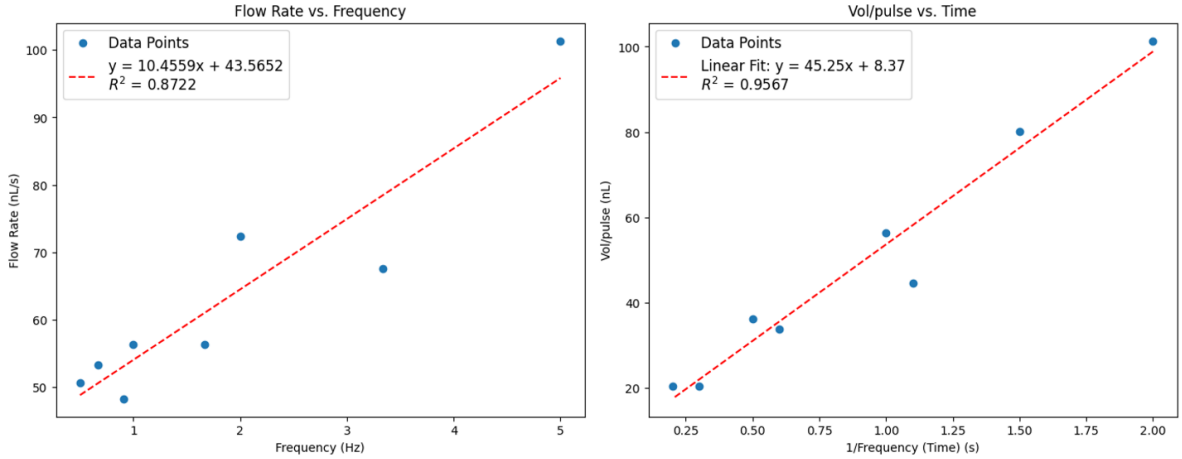

Figure 2.17 The left plot shows the correlation between frequency (Hz) and flow rate (nL/s), highlighting a positive linear relationship. The right plot illustrates the relationship between 1/frequency (Time in seconds) and volume per pulse (nL), also demonstrating a strong linear correlation. The fitted lines and R^2 values indicate the strength and accuracy of these relationships.

2.4.5.1.2 NCV-controlled multi-phase segmented flow

Figure 2.18 illustrates the relationship between droplet detection and valve actuation in a microfluidic system using a Normally Closed Valve (NCV). The x-axis shows time in seconds, while the y-axis represents the normalized intensity and valve actuation status. The plot reveals that droplet detection occurs immediately after the valve is opened, as indicated by the sharp decrease in intensity at the Region of Interest (ROI). The blue line represents the normalized intensity, showing a drop when the valve, initially closed, opens and allows the droplet to pass through. The orange dashed line shows the valve's actuation state, with the transition from closed to open state preceding the detection of the droplet.

The slight delay between the valve opening and the detection of the droplet can be attributed to several factors, including the physical response time of the valve, the system's electronic control lag, the time required for the fluid to travel from the valve to the detection point at the ROI. This

delay may also be influenced by the system's control electronics and fluid dynamics within the microchannels.

Figure 2.19 demonstrates the control of droplet volume by varying the actuation time of a normally closed valve. The data show a clear correlation between the actuation time and the resultant droplet volume, indicating that precise timing control can effectively manipulate droplet size. For the shortest actuation time of 10 ms, the generated droplets are relatively small, with volumes clustered around lower values. As the actuation time increases, the volume of the droplets also

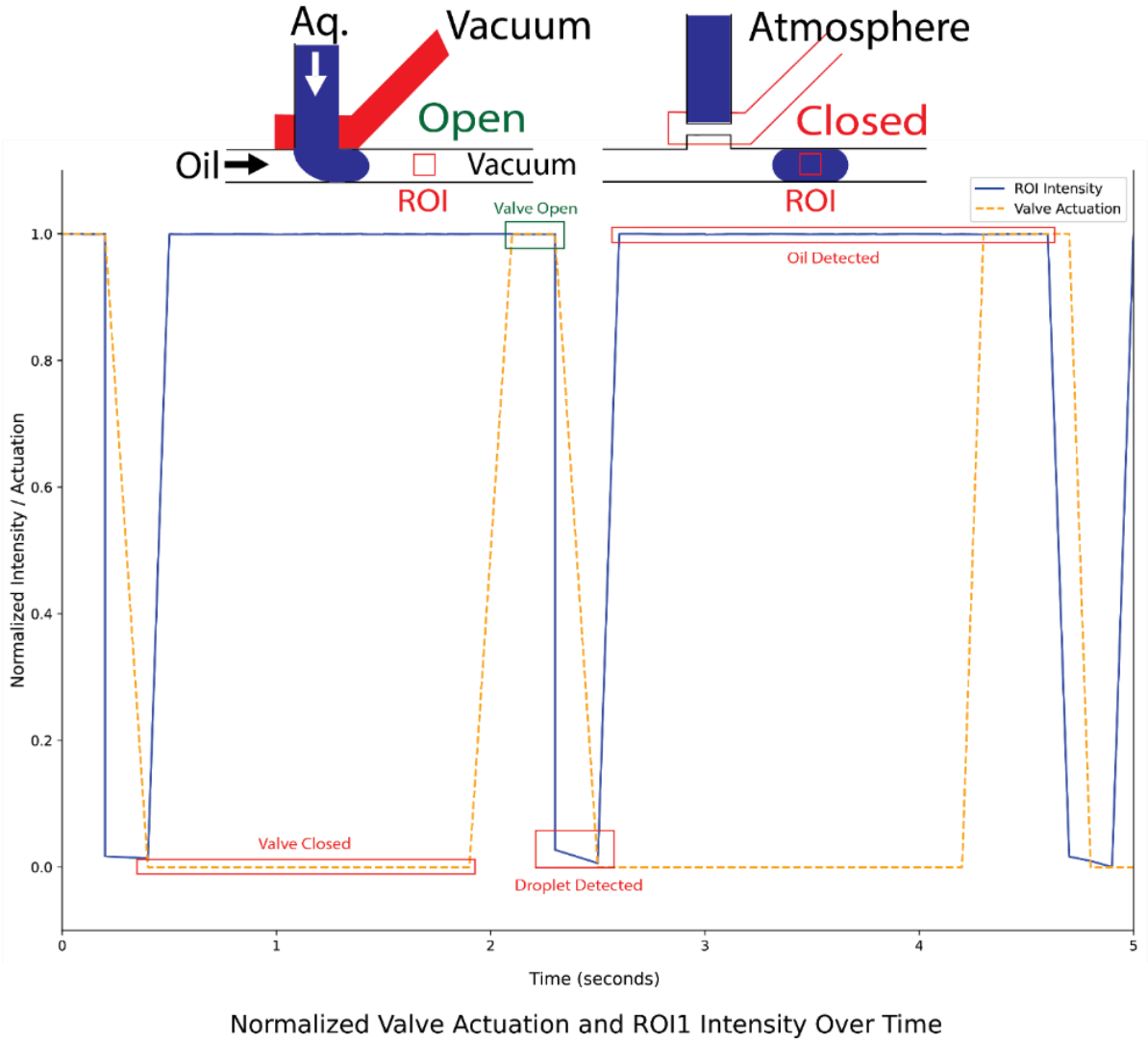

Normalized Valve Actuation and ROI1 Intensity Over Time

Figure 2.18 Schematic of a microfluidic normally closed valve operation

increases. This trend is consistent across the different actuation times tested (100 ms, 250 ms, 500 ms, 750 ms, and 1000 ms), with the largest droplets being produced at the longest actuation time of 1000 ms.

The frequency distribution of droplet volumes for each actuation time shows that the method can produce droplets with a relatively narrow size distribution, particularly at shorter actuation times.

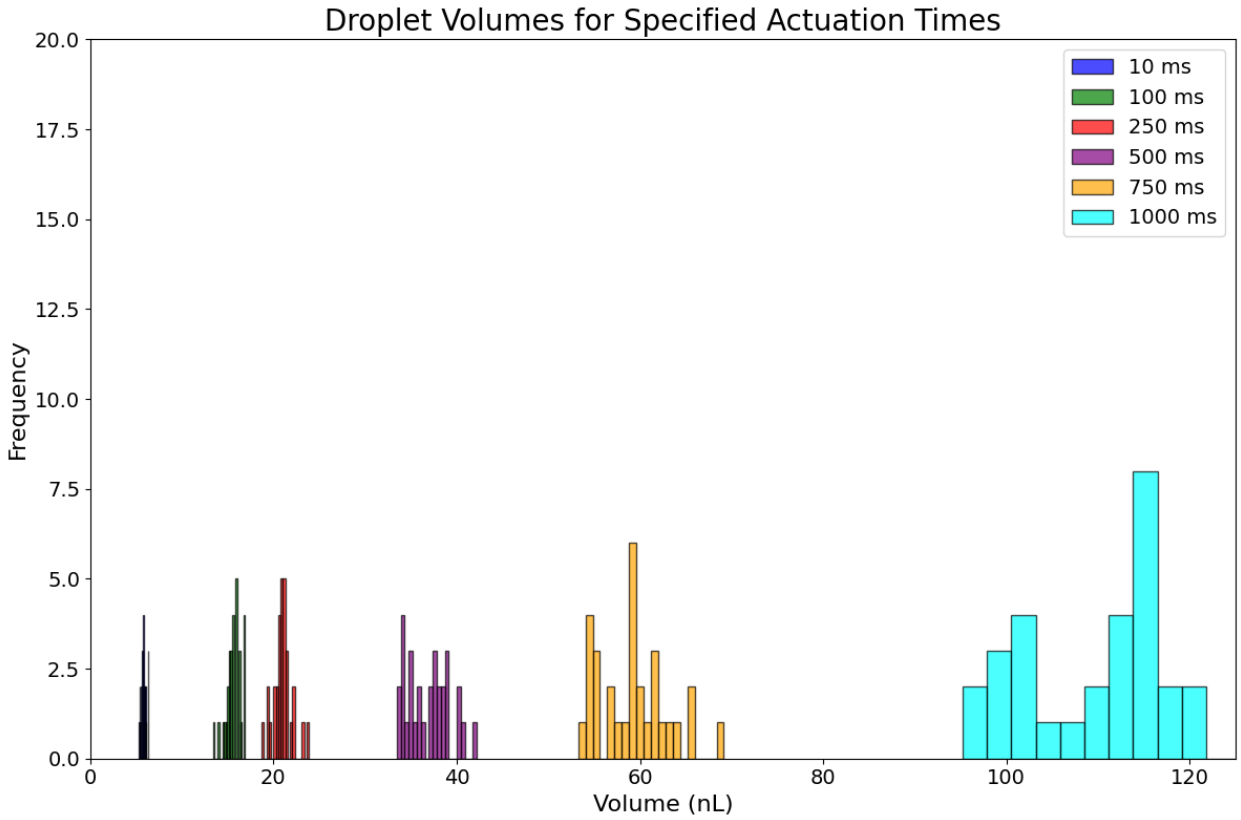

Figure 2.19 the relationship between actuation time and droplet volume for a normally closed valve. Different actuation times (10 ms, 100 ms, 250 ms, 500 ms, 750 ms, and 1000 ms) are shown, highlighting how the droplet volume increases with longer actuation times.

2.4.5.2 Microfluidic Normally Closed Pump

Workflow: The NC pump's workflow is illustrated in Figure 15 (Left) through four sequential steps, showing the states of the valves during the pumping cycle. In step 1, all valves are in the closed state, isolating the pump chamber. In step 2, the top valve opens, allowing fluid to enter the chamber while the bottom and side valves remain closed. Step 3 involves closing the top valve and opening the bottom valve, which creates a pressure differential that drives fluid flow out of the chamber. Finally, in step 4, the bottom valve closes, and the side valves open, resetting the chamber for the next cycle. This cyclic operation effectively pumps fluid through the microfluidic device, demonstrating the practicality of the NC pump design for fluid manipulation.

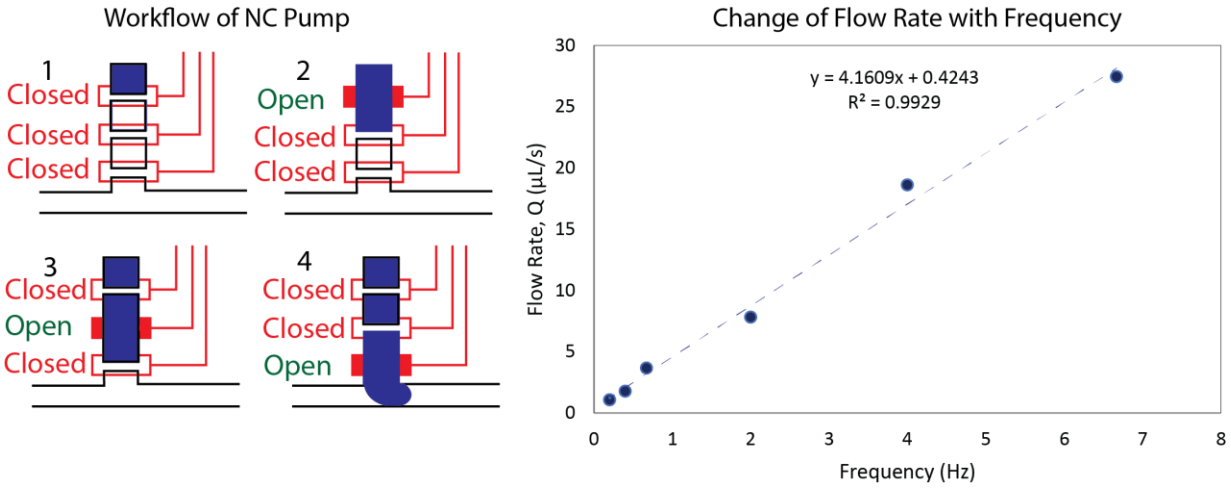

Figure 2.20 Workflow of Normally Closed (NC) Pump and the relationship between flow rate and frequency. (Left) Sequential steps in the operation of an NC pump, showing the states of the valves during the pumping cycle. (Right) Plot depicting the change in flow rate

Change of Flow Rate with Frequency: The plot on the right side of the **Figure 2.20** shows the relationship between the flow rate (Q) and the frequency of the pump cycle. The data points indicate that as the frequency increases, the flow rate also increases linearly, as evidenced by the linear regression line with a slope of 4.1609 and a y-intercept of 0.4243. The high coefficient of determination ($R^2 = 0.9929$) suggests a strong linear correlation between frequency and flow rate.

2.5 Conclusions

In this chapter, we have explored the historical context and technological advancements in the field of microfluidic flow control systems, highlighting the intricate interplay between electronic circuits and microfluidic systems. Beginning with a brief history of electronics, we traced the evolution of computing technology from the early days of ENIAC to modern advancements in molecular and quantum computing. This progression underscores the importance of continuous innovation and the significant milestones that have shaped the current landscape of electronic and microfluidic technologies.

The analogy between electronic circuits and microfluidics provided a conceptual framework for understanding the similarities in design and operation, facilitating the development of sophisticated microfluidic devices. By drawing parallels between fluidic and electronic components, we emphasized how established principles in electronics can be applied to microfluidic systems, enhancing their design and functionality.

The chapter also delved into the use of 3D printing technologies for the fabrication of microfluidic devices, particularly focusing on the integration of PDMS with 3D-printed templates. We discussed the chemical intricacies involved in PDMS curing, the role of platinum catalysts, and the challenges posed by inhibitors present in 3D-printed materials. Through a series of experiments and optimizations, we demonstrated effective methods to overcome these challenges, enabling the reliable production of high-quality PDMS microfluidic devices.

Furthermore, we examined various flow control mechanisms, both passive and active, within microfluidic systems. Passive methods leverage the inherent properties of microscale fluid dynamics, offering simplicity and cost-effectiveness, while active methods utilize external energy sources for precise fluid manipulation. The development of normally closed valves and lock-in detection

techniques were highlighted as significant advancements in achieving controlled and sensitive fluid handling in microfluidic applications.

Our exploration of computer-aided design (CAD) tools, specifically SOLIDWORKS, illustrated the importance of precision and simulation capabilities in designing microfluidic devices. The integration of CAD tools with 3D printing and PDMS fabrication processes was shown to be crucial in achieving the desired device specifications and functionalities.

Overall, the advancements and methodologies discussed in this chapter underscore the dynamic and interdisciplinary nature of microfluidic flow control systems. The integration of electronic principles, advanced fabrication techniques, and innovative flow control mechanisms is paving the way for more efficient and versatile microfluidic devices. As the field continues to evolve, these innovations hold the promise of further enhancing the capabilities and applications of microfluidic systems in various scientific and industrial domains.

Chapter 3
Electronic Automation of Membrane-actuated Microflow Control

3.1 Background

Comprehensive control over the size, flow rate and frequency of droplet formation is possible in several passive ways by regulating the hydrodynamic pressure, channel geometry, surface, and interfacial chemistry. However, active controls with the aid of external energy inputs can provide more authority over both the frequency and order of droplet formation, minimizing the level of inconsistency that may arise in a passively operated system where optimization is not always feasible.

Depending on the kind of energy used, active control systems can be classified as mechanical, electrical, thermal, and magnetic[4, 5]. Our methods of interest, monolithic membrane valves, are one of the most used mechanical means in such purposes due to their ability to regulate the flow rate and frequency[4]. 'Quake' style normally open (NO) valves[31] are used to stop a continuous flow when actuated whereas a normally closed (NC) valve[1] does the opposite, opening the closed gate from a static flow on demand. Both the types can be interfaced with a computer-controlled system for flexibly programming the flow and consequently the droplet formation.

The automation of droplet-based microfluidic devices is a significant step forward, enabled by advancements in normally closed valve systems. One successful implementation involved on-demand droplet release from microwells, highlighting the integration of droplet trapping and fusion functions, which is crucial for precise control in microfluidic systems.

To automate these systems, a programmable microfluidic digital array can be employed. This array includes a pressure source, control line, multiple valves, and an independent valve for automation. Such configurations allow for precise control and manipulation of microdroplets, essential for tasks such as droplet creation, mixing, incubation, and sorting.

Electrowetting-based actuation is another method used for the integrated control of micro-droplets. This technique allows for the positional and formational control of microdroplets without the need for permanent channels or structures, enhancing the flexibility and functionality of the microfluidic devices. Additionally, internal gas pressure components can be utilized to actuate the system and determine the presence or absence of micro-droplets at specific positions, enabling automated control signals for droplet processing.

Moreover, integrated pneumatic micro-pumps have been developed for high-throughput droplet-based microfluidics. These pumps facilitate the precise manipulation of fluids within the microfluidic system, ensuring reliable and efficient operation.

In summary, the automation of droplet-based microfluidic devices using normally closed valve systems is a complex but achievable goal. By leveraging programmable digital arrays, electrowetting-based actuation, and integrated pneumatic micro-pumps, we can create sophisticated systems capable of precise fluid manipulation, paving the way for advanced applications in various fields.

3.2 Objective

The Easley lab has previously reported digitally controlled NO-valve actuated droplet microfluidic devices to automate tissue secretion sampling with continuous reference sampling (**Figure 2**). This dissertation chapter aimed to **automate similar locked-in detection processes**[25-27] **with a more customizable and affordable system that is controlled by normally closed valves and modulated by portable 3D printed pneumatic logic circuits**, thus minimizing number of off-chip digital controls. Here we introduce our in-house designed and developed pneumatic NOT and NOR logic gates that can automate **a four-step droplet sampling sequence** ((sample, probe), oil, (reference, probe), oil) in a recurring manner with the aid of only two electronic controls.

In the previous chapter, we discussed the construction of microfluidic devices using 3D-printed templates with integrated pneumatic control in direct 3D-printed and hybrid-integrated systems. In this one, we delve into the design and functioning of the electronic system used to control the flow through valve manipulation in our developed droplet-based microfluidic system.

In this chapter, we will first explore how to operate the microcontroller system using a computer program and analyze the results. We will demonstrate two types of computer programming: LabVIEW and Arduino. The advantages and disadvantages of each programming language will be discussed.

LabVIEW and Arduino are popular choices for controlling microfluidic devices due to their unique strengths. LabVIEW is known for its graphical programming interface, which simplifies the process of developing complex control systems. It allows for intuitive visual representations of the control processes, making it easier for users to understand and modify their programs. However, LabVIEW can be more expensive and may require more processing power, making it less suitable for low-cost or resource-limited applications.

On the other hand, Arduino offers a cost-effective solution with a straightforward programming environment based on C/C++. Arduino systems are particularly advantageous for rapid prototyping and precise control of servomotors in valve control applications. The simplicity of the Arduino platform, combined with its extensive community support, makes it an accessible option for beginners and experienced developers alike. However, Arduino systems may have limitations in terms of processing power and scalability when compared to more robust platforms like LabVIEW.

For the characterization of the electronics-based valve control system, we will start with a simple droplet generation circuit that includes one oil flow channel and one aqueous flow channel.

Each channel will have a normally closed valve, and the two flows will meet at a T-junction. Initially, both flows will be closed. We will first create the carrier phase of the circuit by opening the oil valve through a vacuum applied via computer programming. After closing the oil valve, we will open the aqueous valve, allowing the aqueous flow to enter the oil stream. Depending on the desired droplet size, we will close the aqueous flow and restart the oil flow. This process will initially demonstrate the formation of an aqueous-in-oil droplet.

The automation of droplet-based microfluidic devices can be achieved using various control methods. For example, electrowetting-based actuation allows for the positional and formational control of microdroplets without the need for permanent channels or structures. This method provides high flexibility and control precision, essential for complex microfluidic operations.

Furthermore, integrating pneumatic micro-pumps within the microfluidic system can enhance high-throughput droplet generation, ensuring efficient and reliable operation. The use of normally closed valve systems, controlled via Arduino or LabVIEW, allows for precise manipulation of fluid flows, demonstrating the potential for automated droplet generation and manipulation in various applications.

3.3 Materials and Methods

3.3.1 Vacuum Control

Tygon polyurethane tubing (1.6 mm ID, 3.2 mm OD) from Component Supply (Sparta, TN, USA) was used to connect to a house vacuum source, which provided an approximate vacuum of -85 kPa. The tubing was sourced. Solenoid valves (Lee Co.; LHDA0533115H) were employed as vacuum switches to regulate the vacuum application. To initiate flow at the microdevice outlets, a small vacuum was applied using a 100 mL glass syringe (SGE Analytical Science, Ringwood, VIC, Australia).

3.3.1.1 LabVIEW Controlled Solenoid System

Our laboratory has traditionally utilized valve-based pumps and merging systems controlled by LabVIEW software, providing a robust solution for microfluidic control. Despite its effectiveness, the LabVIEW-based system comes with challenges such as high costs, limited portability, and complex programming. To address these limitations, we have developed an advanced LabVIEW-controlled solenoid system that maintains precision while improving usability.

The LabVIEW-based control system consists of solenoid valves managed by a National Instruments (NI) data acquisition (DAQ) device, depicted in Figure 5.4. The system uses NI USB-6002 for data acquisition and control, interfaced with LabVIEW software for precise regulation of the solenoids. The power supply is a 24 V (≥ 2 A) AC/DC converter, providing sufficient power for the solenoids and control circuitry.

Each solenoid valve is connected to the NI DAQ device through a relay board, which acts as an intermediary to control the high-power solenoids using low-power signals from the DAQ. The relay board is connected to a 5 V power supply, regulated by an LM7805 voltage regulator to ensure stable operation.

In this system, the LabVIEW software sends signals to the NI DAQ device, which then controls the relays on the board. When the relay is activated, it closes the circuit, allowing current to flow through the solenoid, setting it to the "ON" position. Conversely, deactivating the relay opens the circuit, stopping the current flow and returning the solenoid to the "OFF" position.

3.3.1.2 Arduino Controlled Solenoid System

To address the limitations of our previous valve-based pumps and merging systems, which were stationary and controlled by LabVIEW, we developed a new portable valve control system using an Arduino Mega 2560 board and open-source Arduino software. This new system is more cost-effective, portable, flexible in alternating between pressure and vacuum, and simpler to

program. The custom-built controller, depicted in Figure 5.2, comprises two main components: the Arduino Mega 2560 and a transistor array box that manages the solenoids. The system is powered by an 18.5 V (≥ 3 A) AC/DC converter connected to the Arduino Mega 2560, which operates within its voltage range of 6 to 20 V. A voltage regulator (LM 2596) is used to step down the voltage to 5 V for the transistor array and solenoids.

The transistor array box controls the solenoid movements. Each solenoid is connected to one of the transistor array's outputs, positioned between a 5 V power supply and ground. Transistors switch to complete the circuits that power the solenoids. The Arduino Mega 2560 sends signals to the transistor array, dictating whether each solenoid should be "on" or "off". When a transistor is "on", current flows through the solenoid, setting it to a "HIGH" position. When the transistor is "off", the current flow is interrupted, and the solenoid returns to a "LOW" position.

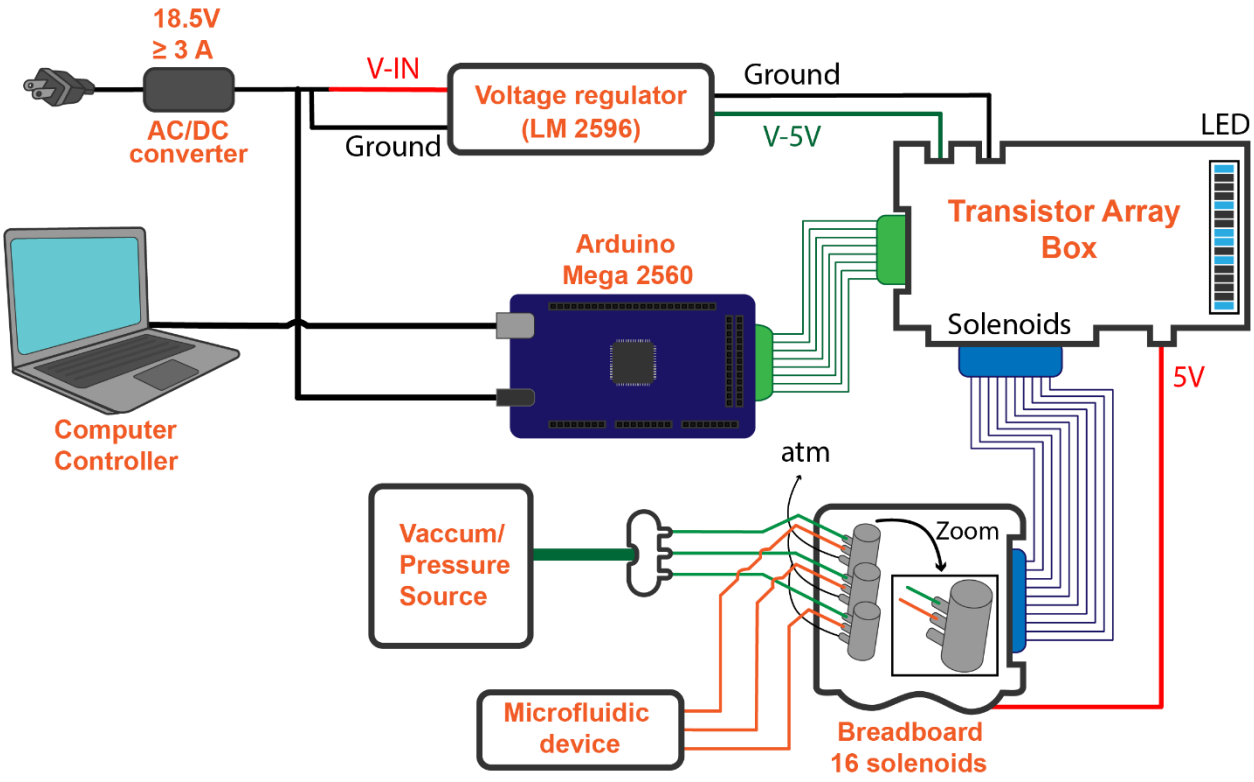

Figure 3.1 Schematic of the custom-built solenoid system controlled by an Arduino Mega 2560. The system can simultaneously control 16 solenoid valves, managing input pressure/vacuum to

atmospheric pressure. This capability makes it suitable for both normally closed and normally-open valve microfluidic devices.

3.3.1.3 Solenoid Structure

Each solenoid has two pneumatic inputs and one output. One input is connected to a high vacuum or high-pressure source, and the other is open to atmospheric pressure. The output connects to the microfluidic device. In our configuration (Figure 5.2), the "HIGH" position corresponds to the high vacuum/pressure connection, and the "LOW" position corresponds to atmospheric pressure. By programming the Arduino to control the transistors, we can precisely manage the solenoids' movements and control the valves' exposure to vacuum/pressure or atmospheric pressure.

To validate the solenoid control system, we tested normally closed valves in PDMS microfluidic device channels, controlled by 3D-printed pneumatic channels (Figure 5.3A). We programmed two aqueous and one oil valve as shown in Figure 5.3B. Using microscopy and video analysis (ImageJ), we precisely analyzed valve movements and confirmed the programmed valve timing during operation (Figure 5.3C). The solid lines indicate the programmed valve movements, with higher signals representing "closed" valves and lower signals representing "open" valves. The image analysis data (dashed lines) closely matched the programmed movements, confirming that the valve timing functioned as intended.

3.3.2 Light, Camera, Detection

A Nikon J1 microscope (Nikon Corporation, Tokyo, Japan) was used as the lighting and detection system. The microscope's built-in lighting system was utilized for illumination. Detection was carried out using the microscope’s integrated camera system.

3.3.3 Data Collection and Analysis

Data from the microscopic imaging system was processed and analyzed using Microsoft Excel, MATLAB and Python to determine the consistency of droplet formation at various frequencies.

3.3.3.1 Pressure/Vacuum Sensor

Two MPX5700AP pressure transducers were mounted to a board, and connected to an Arduino Uno, using 5 volts from the connected batteries for power. The dual sensor board was then enclosed in a 3D printed box. Decoupling capacitors are added between the V+ (0.01 µF and 100 µF) and signal output (470 pF) to ground, Figure 5.11 shows prototyping board and components. The Arduino Uno was programmed to read the pressure data from the transducers and log the measurements.

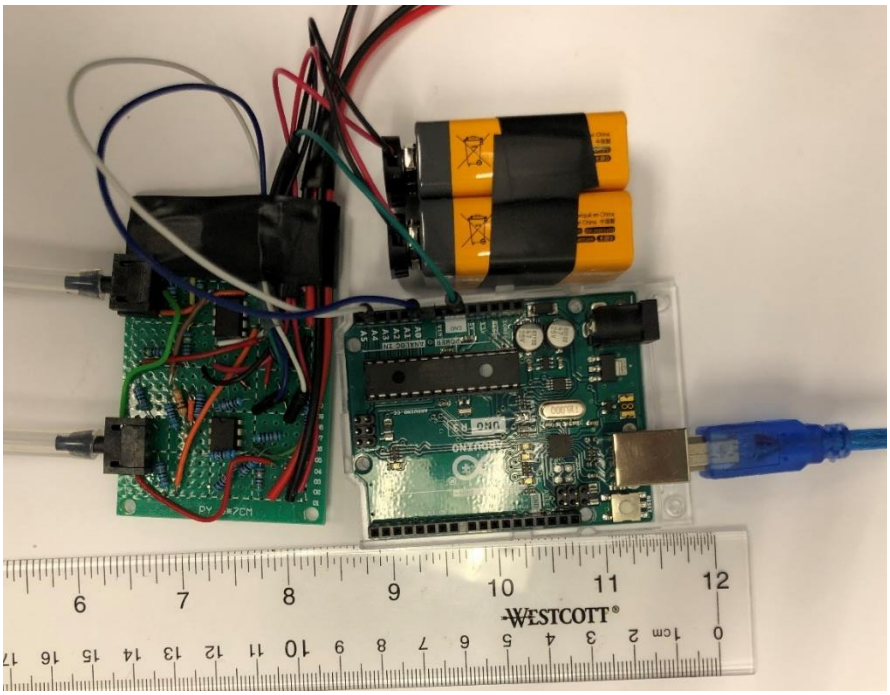

Figure 3.2 Prototype of the pressure sensor system, including the MPX5700AP transducers, Arduino Uno, power supply, and decoupling capacitors mounted on a prototyping board.

3.3.4 System Characterization

The system was set up for experiment by connecting the Tygon tubing to the house vacuum source and solenoid valves and attaching the microfluidic device. LabVIEW/Arduino software were programmed to alternate the actuation of the solenoid valves, applying vacuum to the oil and

aqueous channels at specific intervals. Using the 100 mL glass syringe, we created an initial vacuum to start fluid flow in the microdevice. The Nikon J1 microscope was used for illuminating the microfluidic channels and detecting droplet formation and movement. Control experiments were conducted for both LabVIEW and Arduino based control system to determine the fastest possible frequency at which each system could alternate the vacuum application, while maintaining consistent droplet sizes which was validated by both computer vision and volumetric measurements.

3.3.5 **Sequential Droplet Formation**

The LabVIEW/Arduino software was initially designed to alternate two solenoid valve actuations, controlling one aqueous and one oil flow. Flow initiation was performed by applying an initial vacuum using a plastic syringe. Sequential droplet formation was achieved by introducing a second aqueous flow to create alternating sample and reference droplets. Finally, a third aqueous channel was integrated to produce probe droplets, synchronized with the sample and reference droplets through precise timing control.

A Nikon J1 microscope was employed to illuminate the microfluidic channels and detect droplet formation and alternation. Data was collected in real-time using a USB DAQ system and LabVIEW software, followed by a Python script integrating Arduino for more flexible serial communication. The data collection focused on droplet size, oil spacing, formation rate, and sequence. The characterization involved analyzing the consistency and reliability of droplet formation and the synchronization of probe droplets.

Description of Microfluidic Devices: The microfluidic devices used for this test are depicted in the figure, which shows a later version containing all three sample, reference, and probe channels, along with the oil channel. Each inlet channel includes a reservoir to store the input, a

normally closed valve to gate the flow, and a resistor to minimize the impact of valve actuation noise on the corresponding T-junctions.

The inlet channels are 5 mm long each before the valve and approximately 7 mm after the valve to the T-junction. The incubation channel after the T-junctions can be extended as required. Channels were initially fabricated at 100 micrometers in height and 300 micrometers in width. Later, they were adjusted to 200 micrometers in both height and width as experimental observations indicated greater consistency in squared channels.

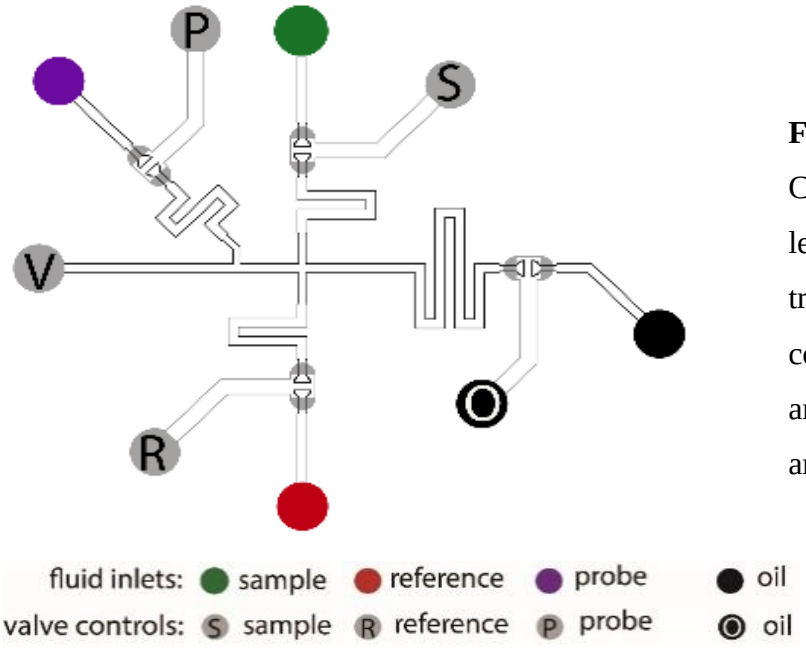

Figure 3.3 Schematic of the CAD layout of a multitype droplet generator. The figure illustrates the microfluidic device containing sample, reference, and probe channels, along with an oil channel. Each inlet chan-

The microfluidic device's design ensures precise control over the flow of liquids, enabling the formation of consistent and reliable droplets. The integration of normally closed valves and resistors effectively minimizes flow disturbances, enhancing the overall performance of the system in generating and synchronizing droplets.

3.4 Results and Discussion

3.4.1 System Characterization

The solenoid-based control system's performance was evaluated by determining the minimum time required to complete a full cycle of operation, which involves sending a command from a computer program through the electronic control system to actuate a normally closed valve on the microfluidic device. Initial tests indicated that the system could theoretically complete this operation in as little as 1 millisecond. This rapid response was confirmed by the integrated LED light actuation on the transistor array box of the solenoid control system (Figure 16).

However, further testing revealed that achieving complete valve actuation required a longer cycle time. Specifically, a minimum cycle time of 10 milliseconds was necessary to ensure reliable serial communication and successful valve operation.

We evaluated the durability of the complex multi-solenoid programs by actuating all 16 solenoid control lines with varying pulse and gap times, ranging from 10 ms to 1000 ms. The results, depicted in Figure 3.4, demonstrate that

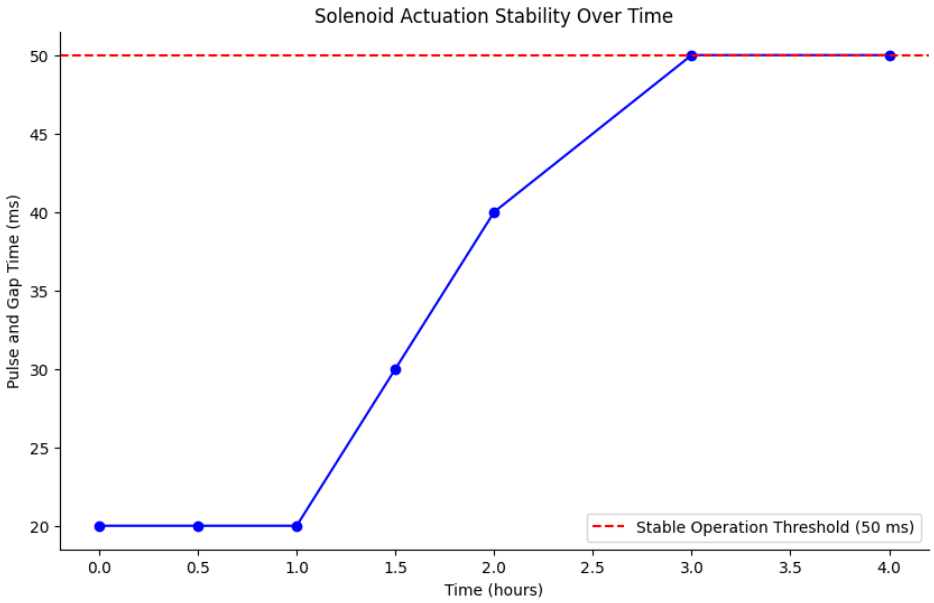

Figure 3.4 Solenoid Actuation Stability Over Time. The plot depicts the stability of solenoid actuation with varying pulse and gap times from 10 ms to 50 ms over a period of up to 4 hours. The red dashed line represents the stable operation threshold at 50 ms. Initial operations with 20 ms pulse and gap times became unstable after 1 hour, while increasing the times to 50 ms ensured stable operation for up to 4 hours.

during the fastest operations, which included 10 ms pulses and 10 ms gaps (a total cycle time of 20 ms), the system began to operate incorrectly after a few minutes to about an hour duration. To address this issue, we gradually increased the pulse and gap times, eventually setting them to 50 ms each (total cycle time of 100 ms). This adjustment allowed the system to run all 16 valves continuously for up to 4 hours without any error, significantly exceeding the typical operational durations required by our systems.

3.4.1.1 Arduino-based Pressure Sensor

The MPX5700DP pressure transducer was selected for its high accuracy (± 2.5% over 0-80°C), wide range (0-700 kPa), and linear output. Its integrated temperature compensation simplifies the circuitry, ensuring reliable performance across varying temperatures.

The developed pressure sensor system was tested to characterize its performance in detecting pressure changes and response time. Both pressure and vacuum pulses were applied via a

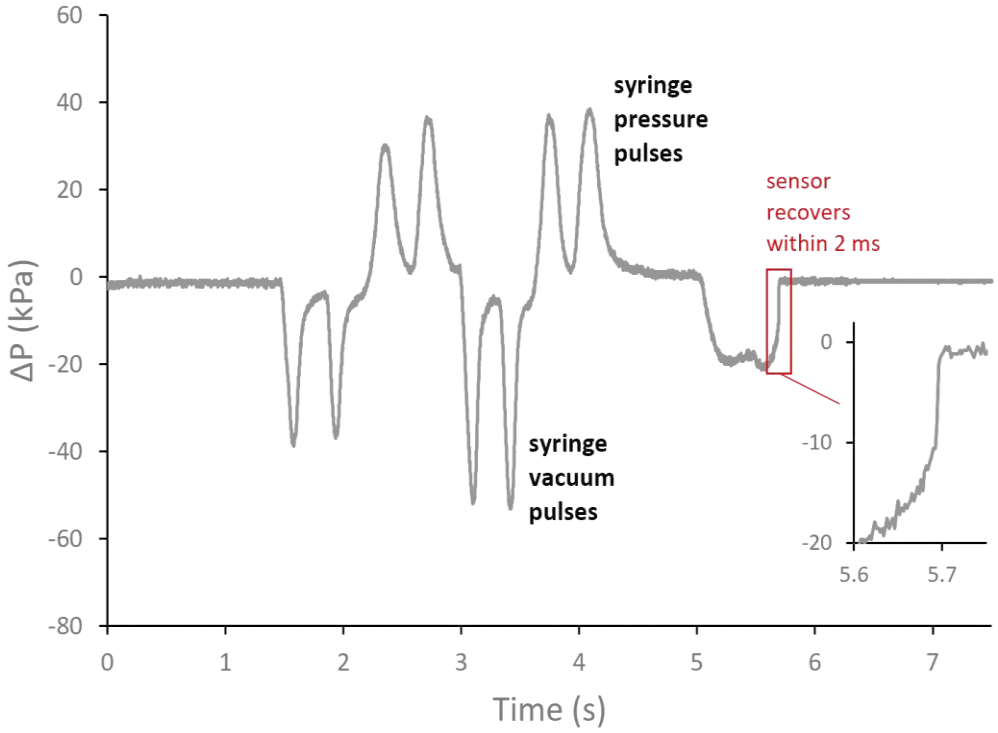

Figure 3.5 Plot of the pressure sensor output (ΔP) over time, demonstrating the sensor's ability to detect pressure and vacuum pulses and its rapid recovery time within 2 milliseconds.

syringe, with pressure pulses reaching up to 40 kPa and vacuum pulses going down to -60 kPa. These limits were chosen based on the typical operational requirements of our systems, which do not generally necessitate pressure changes beyond these ranges.

The pressure transducers demonstrated their capability to accurately detect both the applied pressure and vacuum pulses. The sensor output (ΔP) was plotted against time (shown in Figure 3.5), revealing distinct pressure peaks and troughs that corresponded to the applied pulses. This clear detection of pressure changes underscores the sensor's sensitivity and precision. Furthermore, the sensor exhibited a rapid recovery time, returning to baseline within approximately 2 milliseconds after each pressure change. This quick response time is critical for applications requiring real-time pressure monitoring and control.

3.4.2 Automated Aqueous in Oil Droplet Generation

Single Aq. Phase (Sample Only):

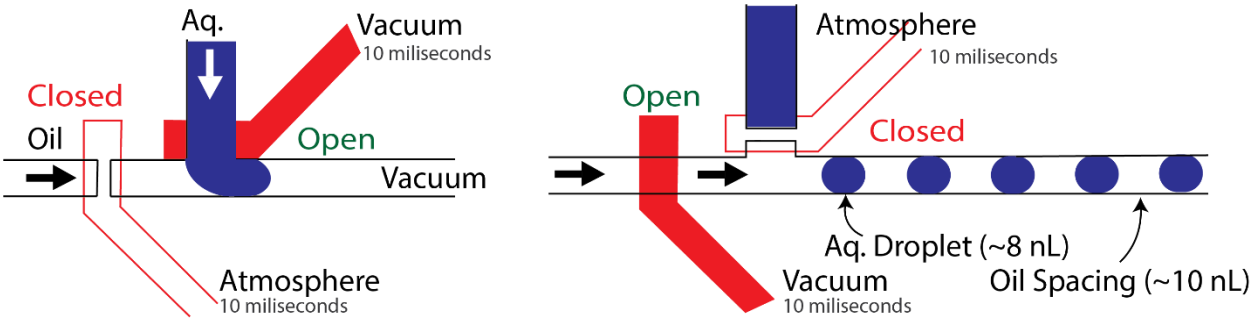

Figure 3.6 Sequential operation of solenoid valves for droplet generation. (Left) The aqueous valve opens while the oil valve remains closed, allowing vacuum pressure to draw the aqueous solution into the droplet formation area. (Right) The aqueous valve closes, and the oil valve opens, pushing the aqueous droplets (~8 nL) into the channel with consistent oil spacing (~10 nL). Each valve operates in 10-millisecond intervals to ensure equal droplet size and spacing.

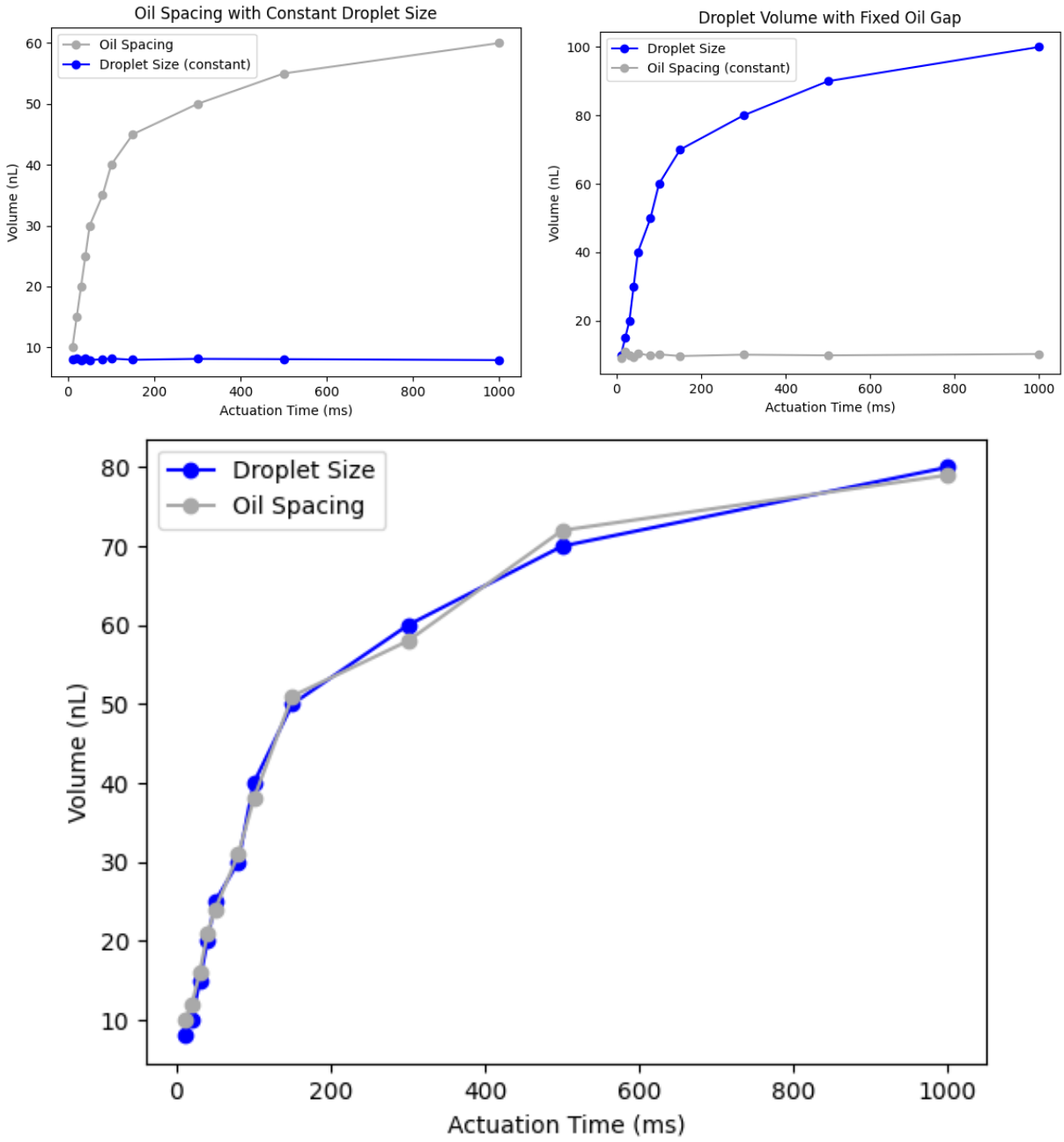

Figure 3.7 (Top Left) The relationship between actuation time and oil spacing while maintaining a constant droplet size with slight variations. The oil spacing increases as the actuation time increases. (Top Right) The change in droplet volume with varying actuation times while keeping the oil gap constant with minor deviations. The droplet volume increases with longer actuation times. Bottom: the simultaneous increase in both droplet size and oil spacing with increasing actuation times. Both parameters show a positive correlation with actuation time, reflecting a more realistic experimental scenario with added variations.

Two Aq. Phase (Sample and Reference)

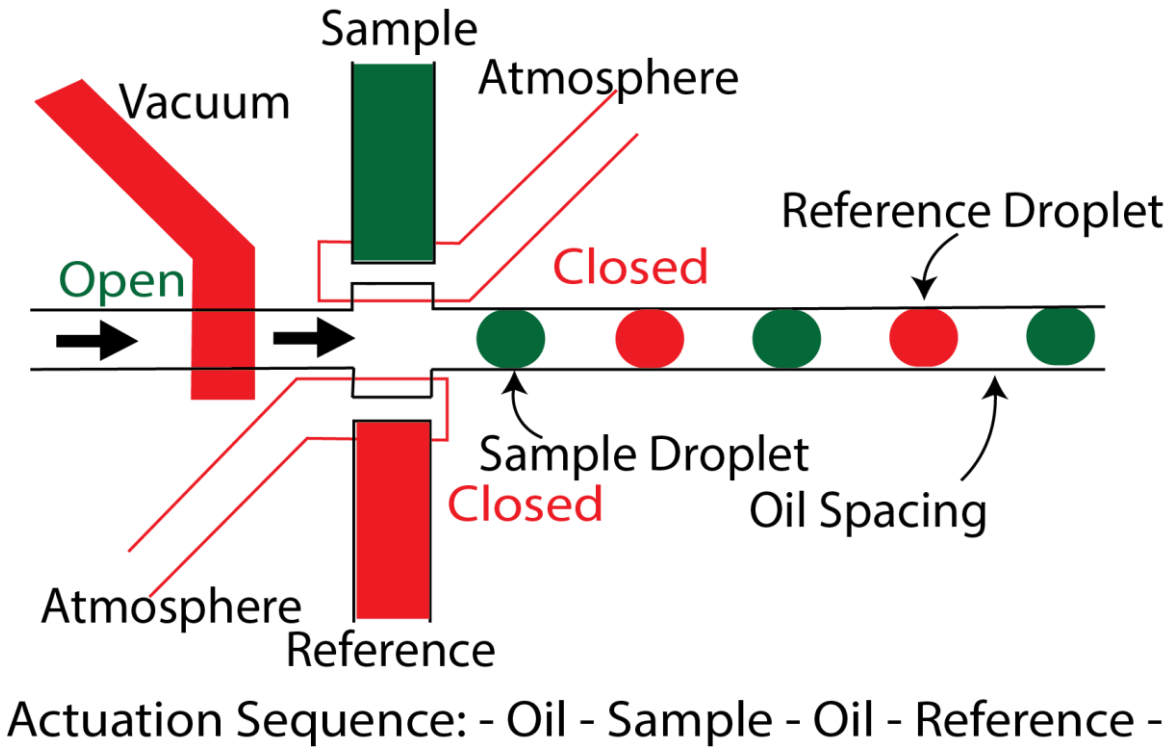

Figure 3.8 The actuation sequence for forming sample and reference droplets. The oil valve is initially opened to introduce an oil segment, followed by closing the sample and reference valves to create alternating sample (green) and reference valves to create alternating sample (green) and reference (red) droplets. The sequence maintains precise oil spacing between the droplets to ensure consistent and reliable formation.

Three Aq. Phase (Adding Probe to Sample and Reference)

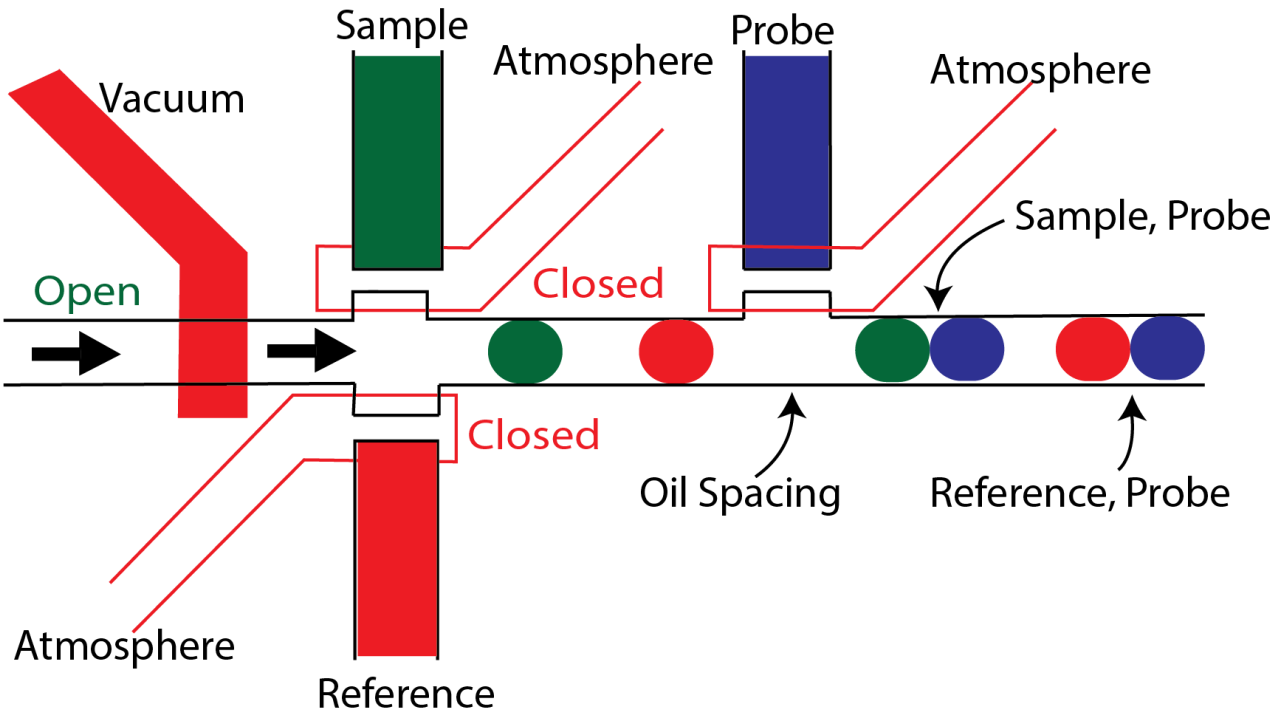

Figure 3.9 the actuation sequence for forming sample (green), reference (red), and probe (blue) droplets. The sequence starts with the oil valve opening, followed by the sample, probe, and reference valves alternately actuating to create the respective droplets.

3.5 **Conclusions**

In this chapter, we explored the intricate process of automating droplet-based microfluidic systems through electronic control mechanisms, particularly focusing on membrane-actuated microflow control. Our investigation covered various active control methods, highlighting the superiority of mechanical control via monolithic membrane valves, specifically normally closed (NC) valves, for precise and flexible droplet formation and manipulation.

Key Findings

Active vs. Passive Control: Passive methods, while effective, often lack the precision and consistency needed for advanced applications. Active control systems, leveraging external energy inputs, provide superior authority over droplet formation, significantly reducing inconsistencies.

Membrane Valves: Monolithic membrane valves, normally closed (NC), demonstrated their effectiveness in regulating flow rates and droplet formation frequencies. These valves, when integrated with computer-controlled systems, allowed for programmable and flexible microfluidic operations.

Programmable Microfluidic Digital Arrays: The implementation of programmable microfluidic digital arrays, incorporating pressure sources, control lines, and multiple valves, enabled precise control over microdroplet manipulation. This system facilitated complex tasks such as droplet creation, mixing, incubation, and sorting.

Integrated Pneumatic Micro-pumps: The development of integrated pneumatic micro-pumps for high-throughput droplet-based microfluidics ensured reliable and efficient fluid manipulation within the system.

LabVIEW vs. Arduino for Control: LabVIEW offered robust and intuitive control through its graphical programming interface but came with higher costs and complexity. Conversely, Arduino provided a cost-effective, portable, and simpler solution, ideal for rapid prototyping and precise control in resource-limited applications.

3.5.1 System Characterization

Minimum Cycle Time: The solenoid-based control system achieved a minimum cycle time of 10 milliseconds for reliable valve actuation, ensuring efficient serial communication and successful operation.

Durability and Performance: The system demonstrated durability under continuous operation, managing 16 solenoid control lines with varying pulse and gap times. The optimal cycle time of 100 milliseconds enabled the system to run continuously for extended periods without errors.

Pressure Sensor Performance: The MPX5700DP pressure transducer exhibited high accuracy and rapid response times, essential for real-time pressure monitoring and control in microfluidic applications.

Automated Droplet Generation

Single, Dual, and Triple Aqueous Phase Operations: The system successfully generated single aqueous phase (sample only) droplets, dual-phase (sample and reference) droplets, and triple-phase (adding probe) droplets, with precise control over droplet size and spacing.

Future Directions

The successful automation of droplet-based microfluidic devices using electronically controlled membrane-actuated systems represents a significant advancement. Future work will focus on further enhancing the precision and scalability of these systems, integrating additional analytical tools, and exploring new applications in various scientific and industrial fields.

By addressing the remaining challenges and continuing to innovate, we can unlock the full potential of automated microfluidic systems, paving the way for more sophisticated and impactful applications in research and technology.

Chapter 4

Pneumatic Automation of Droplet-based Microfluidic Systems

4.1 Background

By enabling precise control and manipulation of small volumes of fluids, droplet microfluidics facilitates high-throughput biochemical assays, synthesis of advanced materials, and biological studies at the single-cell level. Central to the functionality of these systems is the ability to control droplet formation, movement, and interaction within microfluidic devices, often achieved through pneumatic control mechanisms.

Recent advances in pneumatic control systems for droplet microfluidics have focused on enhancing precision, flexibility, and cost-effectiveness. Open-source solutions, such as the pneumatic pressure control system developed by Gao and Hébert (2018), aim to reduce barriers to entry by providing high-performance, affordable alternatives to commercial systems[147]. These systems leverage widely available components and open-source software to enable pulseless pressure-driven flow for nanoliter-sized droplet manipulation.

Choi et al. integrated pneumatic micro-pumps with droplet-based microfluidic systems to eliminate the need for syringe pumps, thereby reducing dead volumes and enhancing high-throughput biological experimentation[148]. Similarly, Han et al. described a microfluidic chip with pneumatic valves for measuring enzymatic kinetics, showcasing the applicability of pneumatic control in biochemical reactions[149].

Pneumatic control has also enabled sophisticated droplet manipulation techniques. Dong and Jiang reported on the formation and repositioning of liquid microlenses within microfluidic channels, controlled through pneumatic manipulation of fluids[150]. This technology allows for tunable focal lengths and precise droplet positioning, essential for advanced optical and analytical applications.

In another significant contribution, Grover et al. developed latching microfluidic valve structures controlled by an on-chip pneumatic demultiplexer. These valves can hold positions without continuous power, significantly reducing the energy requirements of microfluidic systems[151].

The push towards open-source and modular microfluidic systems is exemplified by the work of Filatov et al. (2022), who developed a low-cost, open-source microfluidic pressure controller with modular design. This system can maintain stable droplet generation for extended periods, making it suitable for diverse lab-on-a-chip applications[152].

Nguyen et al. presented a semi-autonomous liquid-handling chip capable of executing complex procedures using on-board pneumatic digital logic. This innovation reduces the need for external control machinery and simplifies the operation of integrated microfluidic systems[153].

The advancements in pneumatic control for droplet microfluidics have significantly expanded the capabilities and applications of these systems. From open-source designs that democratize access to microfluidic technology, to sophisticated valve and pump systems that enhance precision and reduce operational costs, the field is poised for continued innovation. These developments not only improve existing methodologies but also open new avenues for research and application in various scientific and industrial domains.

4.2 Objective

Electronically powered solenoid-based systems offer precise control for automating high-throughput microfluidic valves. However, their complexity and the costly macro-to-micro interfacing with numerous external connections can limit the functionality of such systems[154]. In contrast, our droplet-based devices, which feature normally closed flow gates, do not require any power to keep the valves closed. These sealed channels remain closed until actuated, simplifying the design[155].

To automate a droplet-based sampling process, where droplets of sample and reference are alternately formed in oil, each with a probe, four separate pulses are typically required to open the normally closed flow gates. The third aim of this dissertation is to introduce fundamental pneumatic logic gates and their integrated application to minimize electronic control.

We begin by developing the fundamental pneumatic logic gates, following their electronic counterparts simulated on the open-source circuit simulator, falstad.com. These gates are then designed using SolidWorks, 3D-printed, and assembled. Detailed procedures are provided in the materials and methods section.

Initially, we employ the NOT gate (or inverter) to actuate one of the two normally closed valves in a single-phase aqueous droplet generator. In this setup, either the aqueous or oil flow can be actuated with an electronic pulse from a solenoid, while the pneumatic inverter creates an inverted pulse to alternately actuate the other valve. This approach reduces the need for two electronic pulses to automate a single-phase aqueous-in-oil droplet generator.

Next, we introduce a Pneumatic NOR gate to operate our sample/reference alternator, enabling the automation of the three-valve operation with just two solenoid pulses. For probe introduction for each sample and reference droplet, we integrate our NOR and NOT gates, allowing us to operate four valves (oil, sample, reference, and probe) with only two electronic pulses.

The ultimate objective of this chapter is to develop a fully pneumatically automated, electronics-free system. We achieve this by employing a 5-ring pneumatic oscillator[156,157], which uses a ring of inverter gates, as the sole power source for our control system. Due to the significant natural overlap in the two pulses from the inverter, a phase shift is required to create sufficient oil spacing between each droplet. This phase shift is accomplished by sending the pulses through an AND-NOR integration circuit[157]. With only two pulse inputs from the oscillator, this pneumatic

logic computation can generate four outputs, achieving the four-step droplet sampling sequence described above.

The details of our findings are discussed further in the results and discussion section.

4.3 Materials and Methods

4.3.1 Falstad Simulation

Falstad Circuit Simulator (www.falstad.com) is an open-source, web-based tool designed for simulating and visualizing electronic circuits. It offers an intuitive graphical interface that allows users to easily construct and analyze complex circuit designs. With real-time simulation capabilities, it provides immediate feedback on circuit behavior. In this chapter, we utilize Falstad Circuit Simulator to model and test the electronic counterparts of our pneumatic logic gates before designing them in 3D for physical implementation.

4.3.2 Designing Pneumatic Circuits

The pneumatic circuits were designed using SolidWorks, focusing on creating two separate 3D-printed layers: one for the flow channels and another for the control channels. The design process involved custom designing channel inlets compatible with Lee solenoid structures to fit Tygon tubing.

Both control and flow channels were routed inside the printed substrate, with specific sections extruding to the surface to serve as valve seats, sitters, or inlet/outlet connections. The channels, each less than 1 mm in diameter, were designed to maximize the capabilities of our 3D-printing technology. Our lab continually strives to enhance the resolution of these channels, pushing the boundaries of what can be achieved with current 3D-printing methods.

4.3.3 3D-Printing and Assembling Printed Components

The designs of the pneumatic circuits are converted into digital formats and sliced into layers of the desired thickness to be 3D printed, following the established process. Using Anycubic printers, these pneumatic circuits are direct printed with circular channels typically ranging from 300 to 500 μm in radius.

After printing, the pieces undergo a washing and curing process as previously described. Once cured, the flow and control channel layers are carefully aligned and screwed together. A thin PDMS membrane is sandwiched between the two layers to work as the valve actuator.

4.3.4 Digital Control Set-up

The pneumatic logic gates were initially automated using LabVIEW, and subsequently, an Arduino-based solenoid control system was integrated for enhanced flexibility. Solenoid switches (LHDA0533115H, The Lee Co., Westbrook, CT) were used in both setups, connected to an in-house vacuum source capable of providing logic high (50-90 kPa) and logic low (0-10 kPa) pressures. Four solenoid valves were integrated onto a breadboard, allowing for four separate digital controls.

The pneumatic control channels, designed to be directly actuated with electronic power, were connected to the corresponding solenoid switches via polyurethane tubing with an inner diameter of 1.6 mm and an outer diameter of 3.2 mm (Component Supply, Sparta, TN).

Initially, custom LabVIEW programs were written to manage the solenoid operations. The first program was designed to alternately turn two solenoid switches on and off, which was then transduced through the pneumatic circuit for further logic computation. The second program aimed

to fully automate the system, using solenoid valves to characterize the full potential of the droplet generation device.

To further enhance the system, an Arduino-based solenoid control system was developed. This setup allowed for more flexible serial communication and user-friendly options.

4.4 Results and Discussion

4.4.1 Characterization of Fundamental Logic Gates

NOT Gate: A pneumatic NOT gate inverts the pressure signal applied to it, converting a high control pressure (vacuum) into a low output pressure (atmospheric) and vice versa. The input (control) pressure, either vacuum or

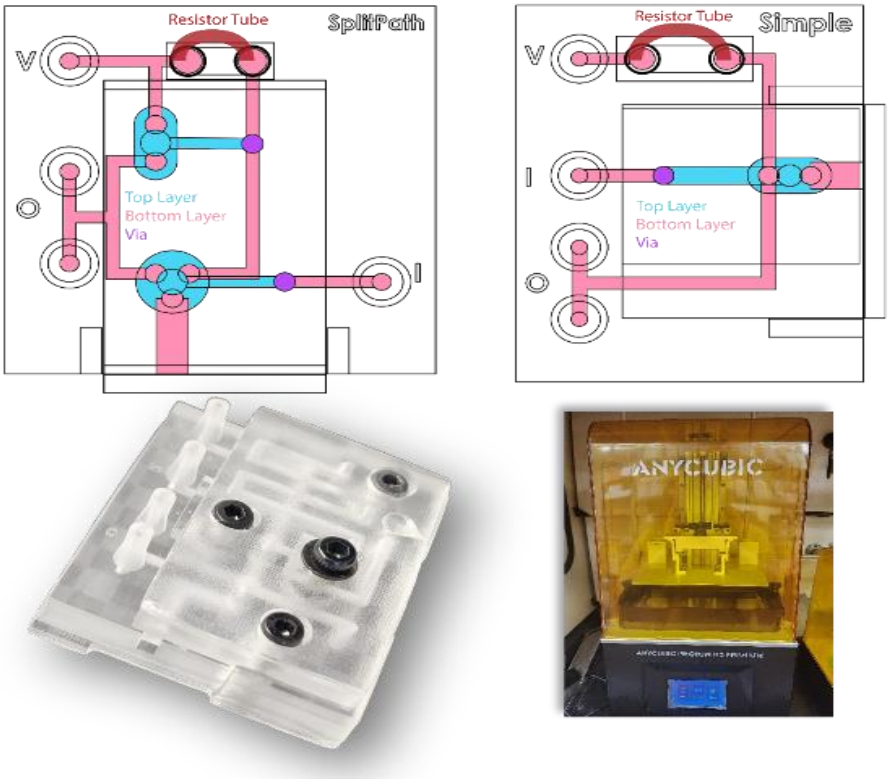

Figure 4.1. (Top) CAD layout of simple and split-path inverter. (Bottom left) Assembled inverter after printing with (bottom right) Anycubic Primo 8K from Anycubic, China.

atmospheric pressure is applied to the valve chamber within the pneumatic circuit as illustrated in Figure. The control pressure determines the position of the flexible PDMS membrane. When the control pressure is high (vacuum applied), it pulls the membrane down, opening the output channel to atmospheric pressure.

Output Pressure Response:

- **High Control Pressure (Vacuum)**: When the control pressure is high (strong vacuum), the membrane is pulled down, opening the output channel to atmospheric pressure. This results in a low output pressure (atmospheric pressure).
- **Low Control Pressure (Atmosphere)**: When the control pressure is low (atmospheric pressure), the membrane relaxes, closing the output channel to atmospheric pressure and connecting it to the vacuum source. This results in a high output pressure (vacuum).

Characterization of the developed pneumatic NOT gate is illustrated in the **Figure 4.2**. The plot illustrates the output pressure (purple line) and control pressure (red line) over time. The control pressure initiates at approximately 0 kPa, gradually increasing to around -40 kPa, and then returns to its initial value. Correspondingly, the output pressure

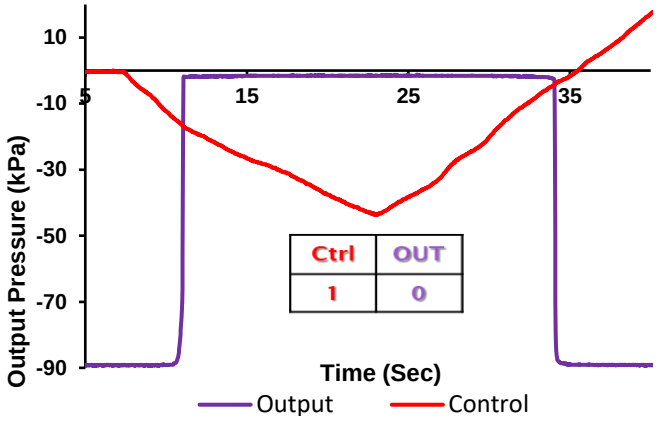

Figure 4.2 Characterization of a Pneumatic NAND Gate. The graph illustrates the output pressure (purple line) in response to the control pressure (red line) over time. The NAND gate maintains a high output (logical '1') when the control pressure is low (atmospheric pressure) and transitions to a low output (logical '0') when the control pressure is high (vacuum applied). The inset table shows the logical state of the control (Ctrl) and the output (OUT) corresponding to the pressure conditions.

remains stable near -90 kPa during the initial phase when the control pressure is low. As the control pressure increases, the output pressure drops sharply to slightly above 0 kPa. This indicates the successful inversion characteristic of the NOT gate, where a low control pressure (high vacuum) results in a high output pressure and vice versa. The rapid transition between states, observable at the beginning and end of the control pressure pulse, demonstrates the responsiveness of the pneumatic NOT gate.

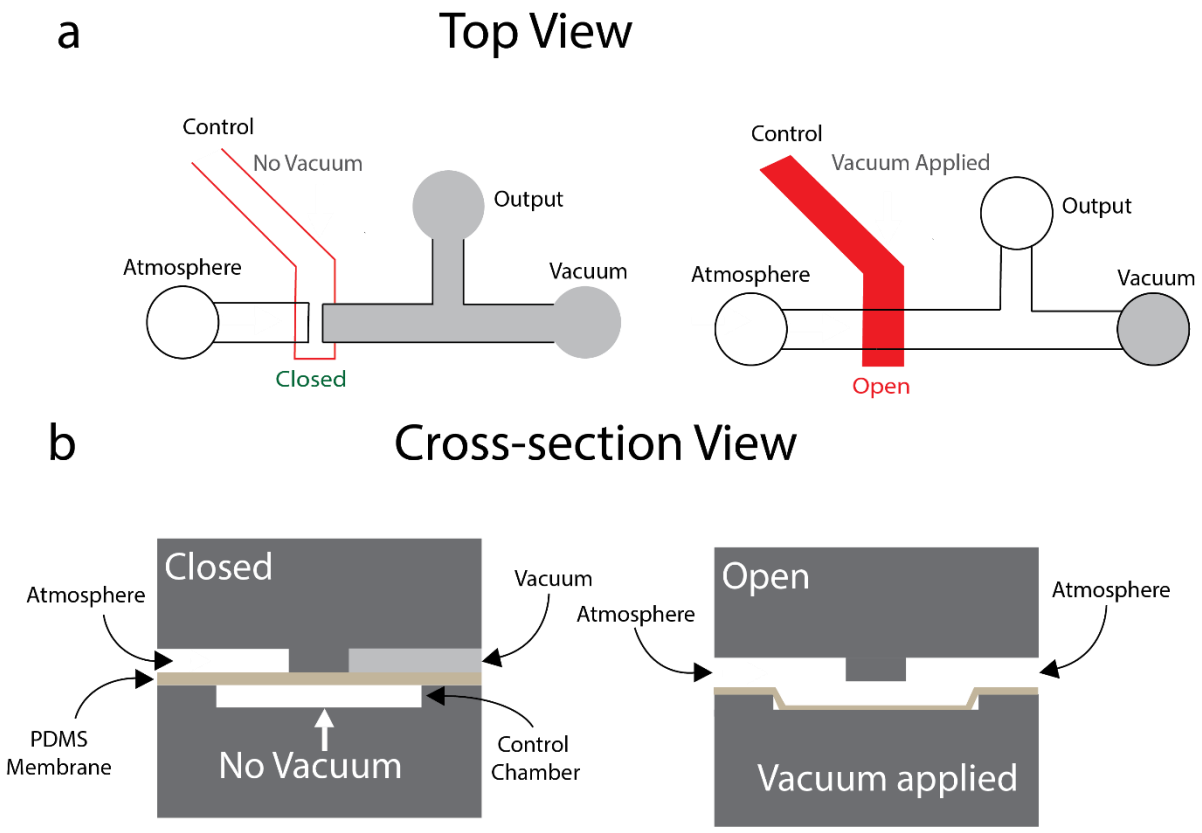

Figure 4.3 Schematic of a pneumatic NOT gate mechanism. (a) Top view: The control pressure (either atmospheric or vacuum) determines the state of the output. When no vacuum is applied (left), the valve is closed, and the output remains at atmospheric pressure. When vacuum is applied (right), the valve opens, connecting the output to vacuum. (b) Cross-section view: Illustrates the position of the PDMS membrane in response to the control pressure. With no vacuum (left), the membrane remains closed, maintaining atmospheric pressure at the output. When vacuum is applied (right), the membrane opens, connecting the output to vacuum.

Figure 4.4 further characterizes the relationship between output pressure and control pressure, forming a distinct NOT gate behavior. As the control vacuum decreases from -80 kPa to -20 kPa, the output vacuum increases from nearly 0 kPa to -90 kPa. This inverted relationship confirms the NOT gate's functionality: when the control pressure is low (strong vacuum), the output pressure is high, and when the control pressure is high (weak or no vacuum), the output pressure is low. The sharp transitions at the boundaries indicate the gate's ability to switch states efficiently and reliably.

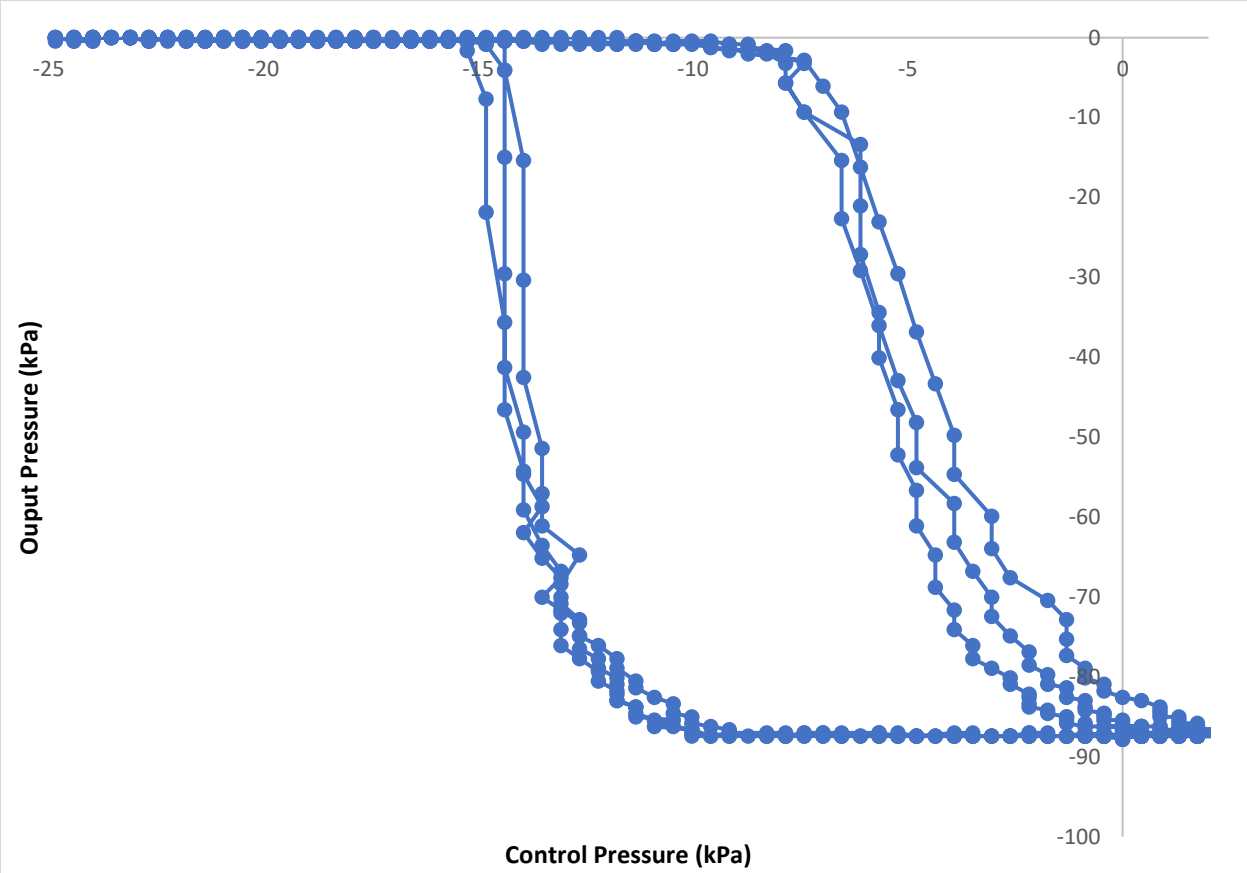

Figure 4.4 Plot showing the relationship between control pressure and output pressure for a pneumatic NOT gate. The control pressure varies from -25 kPa to 0 kPa, while the output pressure ranges from 0 kPa to -100 kPa. The graph illustrates how the output pressure responds to changes in the control pressure.

NOT Gate

Input	Output
0	1
1	0

NOR Gate

A	B	Output
0	0	1
0	1	0
1	0	0
1	1	0

NAND Gate

A	B	Output
0	0	1
0	1	1
1	0	1
1	1	0

Figure 4.5 Truth tables for NOT, NOR, and NAND gates. Each table lists the possible input combinations and their corresponding outputs. The NOT gate inverts a single input, the NOR gate outputs true only when both inputs are false, and the NAND gate outputs false only when both inputs are true.

The characterization results confirm that the pneumatic NOT gate operates effectively, with clear and sharp transitions between high and low states in response to the control pressure. The data indicates that the system can reliably invert the control signal, providing a high output pressure when the control pressure is low and vice versa.

NOR Gate: A pneumatic NOR gate is a logic gate that outputs a logic high (vacuum) only when both inputs are at logic low (atmospheric pressure). It uses atmospheric pressure and vacuum to achieve the desired logical operation. When both control inputs are at atmospheric pressure, the valve remains in a closed position due to the lack of vacuum pressure. The output line is connected to the vacuum source, resulting in a vacuum output, representing a logical '1'. When either or both control inputs are at vacuum pressure, the valve opens, allowing atmospheric pressure to enter the output line. This results in the output being at atmospheric pressure, representing a logical '0'.

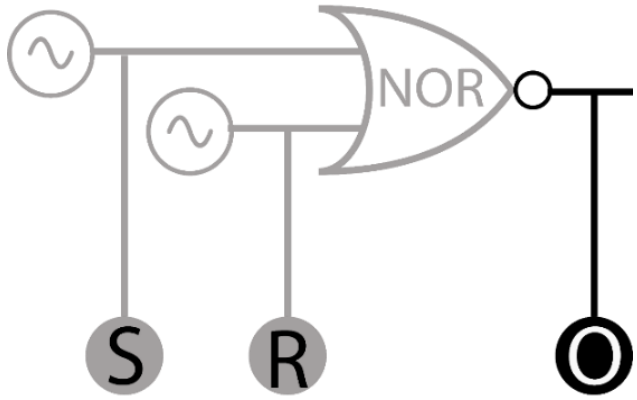

Figure 4.6 Schematic of a NOR Gate

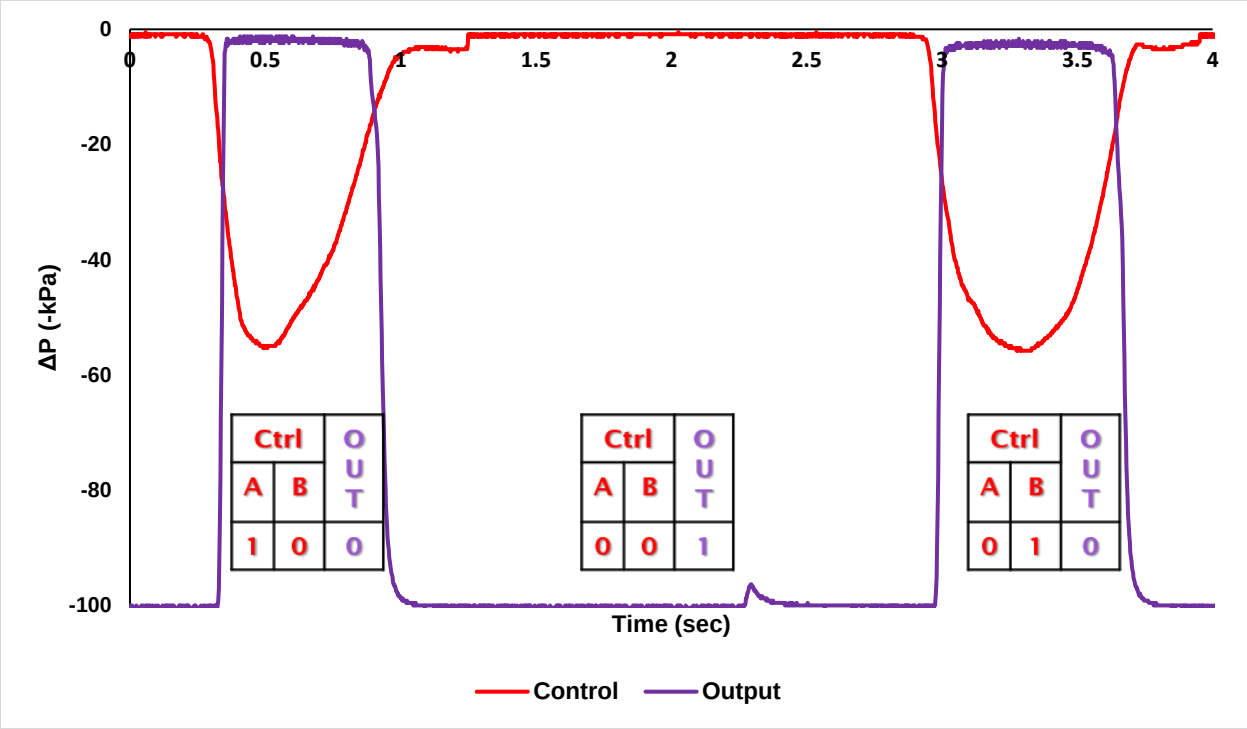

Figure 4.7 Output pressure and control signals for a pneumatic NOR gate. The graph illustrates the relationship between the control inputs (A and B) and the resulting output pressure (OUT). The control pressures vary to represent different logic states (0 and 1) The output pressure transitions accordingly, demonstrating the NOR gate logic: when both A and B are low (0), the output is high (1), otherwise, the output remains low (0).

The pneumatic NOR gate was characterized by measuring the output pressure in response to varying control pressures. The control signals (A and B) were manipulated to represent different logic states (0 and 1), and the resulting output pressure (OUT) was recorded, as shown in **Figure 4.7**. The control signals (A and B) are shown in red, and the resulting output pressure (OUT) is shown in purple. The key observations are as follows:

Initial State (0, 0):

- At the beginning of the test, both control signals (A and B) are low (0).
- The output pressure is high (1), reaching approximately -90 kPa. This corresponds to the expected NOR gate behavior where both inputs being low results in a high output.

Control Signal Change (1, 0):

- At around 0.4 seconds, control signal A transitions to high (1) while B remains low (0).
- The output pressure drops to low (0), reaching approximately -90 kPa, indicating that the NOR gate correctly interprets one high input as a low output.

Control Signal Change (0, 1):

- At around 1 seconds, control signal A returns to low (0), and control signal B transitions to high (1).
- The output pressure remains low (0), reinforcing the NOR gate logic where any high input results in a low output.

Both Control Signals High (1, 1):

- At around 3 seconds, both control signals (A and B) are high (1).
- The output pressure remains low (0), consistent with the NOR gate's logic that the output should be low if either or both inputs are high.

Return to Initial State (0, 0):

- At around 3.6 seconds, both control signals return to low (0).
- The output pressure rises back to high (1), confirming the NOR gate's behavior where both inputs being low results in a high output.

The experimental results align well with the expected behavior of a pneumatic NOR gate. The plot clearly shows the inverse relationship between the control signals and the output pressure, validating the functionality of the pneumatic NOR gate. The system's response time is quick, with transitions between high and low states occurring rapidly, demonstrating the gate's efficiency in switching operations. These findings confirm that the pneumatic NOR gate can reliably perform logical operations using vacuum and atmospheric pressure. The gate's performance is consistent and predictable, making it suitable for integration into more complex pneumatic logic systems.

NAND Gate: A pneumatic NAND gate is a logic gate that outputs a logic high (vacuum) unless both inputs are at logic high (vacuum). It operates using atmospheric pressure and vacuum to perform the desired logical operation. The mechanism involves the following steps:

Both Inputs Low (Atmospheric Pressure):

- When both control inputs are at atmospheric pressure, the valve remains in a closed position because there is no vacuum pressure to actuate it.
- The output line remains connected to the vacuum source, resulting in a vacuum output, representing a logical '1'.

One Input High (Vacuum) and One Low (Atmospheric Pressure):

- If one control input is at vacuum and the other is at atmospheric pressure, the valve partially opens, allowing a mix of vacuum and atmospheric pressure to enter the output line.
- This results in the output being closer to atmospheric pressure, but due to the design, it remains at vacuum, representing a logical '1'.

Both Inputs High (Vacuum):

- When both control inputs are at vacuum pressure, the valve fully opens, allowing atmospheric pressure to enter the output line.
- This results in the output being at atmospheric pressure, representing a logical '0'.

By using this configuration, the pneumatic NAND gate ensures that the output remains at vacuum (logical '1') unless both inputs are at vacuum (logical '0'), fulfilling the NAND gate logic (**Figure 4.8**).

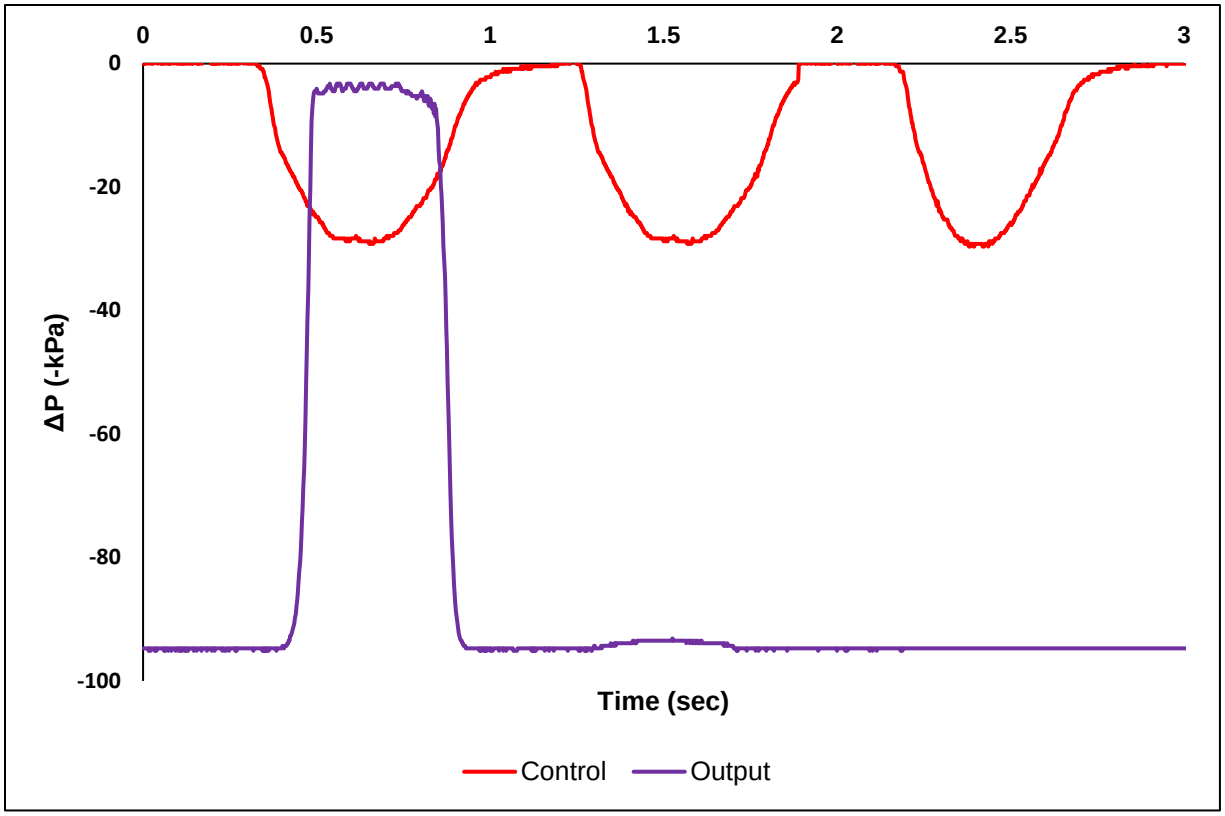

Figure 4.8 The output pressure (purple) and control signals (red) for a pneumatic NAND gate. The control signals represent the inputs to the gate, while the output pressure represents the logical state of the gate. The NAND gate outputs a logical high (vacuum) except when both inputs are high (vacuum), in which case the output is low (atmospheric pressure). This behavior is evident from the graph, where the output pressure remains high when either or both control signals are low and drops to low when both control signals are high. The data demonstrates the correct operation of the NAND gate in converting pneumatic control signals into the expected logical output.

4.4.2 NOR-NOT Integration

To automate the process of droplet generation in the desired order of (probe, sample) and (probe, reference), a four-stage program (1000, 0101, 1000, 0011) is required for 4 different valve controls (oil, sample, reference, probe) as illustrated on **Table 03**. In pursuit of eventually controlling our devices completely electronic powerless as discussed in goal 03, two digital control lines

were employed - instead of four separate ones- as we accomplish the four-stage program. A NOR and NOT gate in series (**Figure 4.9 (b)**) should logically convert the two solenoid controls into four time-resolved pulses. The two digital controls, along with actuating sample and reference valves, are simultaneously sent as inputs to the NOR gate. Output of the NOR gate controls the oil valve, making sure that oil flows only when neither sample nor reference is flowing. To ensure a probe drop is formed with each sample and reference drop, a split output of the NOR gate is sent as input to a NOT gate, the inverted output of which is sent to control the probe valve.

Therefore, the integrated pneumatic circuit is intended to generate the logic statement {((s OR r) AND p) NOT o} and therefore produce droplets in desired pairs of (probe, reference) and (probe, sample) with each pair remaining separated by a certain amount of oil to prevent undesired coalescence before dedicated merging downstream. The desired pneumatic logic combination was first tested for electronic circuits (**Figure 4.9 (a)**) by a free web application (falstad.com/circuit), based on a P-channel metal oxide semiconductor field effect transistor (p-MOSFET) analogy, where the gate is considered as the control channel, as flow proceeds from the source to the drain.

Constant voltage sources are tested against different resistance values with necessary capacitors and ground connections to produce real time current flow in desired direction and rate, thus predicting the role of a pneumatic analog in controlling fluidic flow. The response of a current

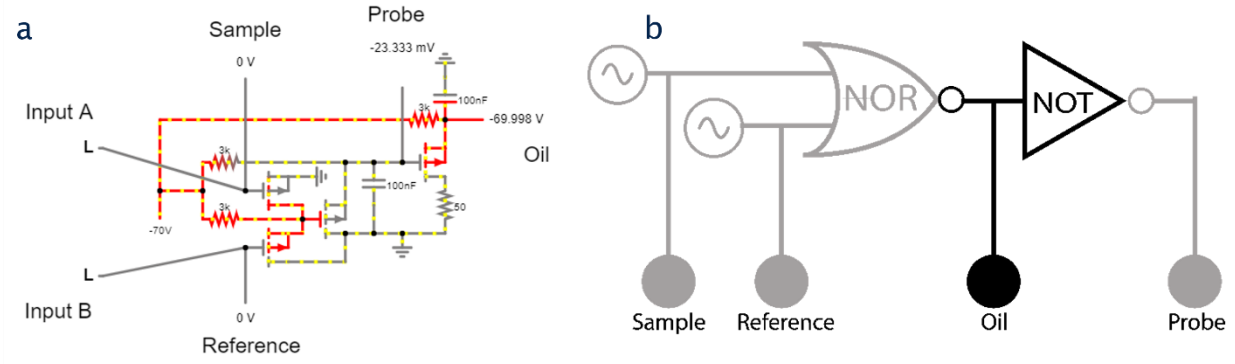

Figure 4.9. Schematic of (a) the electronic circuit and (b) its equivalent pneumatic circuit proposed to automate a 4-step droplet program using only two electronic controls.

flow, I, against voltage, V, and electrical resistance, R_E, from Ohms law $V = I*R_E$ is respectively analogous to volumetric flow rate, Q (mm^3s^{-1}), pressure difference, ΔP (kPa), and hydrodynamic resistance, R_h (kPa s mm^{-3}) in the Hagen-Poiseuille Law $\Delta P = Q*R_h$. Pneumatic counterparts with optimized channel dimensions, valve controls and atmospheric connections are designed accordingly to actuate a pneumatic flow of desired rate.[41-43]

Table 3: Truth table for NOR-NOT integration

Digital Control 1	Digital Control 2	NOR	NOT	Output
0	0	1	0	Oil
1	0	0	1	Sample, Probe
0	0	1	0	Oil
0	1	0	1	Reference, Probe

4.4.3 Complete Pneumatic Automation

A Falstad simulation of the electronic circuit designed to emulate the behavior of a complete pneumatic automation system is lustrated in Figure 4.10. This simulation includes various logic gates and control lines, mimicking the operations that will be later translated into a microfluidic design using CAD tools. The electronic logic gates, such as NAND, NOR, and NOT, process input voltages to produce specific outputs, which are then used to control the microfluidic logic gates in the

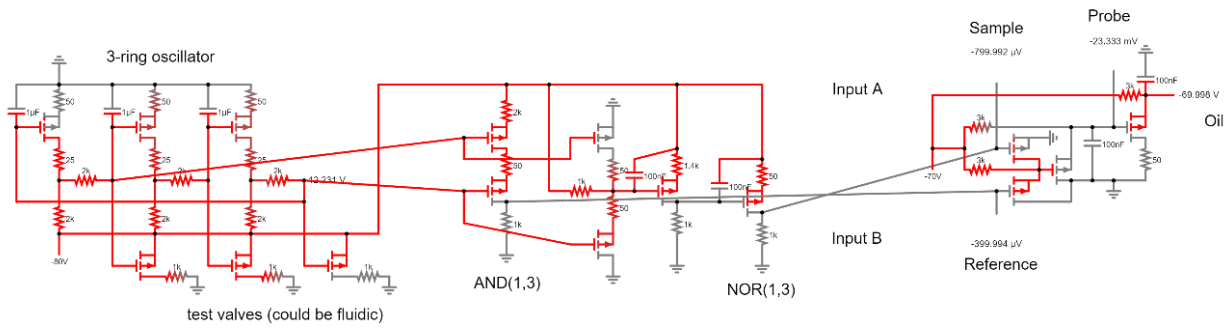

Figure 4.10 Electronic Simulation of Complete Pneumatic Automation Circuit

final design. This approach ensures the efficient transition from electronic to pneumatic systems, enabling the automation of complex droplet generation processes in a microfluidic device.

The pneumatic logic circuit designed for electronics-free automation of a four-step droplet generation process is illustrated in **Figure 4.11**. Below a breakdown of the components and their functions:

1. **5-Ring Oscillator:** This component generates a continuous sequence of pulses. It serves as the timing element, initiating the control signals for the entire system.
2. **Pulse 1 and Pulse 3:** The red and blue lines represent alternative pneumatic control pulses (pulse 1 and pulse 3) carrying vacuum and atmospheric pressure signals from the oscillator to the phase optimization part of the circuit.
3. **NAND Gate:** This gate takes inputs from the oscillator pulse, combining their signals. In this

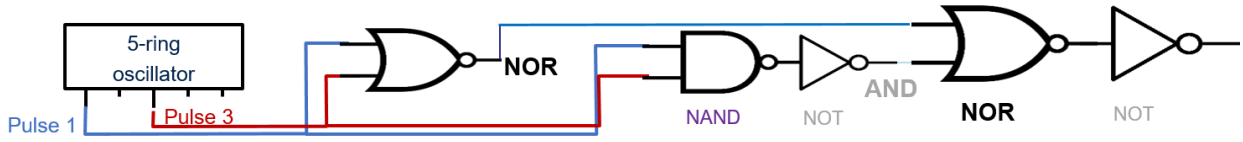

Figure 4.11. The proposed pneumatic logic circuit for electronics-free automation of the 4-step droplet automation.

   logic gate, the output is high (vacuum) unless both inputs are high (vacuum), in which case the output is low (atmospheric pressure).
4. **NOT Gates:** These invert the signals from the NAND gate and possibly other control lines. When the input is high (vacuum), the output is low (atmospheric pressure), and vice versa.
5. **AND Gate:** Combines multiple control signals. The output of the AND gate is high (vacuum) only when all inputs are high (vacuum).

This configuration allows for a sequence of pneumatic signals to control the automation process without the need for electronic components, making it suitable for environments where electronics might be impractical.

Table 4: Truth table for complete pneumatic oscillation

Oscillator Pulse 1	Oscillator Pulse 2	AND	NOR	Output
0	0	0	1	Resolved 1
1	0	0	0	0
0	1	0	0	0
1	1	1	0	Resolved 2

4.4.4 Applications

4.4.4.1 Single Aqueous Phase Droplet Generation in Oil

Successful actuation of the normally closed valves is shown in **Figure 5** where 8-bit imaging intensity at the valve actuation region is plotted against time to demonstrate consistent opening and closing of a valve. The proposed fabrication method is then applied to develop a single aqueous-in-oil droplet generator and to automate the process with an on-chip pneumatic inverter, powered

Figure 4.12. Vacuum actuated signals deflecting a thin PDMS membrane from a 5-ring pneumatic oscillator (a) before and (b-d) after phase-optimization.

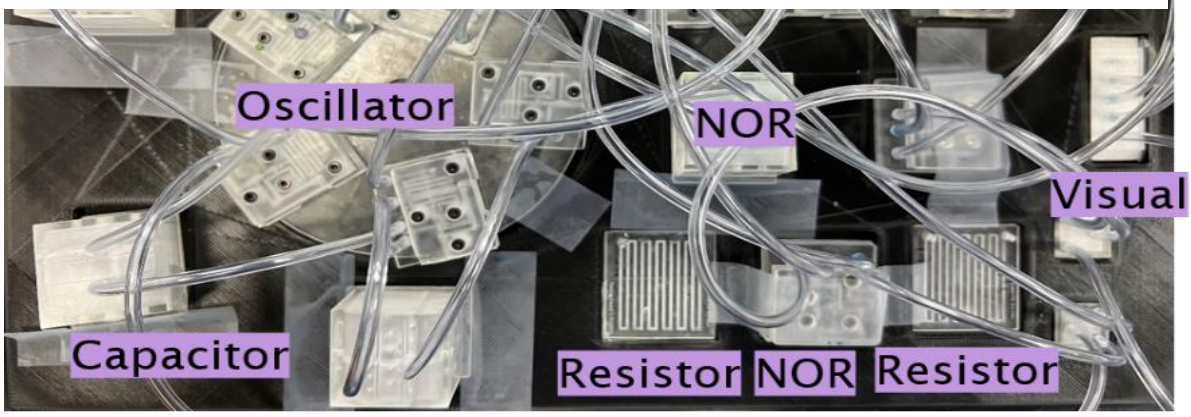

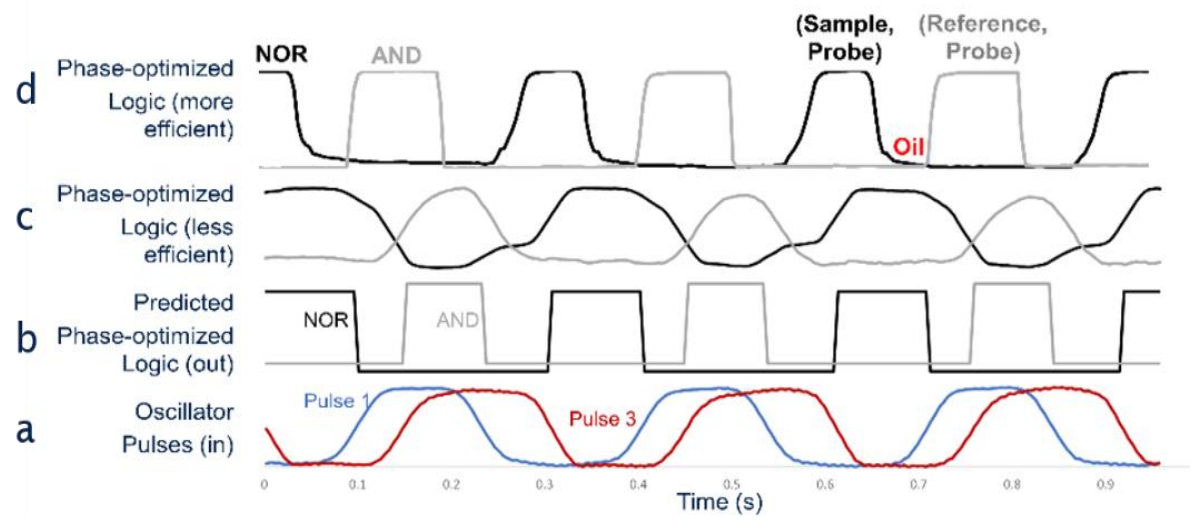

Figure 4.13 Step by step phase optimization of oscillator pulses

by a single electronic pulse, to alternatively actuate the oil and aqueous flow and therefore providing required control over the droplet size and frequency, as demonstrated in **Figure 4.14**.

The following approach incorporated an additional NCV-controlled aqueous input to form sample and reference droplets. Two solenoid valves were LabVIEW programmed to alternatively actuate the sample and reference valves, thus enabling continuous calibration of sample droplets with time-stamped reference droplets. An on-chip NOR gate was introduced to open the oil valve

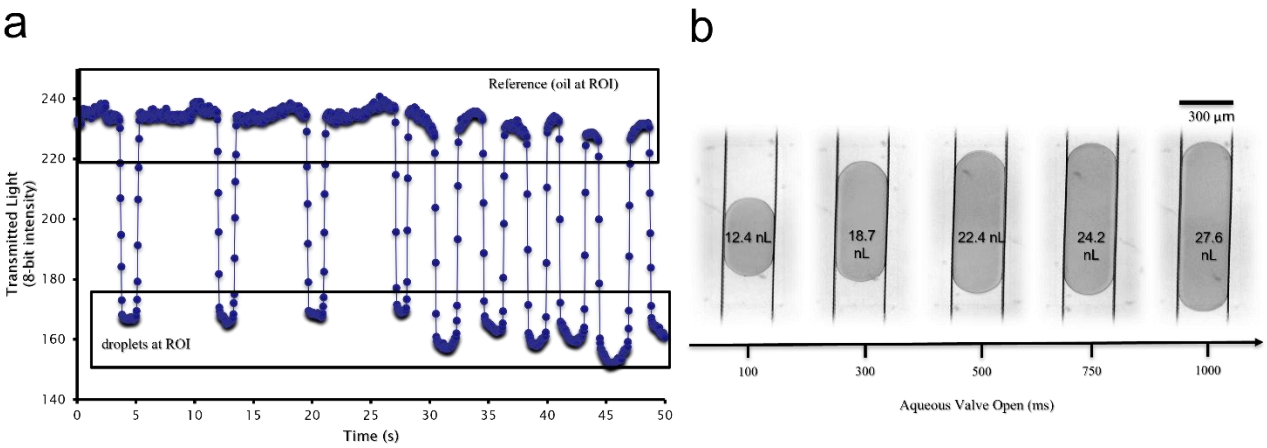

Figure 4.14. (a) Control over droplet generation frequency and (b) microscopic images of droplets controllably formed varying valve opening time.

only when both the sample and reference valves were closed.

4.4.4.2 Alternating Sample and Reference Segmentation

4.4.4.3 Adding Probe to Sample/Reference Droplets

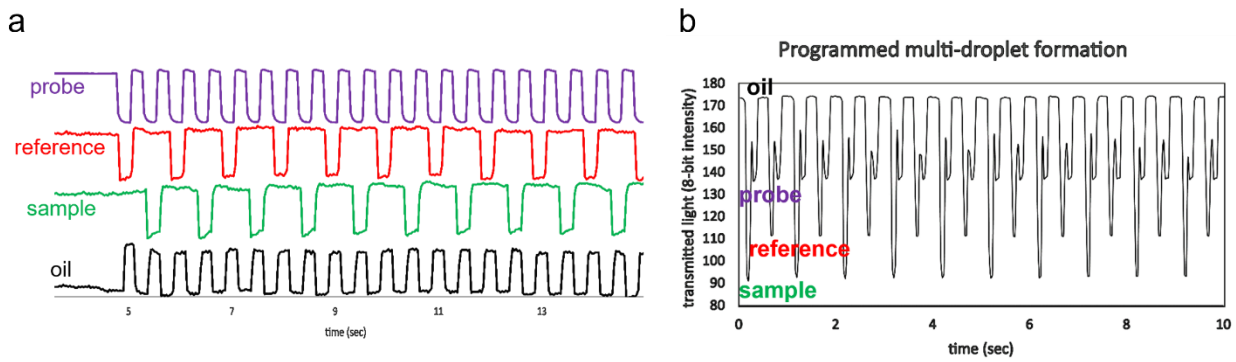

Figure 4.15 (a) Vacuum actuation signals deflecting a thin PDMS membrane, recorded with high-resolution (30 fps) iPhone 13 pro camera using standard laboratory room light. (b) Colorimetric detection of droplets formed at desired order, captured with Nikon 1J (400 fps) coupled with 4X lens.

4.5 Conclusions

In this chapter, we explored the development and implementation of pneumatic automation systems for droplet-based microfluidics. Our focus was on creating a fully automated, electronics-free microfluidic control system using pneumatic logic gates and oscillators. Here are the key conclusions drawn from our work:

Advancements in Pneumatic Control: Pneumatic control systems offer precise and reliable manipulation of droplets in microfluidic devices. The integration of pneumatic micro-pumps and valves enhances high-throughput experimentation by eliminating the need for syringe pumps and reducing dead volumes.

Open-Source and Modular Designs: We highlighted the potential of open-source solutions, such as the pneumatic pressure control system developed by Gao and Hébert, to democratize access to high-performance, affordable microfluidic technologies. These systems are designed using widely

available components and open-source software, making them accessible to a broader range of researchers.

Pneumatic Logic Gates: We successfully developed and characterized fundamental pneumatic logic gates, including NOT, NOR, and NAND gates. These gates were crucial for creating a sequence of operations needed for droplet generation and manipulation. The pneumatic NOT gate effectively inverted pressure signals, while the NOR gate produced a high output only when both inputs were low, and the NAND gate maintained a high output unless both inputs were high.

Integration and Automation:

- By integrating NOR and NOT gates, we automated the process of droplet generation with reduced electronic controls. This integration allowed for precise droplet formation and separation, essential for applications requiring high precision and consistency.
- The use of a 5-ring pneumatic oscillator and AND-NOR integration circuits enabled the development of a completely pneumatically automated system. This system demonstrated the potential to operate without electronic components, making it suitable for environments where electronics may be impractical.

Applications and Validation:

- The automated system was validated through the successful generation of single aqueous phase droplets in oil, as well as the alternating segmentation of sample and reference droplets. These results confirm the system's capability to perform complex droplet manipulations autonomously.

- The developed pneumatic automation techniques offer significant improvements in cost-effectiveness, portability, and scalability compared to traditional electronic systems.

In conclusion, our work demonstrates the feasibility and advantages of using pneumatic automation for droplet-based microfluidic systems. The developed techniques provide a robust and flexible platform for high-throughput biochemical assays, material synthesis, and single-cell studies, paving the way for broader applications and innovations in microfluidics.

Chapter 5

Development of an Integrated Valve Control and Monitoring Framework with User-friendly Interface

*(**Special acknowledgement:** The author would like to extend sincere gratitude to the artificial intelligence platforms that significantly contributed to the development of the software system described in Chapter 5 of this dissertation. The assistance provided by ChatGPT, Copilot, and Google Gemini was invaluable in crafting and refining the complex code required for this project.*

ChatGPT: Its advanced language processing capabilities were instrumental in generating insightful and accurate code snippets, debugging, and providing explanations that enhanced the author's understanding and facilitated efficient problem-solving throughout the development process.

Copilot: Its context-aware coding suggestions streamlined the writing of numerous functions and modules, significantly accelerating the development timeline. Copilot's ability to anticipate coding needs and offer relevant suggestions was particularly beneficial in overcoming various programming challenges.

Google Gemini: Its powerful machine learning algorithms and comprehensive coding assistance played a crucial role in optimizing and testing the software. Google Gemini's contributions ensured that the system was robust, efficient, and capable of meeting the project's objectives.

The author acknowledges these platforms for their indispensable support and contributions, which have been crucial in the successful completion of this project.)

5.1 Background

The significance of microfluidics lies in its unparalleled ability to create controlled environments for manipulating small biological and chemical samples, enabling precise control over biochemical conditions and reactions[158]. This precision is vital for various applications ranging from biological assays to chemical synthesis, where the ability to control and monitor reactions at such a small scale can lead to significant advancements in both fundamental research and practical applications. The core of microfluidic technology is the precise control and monitoring of fluid flow within the microchannels of the devices. This control is essential for the success of a wide array of experiments and applications, such as drug development, diagnostics, and environmental monitoring. One of the fundamental components in these setups is the valve control system, which directs fluid flow and manages the mixing of reagents. The ability to automate these processes is crucial for ensuring reproducibility and scalability[159]. Effective valve control not only enhances the efficiency and reliability of microfluidic devices but also expands their functionality, enabling complex and high-throughput experiments that would be challenging to perform manually.

Moreover, real-time monitoring and data visualization are critical components of modern microfluidic systems. These capabilities enable the immediate assessment of experiments and

processes within microfluidic devices, allowing researchers and technicians to make timely adjustments based on real-time data. This real-time feedback loop can significantly enhance the outcomes and efficiency of microfluidic experiments by optimizing parameters on-the-fly and ensuring that experiments are conducted under the best possible conditions[160]. The integration of real-time monitoring with data visualization tools provides a comprehensive view of the ongoing processes, facilitating better decision-making and more precise control over the experimental conditions.

In response to the growing needs for enhanced control and visualization in microfluidic applications, this chapter focuses on the development of an integrated software system designed to improve the control and visualization of microfluidic processes. This system addresses several gaps in current technologies by offering a robust and user-friendly interface for controlling microfluidic valves and visualizing the flow and reaction results in real-time. The development of this software system involves creating sophisticated algorithms and interfaces that allow for precise valve control, real-time data acquisition, and dynamic visualization of experimental outcomes. By improving the monitoring and control of microfluidic experiments, this project aims to significantly advance research and development in fields that rely heavily on microfluidic technologies.

The implications of developing such integrated systems extend beyond academic research. They have the potential to facilitate the broader adoption of microfluidic technologies across various industries. For instance, in the biomedical field, improved microfluidic systems can lead to the development of more efficient diagnostic devices that require minimal sample volumes and provide rapid results. In pharmaceuticals, microfluidic systems can be used to conduct high-throughput screening of drug candidates, accelerating the drug discovery process. In environmental engineering, microfluidic devices can be employed for real-time monitoring of pollutants and

other environmental parameters[161162]. By addressing the need for precision, efficiency, and adaptability, the project contributes to the ongoing revolution in scientific research and industrial processes, positioning microfluidics as a cornerstone technology in the 21st century.

5.2 Objective

The goal of this project was to develop and test a system capable of generating aqueous droplets in an oil stream with precise control over the droplet size and timing. This is achieved by alternating the actuation of oil and aqueous valves based on real-time feedback from a region of interest (ROI) at a microfluidic T-junction. The system aims to demonstrate the feasibility of using automated feedback control for consistent and repeatable droplet formation in a lab-on-a-chip device. The ultimate goal is to develop an integrated software system that enhances the control and visualization capabilities of microfluidic experiments. This system aims to:

1. Provide precise control over microfluidic valves to manage fluid flow within microchannels.
2. Integrate real-time monitoring and data acquisition to facilitate immediate assessment and adjustments during experiments.
3. Offer dynamic visualization tools that provide a comprehensive view of ongoing processes, aiding in better decision-making and experimental optimization.
4. Create a user-friendly interface that simplifies the interaction with the microfluidic system, making advanced control and monitoring accessible to a broader range of users.

5.3 Materials and Methods

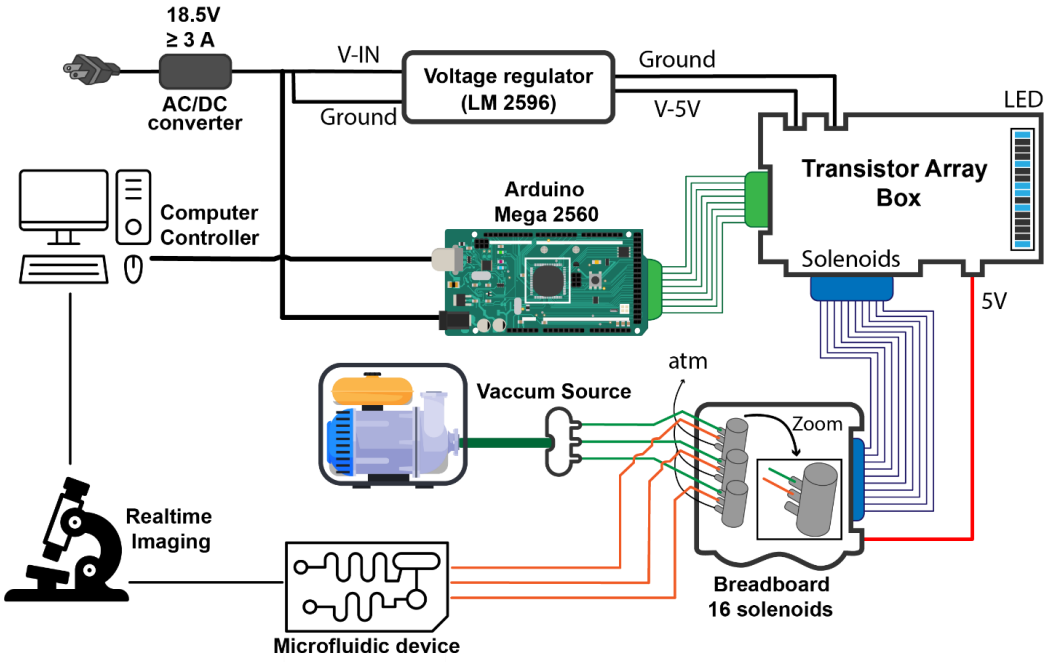

Figure 5.1 Schematic of a computer vision controlled closed-loop microfluidic control system

Backend Development

The software system designed for controlling microfluidic experiments leverages Python, a programming language acclaimed for its readability and extensive library support. The system integrates advanced features such as serial communication, computer vision, and closed-loop automation to create a comprehensive control environment for microfluidic experiments. This section provides a detailed overview of the integration of these components:

Python and PyQt Framework

The core of the software is developed using Python, with PyQt—a set of Python bindings for the Qt application framework—used to create the graphical user interface (GUI). PyQt enables the development of professional, responsive interfaces that integrate elements such as buttons, charts,

and live video feeds essential for real-time monitoring and control. This facilitates a user-friendly experience, allowing researchers to interact seamlessly with the microfluidic system.

Serial Communication

Serial communication is critical for interfacing with hardware devices like pumps and valves, which are controlled by an Arduino microcontroller (Arduino Uno, Arduino, Somerville, MA, USA; Arduino Store). The pySerial library in Python enables this functionality, allowing the software to send commands to and receive responses from the microcontroller. For instance, commands to open or close a valve are sent as serial messages constructed in Python and transmitted through the connected COM port. Robust error handling mechanisms are implemented to manage communication failures or disconnects, ensuring reliable operation (PySerial Documentation).

Computer Vision

Computer vision capabilities are integrated using the OpenCV library, renowned for its real-time image processing capabilities. OpenCV processes video or image data to identify and analyze regions of interest (ROIs), such as droplets. Metrics including size, shape, and intensity are measured and can trigger automatic adjustments in the system, such as modifying flow rates or chemical concentrations based on detected changes. This allows for precise and automated control of the microfluidic environment.

Closed-Loop Automation

Closed-loop automation is a sophisticated feature where the system continuously adjusts outputs (e.g., valve states, flow rates) based on real-time sensor data or image analysis results to maintain optimal experimental conditions. Python threads or QThread (from PyQt) manage background tasks such as data monitoring and device control, ensuring the GUI remains responsive. These

threads process data, update GUI elements, and execute control commands concurrently, enabling real-time adjustments and dynamic responses to experimental conditions.

Integration and Coordination

The main Python application coordinates all elements, with the GUI serving as the command center. It handles user inputs and displays system status and analysis results. Background threads manage time-intensive tasks, maintaining GUI responsiveness. Event-driven programming allows the system to efficiently react to user actions, sensor outputs, or scheduled events, ensuring smooth and effective operation.

Data Management

Efficient data management is crucial for analysis and reporting. Python libraries like Pandas and CSV support data storage, management, and analysis. The system can save data in various formats, facilitate quick retrieval, and enable comprehensive data visualization. This ensures that all experimental data is accurately recorded, easily accessible, and ready for detailed analysis.

This integrated approach ensures high precision and efficiency in microfluidic experiments, adapting dynamically to changing experimental conditions. The advanced control and visualization capabilities significantly enhance the performance and reliability of microfluidic systems, supporting both research and industrial applications.

The Frontend

The core of the software is structured around three main tabs: Pre-Analysis, Real-Time Analysis, and Post-Analysis, each tailored to specific phases of the experimental workflow:

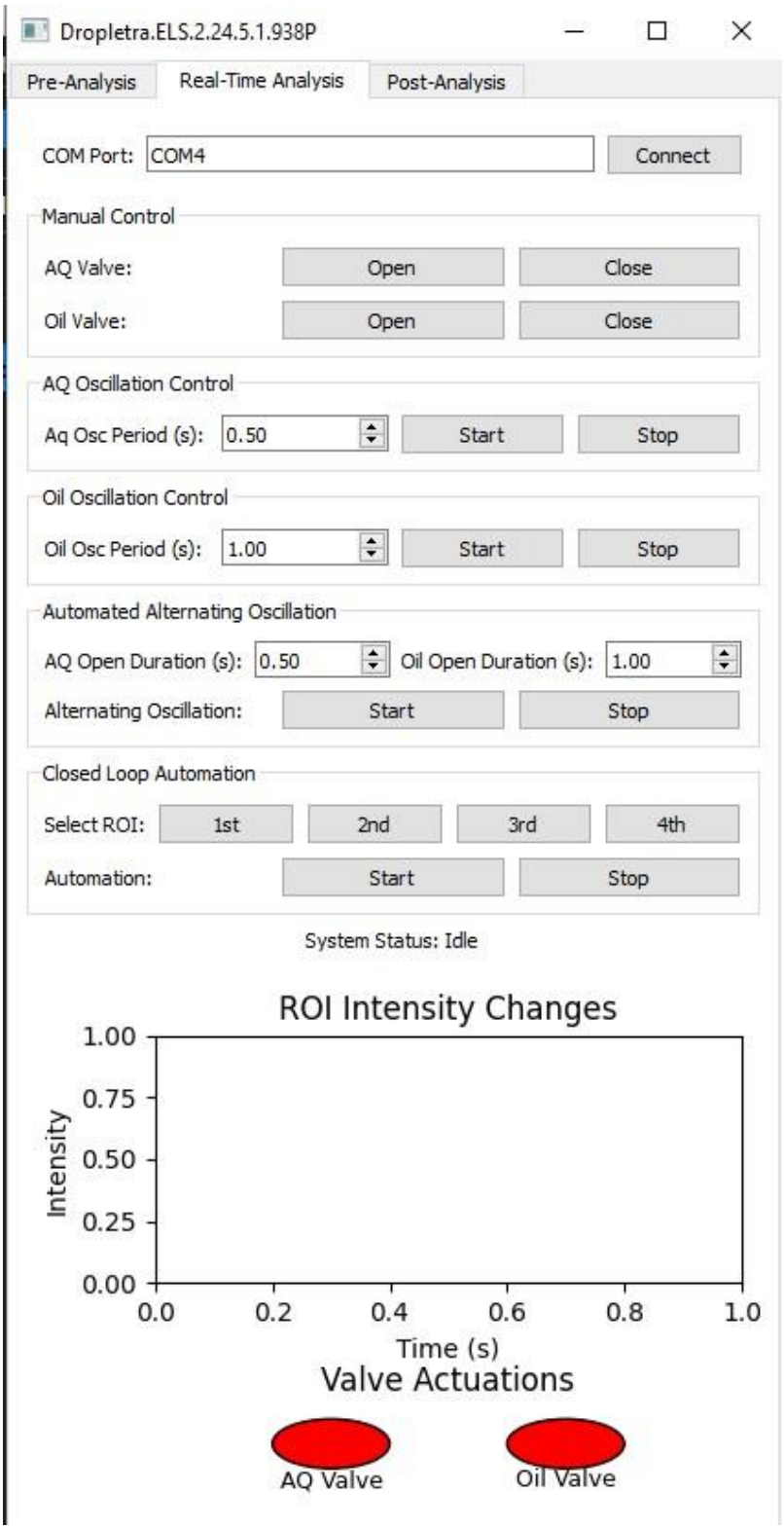

Figure 5.2 GUI for single aquoues in oil droplet control

Pre-Analysis Tab: This tab facilitates the initial setup, allowing users to configure droplet generation parameters such as size, intensity, and quantity through intuitive controls. This preparatory stage is crucial for standardizing the initial conditions of experiments.

Real-Time Analysis Tab: The focal point of the software, this tab provides real-time control and monitoring of the experiments. As illustrated in **figure 5.2**, it includes manual and automated valve control for precise fluid handling, integrated image analysis for on-the-fly adjustment based on ROI intensity, and live visual feedback through a plotting canvas. This section also incorporates advanced features like valve oscillation and closed-loop

feedback systems that react dynamically to changes in detected intensities, ensuring meticulous management of the microfluidic processes.

Manual and Automated Valve Control

The tab is equipped with both manual and automated valve controls, enabling users to manage fluid flows within the microfluidic device directly. Users can manually open or close valves to adjust the flow paths, which is useful for setting up experiments or making quick adjustments. The automated valve control extends this functionality by allowing the software to control valve states based on predefined conditions or in response to real-time experimental data. This dual-mode control ensures flexibility in experiment management, accommodating both static and dynamic experimental setups.

Integrated Image Analysis

A critical feature of this tab is its integrated image analysis capability. The software continuously analyzes images from the microfluidic device to detect regions of interest (ROIs) based on criteria such as droplet size, color, or intensity. Adjustments to the experimental conditions can be made on-the-fly, based on changes in the ROI data. For instance, if the intensity within a specific ROI falls below a threshold, the software can trigger valves to modify fluid flow to correct this variance.

Live Visual Feedback through Plotting Canvas

The tab also includes a plotting canvas that provides live visual feedback of the experiment. This feature plots various parameters such as fluid intensity, droplet size, and valve status over time,

offering a real-time graphical representation of the experiment's progress. This immediate feedback is invaluable for monitoring the experiment and making informed decisions quickly.

Advanced Features: Valve Oscillation and Closed-Loop Feedback Systems

One of the advanced features integrated into the Real-Time Analysis Tab is valve oscillation. This feature allows for the periodic opening and closing of valves at set intervals, creating oscillations in fluid flow. Such oscillations can be useful in applications like droplet formation and mixing.

Moreover, the tab includes a sophisticated closed-loop feedback system. This system automatically adjusts the microfluidic device's operations in response to real-time changes in measured variables. For example, if the detected intensity of a fluid within a droplet deviates from a set target, the feedback system can adjust the flow rates or mix ratios automatically to bring the process back to the desired state. This dynamic adjustment is crucial for maintaining the integrity of the experiment under varying conditions and reducing the need for manual intervention.

Overall, the Real-Time Analysis Tab is designed to facilitate a high degree of control over microfluidic experiments, ensuring precision and adaptability. By integrating manual and automated controls, live data feedback, and advanced regulatory systems, it provides a robust platform for conducting sophisticated experiments in the field of microfluidics. This integration of advanced technologies enhances the capability to perform controlled and detailed experiments, thus pushing the boundaries of what can be achieved in microfluidic research.

The experiments were conducted using 3D-printed and assembled normally closed flow-controlled aqueous (AQ) and oil T-junction droplet generators. The setup consisted of three

separate configurations, each designed to explore different control mechanisms for droplet generation. The following describes the methodology and sequence of operations for each configuration:

Single AQ Valve Control:

Device Configuration: A single AQ valve controlled the flow of the aqueous phase, with no oil valve present.

Control Mechanism: The AQ valve was controlled using intensity measurements from two ROIs positioned downstream of the T-junction.

Dual Valve Control (One AQ and One Oil Valve):

Device Configuration: One AQ valve and one oil valve controlled the flow of the aqueous and oil phases, respectively.

Control Mechanism: The AQ and oil valves were controlled using intensity measurements from two ROIs positioned downstream of the T-junction, ensuring that when the AQ valve opened, the oil valve closed, and vice versa.

Triple Valve Control (Two AQ and One Oil Valve):

Device Configuration: Two AQ valves and one oil valve controlled the flow of multiple aqueous droplets and the oil phase.

Control Mechanism: The AQ and oil valves were controlled using intensity measurements from three ROIs positioned downstream of the T-junction, facilitating the generation of two AQ droplets separated by oil.

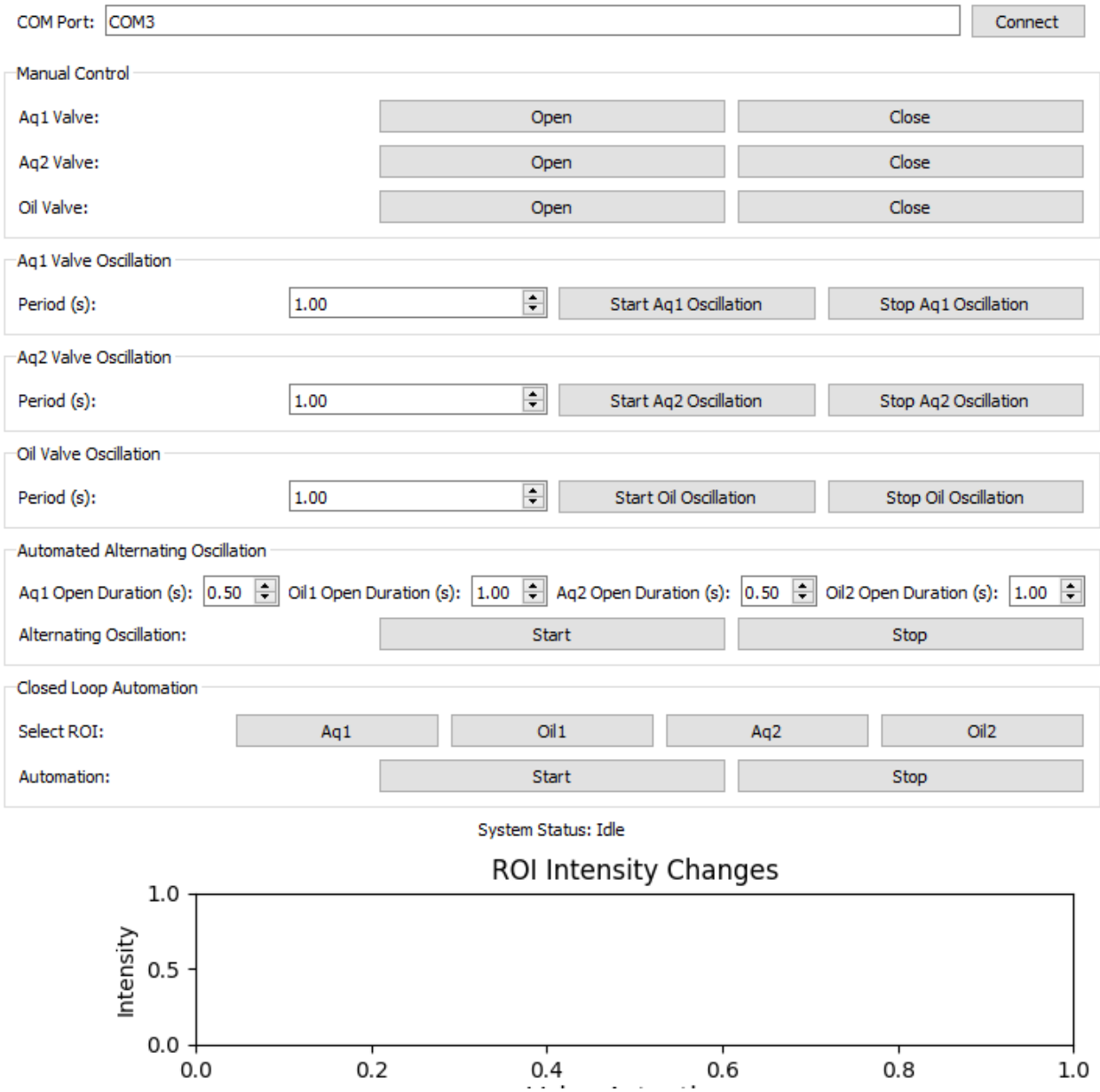

Figure 5.3 Graphical User Interface (GUI) for Automated Microfluidic System: This interface, developed using PyQt, allows for precise control and automation of solenoid valve actuation within the microfluidic setup. The GUI includes options for manual control of individual valves, oscillation of each valve with adjustable periods, and automated alternating oscillation with customizable open durations. The closed-loop automation feature allows selection of Regions of

Interest (ROIs) and initiates automated valve control based on real-time feedback. The system status and ROI intensity changes are displayed for monitoring the ongoing processes.

Hardware Setup

The system utilizes an Arduino microcontroller to manage the actuation of the valves that control the oil and aqueous flow. The Arduino is connected to a computer running a Python script that analyzes live video feed from a camera positioned at the T-junction. This camera monitors the ROI to determine the coverage of the aqueous solution within the oil stream.

Software Implementation

The Python script captures the ROI's live video feed and processes the images to detect the percentage coverage of the aqueous solution. Based on predefined thresholds (90%, 75%, 50%, and 25%), the script sends commands to the Arduino to open or close the aqueous and oil valves accordingly. The initial cycle begins with the oil valve opening for 5 seconds to establish an oil stream. Subsequently, the aqueous valve is actuated to form droplets, with the cycle's timing and sequence adjusted based on the ROI coverage observed.

Feedback Control Logic

The feedback control logic is implemented in the Python script, which continuously analyzes the ROI to adjust the valve actuations in real-time. This ensures that the droplets are generated according to the specified coverage thresholds, thereby achieving precise control over the droplet formation process.

5.3.1 Experimental

Single AQ Valve Control:

Initial Valve Opening: The AQ valve was initially kept open to allow the aqueous phase to flow until it reached ROI1. As the AQ phase reached ROI1, the intensity detected by ROI1 was high, indicating the presence of the aqueous fluid.

Detection and Valve Closure: When the intensity at ROI1 dropped from high to low, indicating the leading edge of the aqueous phase had passed, the AQ valve was closed, forming a discrete droplet within the continuous oil phase.

Detection by ROI2 and Valve Reopening: As the generated droplet moved downstream, it was detected by ROI2, which monitored the intensity. The intensity at ROI2 transitioned from low to high as the droplet passed, signaling the AQ valve to reopen for the next droplet generation cycle.

Dual Valve Control (One AQ and One Oil Valve)

Initial Valve Opening: The AQ valve was initially kept open to allow the aqueous phase to flow until it reached ROI1. Simultaneously, the oil valve was kept closed to prevent the oil phase from flowing.

Detection and Valve Switching: When the intensity at ROI1 dropped from high to low, indicating the leading edge of the aqueous phase had passed, the AQ valve was closed and the oil valve was opened, forming a discrete droplet within the continuous oil phase.

Detection by ROI2 and Valve Switching: As the generated droplet moved downstream, it was detected by ROI2, which monitored the intensity. The intensity at ROI2 transitioned from low to high as the droplet passed, signaling the AQ valve to reopen and the oil valve to close for the next droplet generation cycle.

Triple Valve Control (Two AQ and One Oil Valve)

Initial Valve Opening: The AQ valve was initially kept open to allow the aqueous phase to flow until it reached ROI1. Simultaneously, the oil valve was kept closed to prevent the oil phase from flowing.

Detection and Valve Switching: When the intensity at ROI1 dropped from high to low, indicating the leading edge of the aqueous phase had passed, the AQ valve was closed and the oil valve was opened, forming a discrete droplet within the continuous oil phase.

Detection by ROI2 and Valve Reopening: As the generated droplet moved downstream, it was detected by ROI2, which monitored the intensity. The intensity at ROI2 transitioned from low to high as the droplet passed, signaling the AQ valve to reopen and the oil valve to close for the next droplet generation cycle.

Second AQ Droplet Generation: The AQ valve remained open to generate a second AQ droplet. As the second droplet reached ROI1, the process repeated: the AQ valve closed, and the oil valve opened, separating the two AQ droplets with a segment of oil.

Third ROI for Second AQ Droplet: The third ROI (ROI3) was introduced to control the generation of the second AQ droplet. As the second AQ droplet moved downstream and was detected by ROI3, the AQ valve was closed, and the oil valve was opened to create a consistent separation between the two AQ droplets.

5.4 Results and Discussions

During initial testing, the system successfully alternated between the oil and aqueous valves to generate droplets at the specified coverage thresholds. The first cycle involved opening the oil

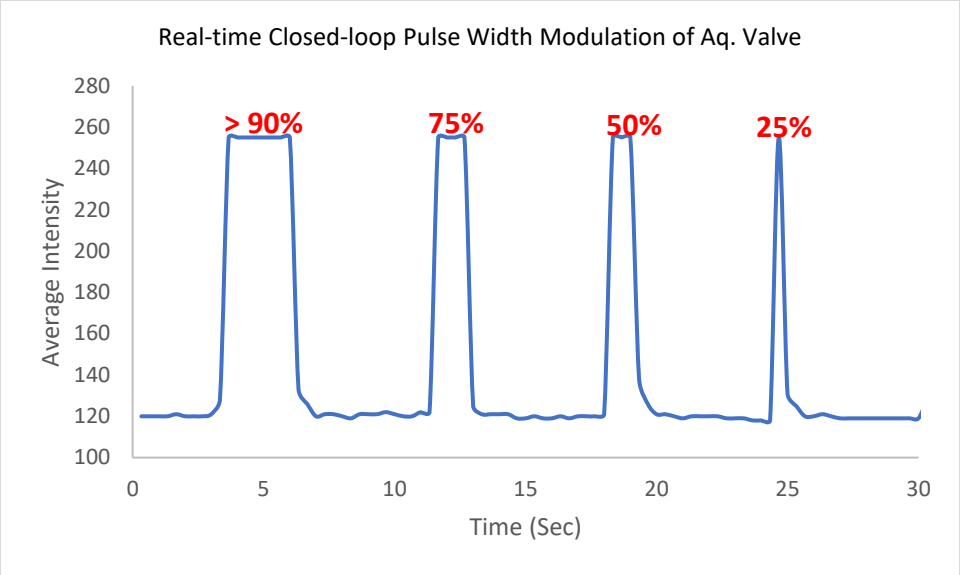

Figure 5.4 Closed-loop pulse width modulation

valve for 5 seconds, followed by the actuation of the aqueous valve until the ROI was 90% covered with the aqueous solution. Subsequent cycles adjusted the coverage thresholds to 75%, 50%, and 25%, demonstrating the system's ability to vary droplet sizes based on real-time feedback.

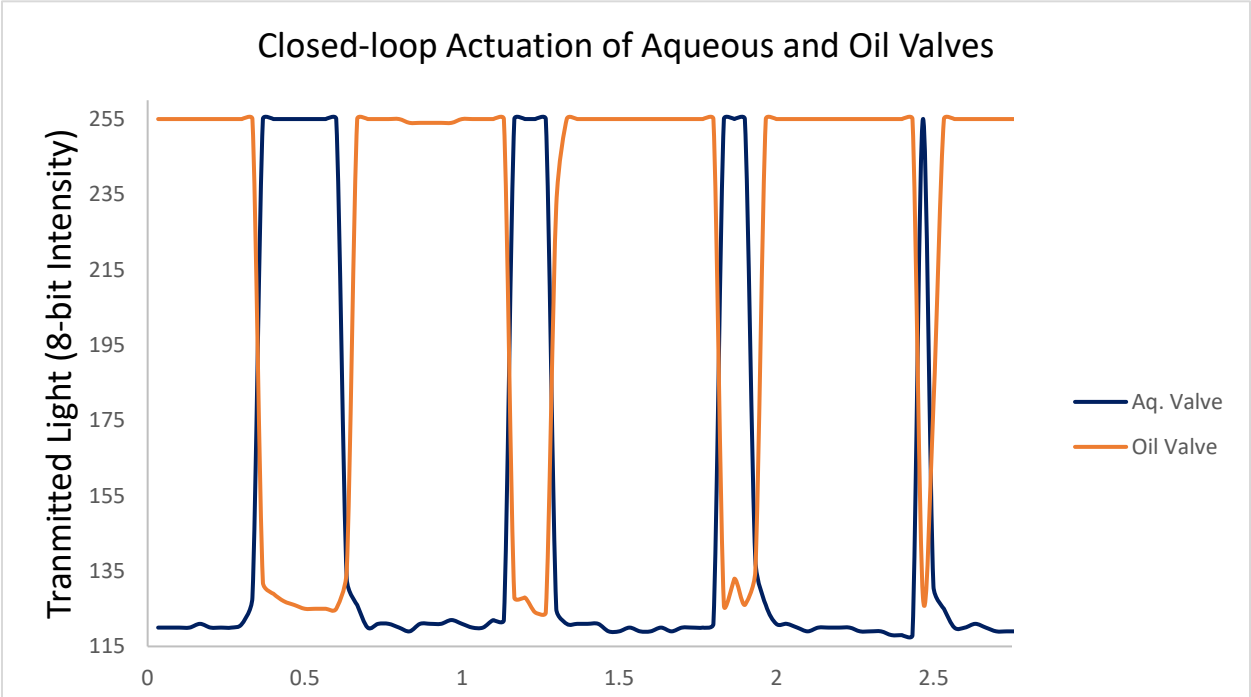

Figure 5.5 Closed-loop pulse width modulation for aq. and oil valve control

Visual observation and video recordings of the droplet formation process confirmed that the system could consistently generate droplets with the desired coverage within the ROI. The timing and sequence of valve actuations were found to be in accordance with the program's logic, validating the effectiveness of the feedback control system. Results are illustrated in **figures 5.4 and 5.5**.

Characterization of Closed-Loop Control

We then utilized the developed system to control size of droplets without any manual intervention. As shown in **figure 5.6** the system uses the first Region of Interest (ROI) to detect the presence of aqueous flow. Upon detection, the system automatically switches the aqueous valve to the "OFF" position and the oil valve to the "ON" position. This action initiates the formation of an oil segment that follows the aqueous phase.

The system utilizes the second ROI to detect the presence of the newly formed aqueous droplet. Once the droplet is detected, the system switches the aqueous valve back to the "ON" position and the oil valve to the "OFF" position, preparing for the next droplet formation cycle.

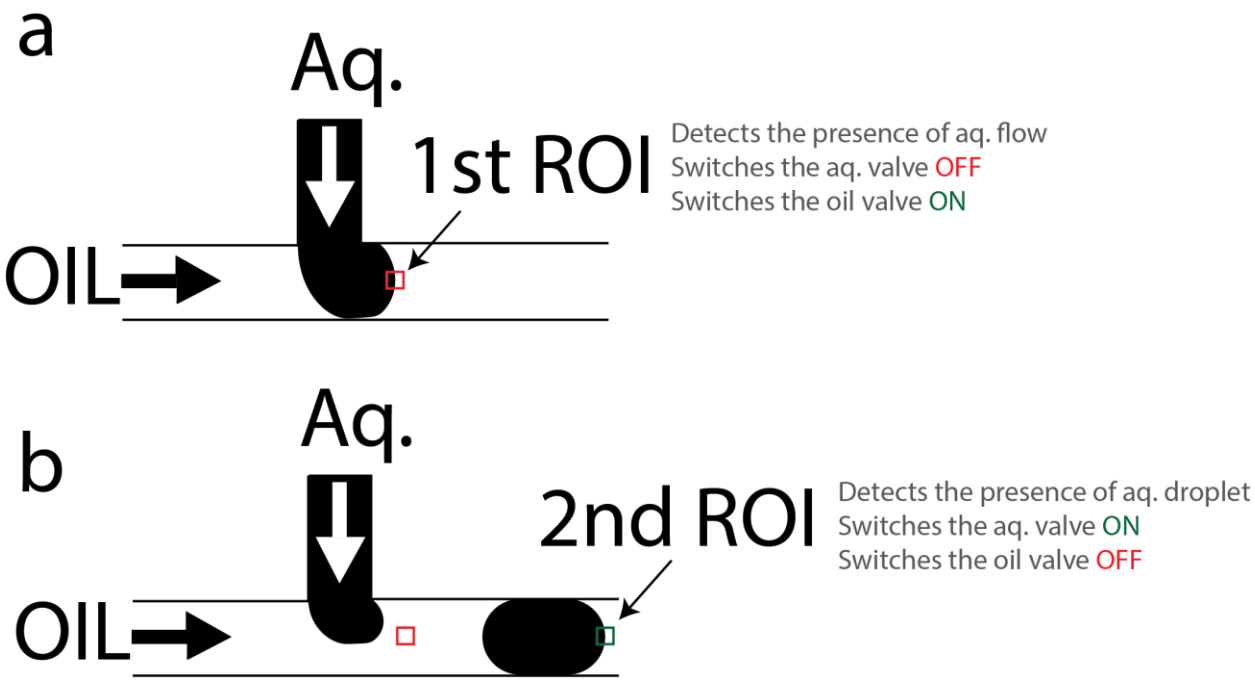

Figure 5.6 Computer-vision technique to actuate the aquous and oil valves for closed-loop control.

The data collected during the experiments provided insights into the intensity variations at all ROIs and the corresponding valve states. The following observations were made:

Intensity Measurements: ROI1, ROI2, and ROI3 Intensity: The intensity values at each ROI indicated the presence of the aqueous phase and the transition points for valve switching, ensuring proper generation and separation of the droplets.

Valve State Transitions: The 'Valve State' columns in the data recorded the binary states (1 for open and 0 for closed) of the AQ and oil valves, showcasing the precise control over the droplet generation process. The synchronization between the intensity readings and valve state transitions demonstrated the effectiveness of the control mechanisms.

Data Visualization

The data visualization plot below illustrates the ROI intensities and the corresponding valve states over time:

- The plot shows the intensity values for ROI1, ROI2, and ROI3, highlighting the moments when the AQ and oil valves were actuated.
- The binary valve state transitions are aligned with the intensity changes, confirming the control logic's accuracy.

The experiments successfully demonstrated the capability of the 3D-printed T-junction droplet generator to produce droplets with varying configurations of AQ and oil valves. The integration of real-time intensity monitoring using multiple ROIs and automated valve control facilitated

efficient and reproducible droplet generation. This system can be utilized for various applications in microfluidics, where controlled droplet generation is essential.

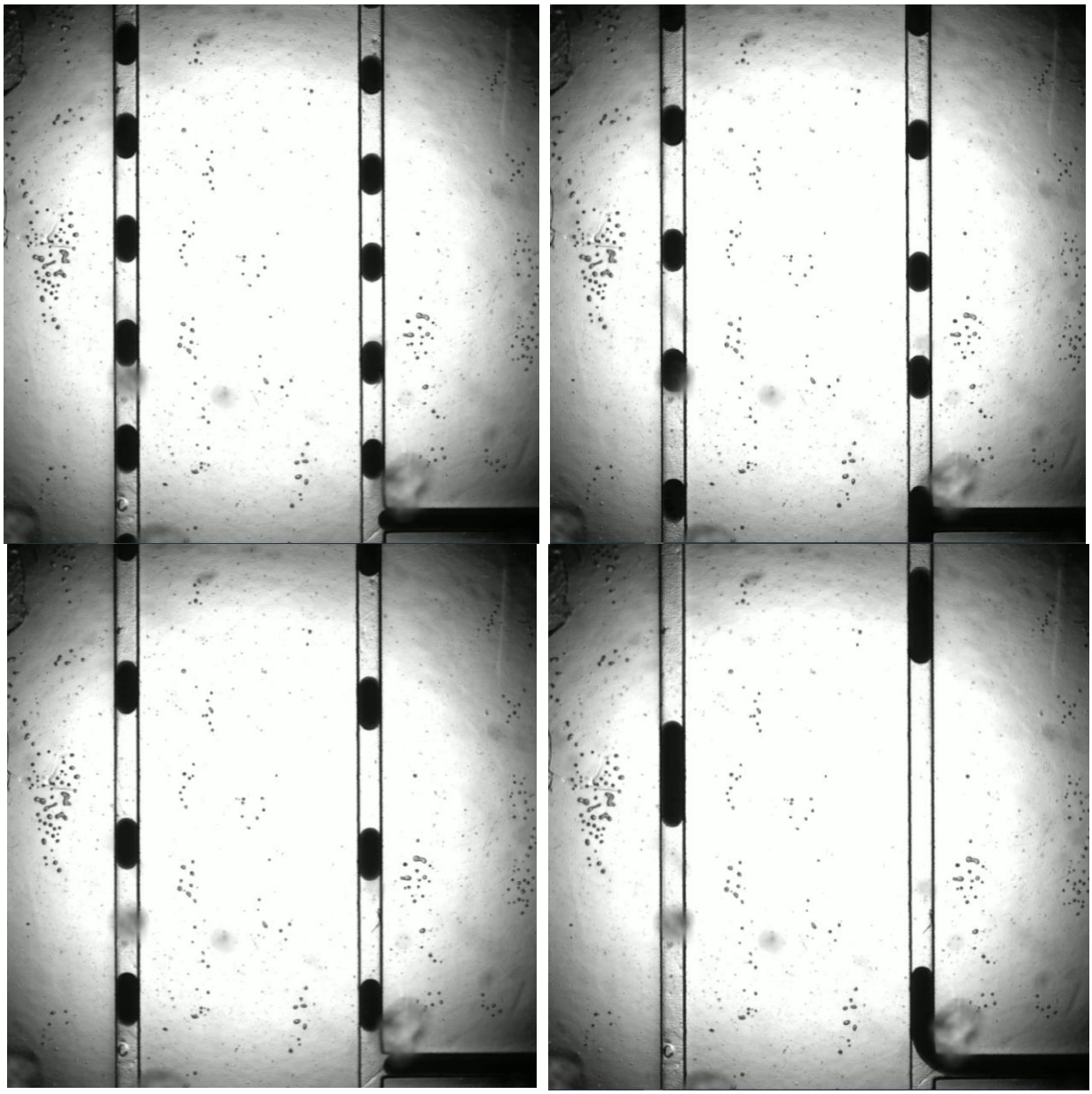

Figure 5.7 Progressive Increase in Droplet Spacing Through Enhanced ROI Differentiation. This series of images demonstrates the gradual increase in spacing between droplets achieved by systematically increasing the region of interest (ROI) difference. The images illustrate how precise control over the ROI can be used to manipulate droplet spacing effectively within a microfluidic device.

In **Figure 5.7**, we demonstrate the impact of adjusting the region of interest (ROI) on droplet spacing within a microfluidic device. This series of images shows the progressive increase in the spacing between droplets achieved by systematically increasing the ROI differentiation. By altering the ROI, the system can effectively manipulate the timing of valve actuation, thus controlling the distance between consecutive droplets. This precise control is crucial for applications requiring specific droplet volumes and spacing, such as in droplet-based assays and high-throughput screening. The images illustrate how fine-tuning the ROI can enhance the functionality and efficiency of droplet microfluidic systems.

The integrated software system was successfully implemented, providing a robust and user-friendly platform for the control and visualization of microfluidic processes. The system's functionality was evaluated across several key areas: droplet generation, real-time control, image analysis, and data management.

In **Figure 5.8**, the graph illustrates the relationship between valve actuation and the intensities recorded at two regions of interest (ROI1 and ROI2) over a 5-second period. The dashed orange line represents the state of the valve actuation, alternating between open (1) and closed (0). The solid blue line shows the intensity at ROI1, which directly correlates with the valve's open state, increasing when the valve is open and decreasing when it is closed. Conversely, the solid green line indicates the intensity at ROI2, which inversely correlates with the valve's state, decreasing when the valve is open and increasing when it is closed. This visualization demonstrates the system's control dynamics and response, highlighting how changes in valve actuation affect the intensities detected at specific points within the microfluidic channel, thus providing insights into the real-time control of droplet formation.

The Real-Time Analysis tab facilitated meticulous control over the microfluidic processes. Manual and automated valve controls enabled precise management of fluid flows. Automated controls, driven by real-time data, allowed the system to respond dynamically to changes in experimental conditions. Valve oscillation and closed-loop feedback systems maintained consistent

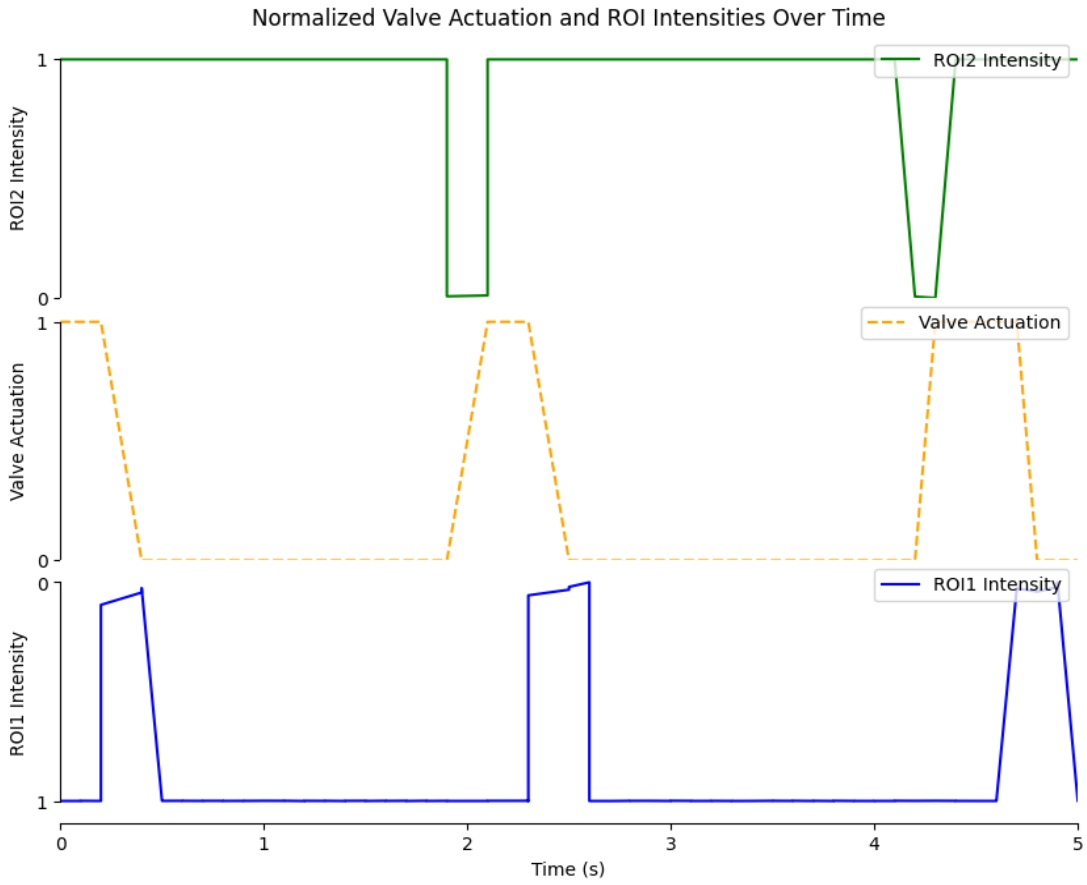

Figure 5.8 The relationship between valve actuation and the intensities recorded at two regions of interest (ROI1 and ROI2) over a 5-second period. The dashed orange line represents the valve actuation state, alternating between open (1) and closed (0). The solid blue line shows ROI1 intensity, which correlates directly with the valve's open state, while the solid green line shows ROI2 intensity, which inversely correlates with the valve's state. This visualization demonstrates the system's control dynamics and response.

experimental conditions by adjusting flow rates and mixing ratios automatically in response to real-time sensor data.

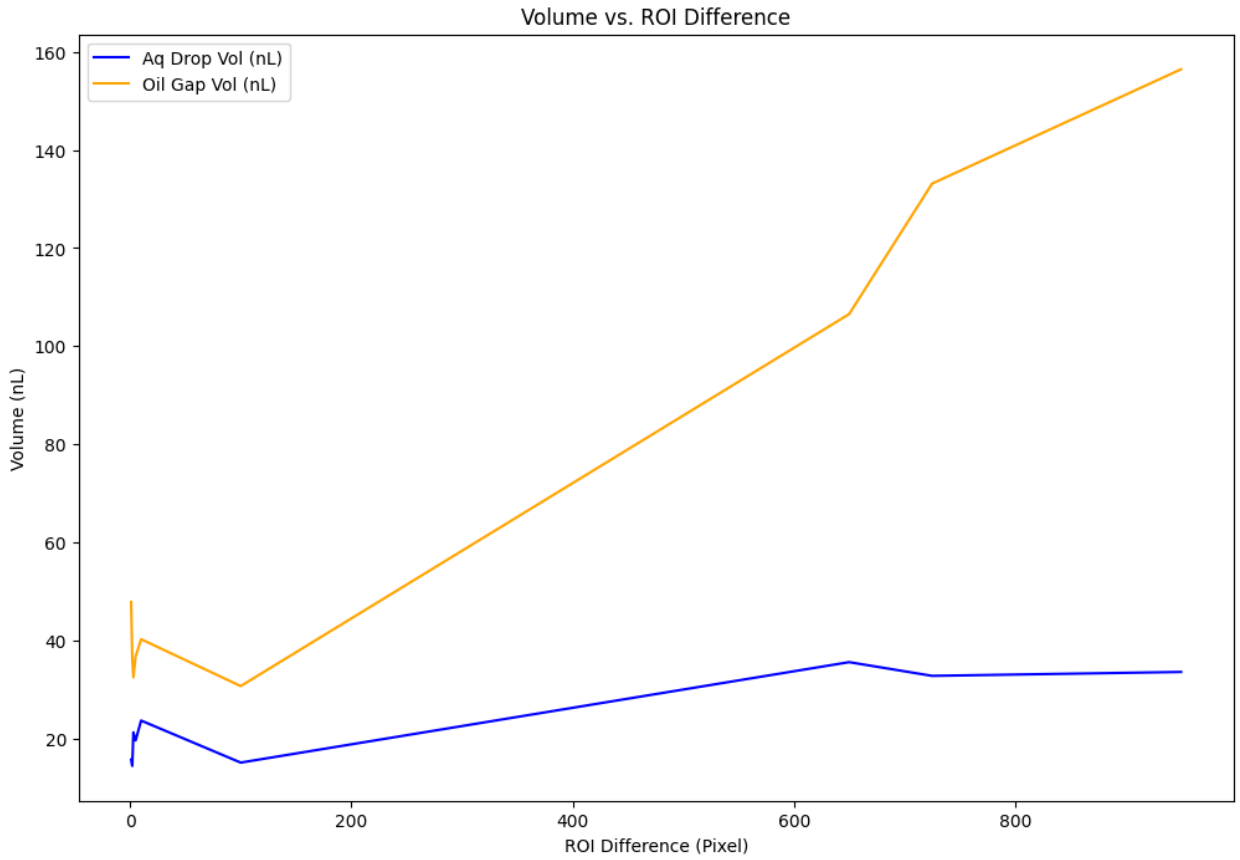

Figure 5.9 The plot illustrates the relationship between the volumes of aqueous droplets and oil gaps with respect to the difference in Regions of Interest (ROI) measured in pixels. The blue line represents the volume of aqueous droplets (Aq Drop Vol) in nanoliter (nL), while the orange line depicts the volume of oil gaps (Oil Gap Vol) in nanoliters (nL). The data shows that as the ROI difference increases, the volume of oil gaps also increases when the droplet volume remains within a narrow range.

In **Figure 5.9**, the plot illustrates the relationship between the volumes of aqueous droplets and oil gaps concerning the difference in Regions of Interest (ROI) measured in pixels. The blue line represents the volume of aqueous droplets (Aq Drop Vol) in nanoliters (nL), while the orange line depicts the volume of oil gaps (Oil Gap Vol) in nanoliters (nL). The data shows that as the ROI difference increases, the volume of oil gaps also increases, while the droplet volume remains

relatively stable within a narrow range. This indicates that adjustments in ROI difference can be used to control the spacing between droplets in a microfluidic system, allowing for precise regulation of fluidic flow dynamics.

Integrated Image Analysis: The integrated image analysis feature performed effectively, continuously monitoring the microfluidic device to detect regions of interest (ROIs). The software was

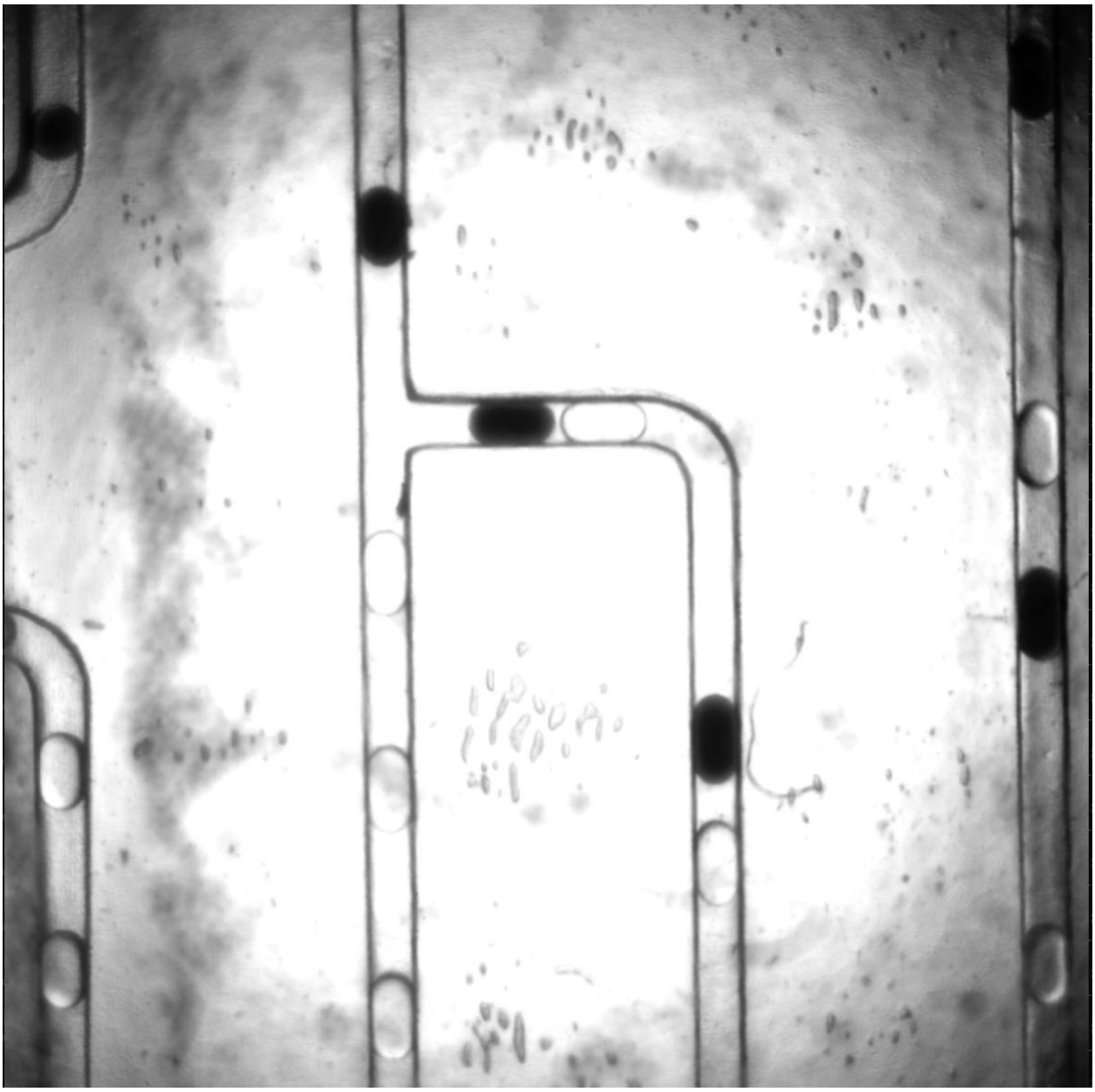

Figure 5.10 Control of two aqueous and one oil valve for alternating sample/reference flow using closed-loop automation

able to detect changes in droplet size, color, and intensity, and trigger appropriate responses, such as adjusting fluid flow. This capability significantly improved the precision and responsiveness of the system.

In **Figure 5.10**, the image depicts the control of two aqueous and one oil valve for alternating sample/reference flow using closed-loop automation. The microfluidic device shown utilizes precise valve actuation to manage the sequence and spacing of sample and reference droplets, interspersed with oil segments. This setup exemplifies the advanced control capabilities achieved through the integration of computer vision techniques and automated valve systems, allowing for highly controlled fluidic manipulation in microfluidic devices.

Live Visual Feedback: The plotting canvas provided real-time visual feedback, displaying parameters such as fluid intensity, droplet size, and valve status. This immediate feedback was invaluable for monitoring the progress of experiments and making informed decisions quickly. The

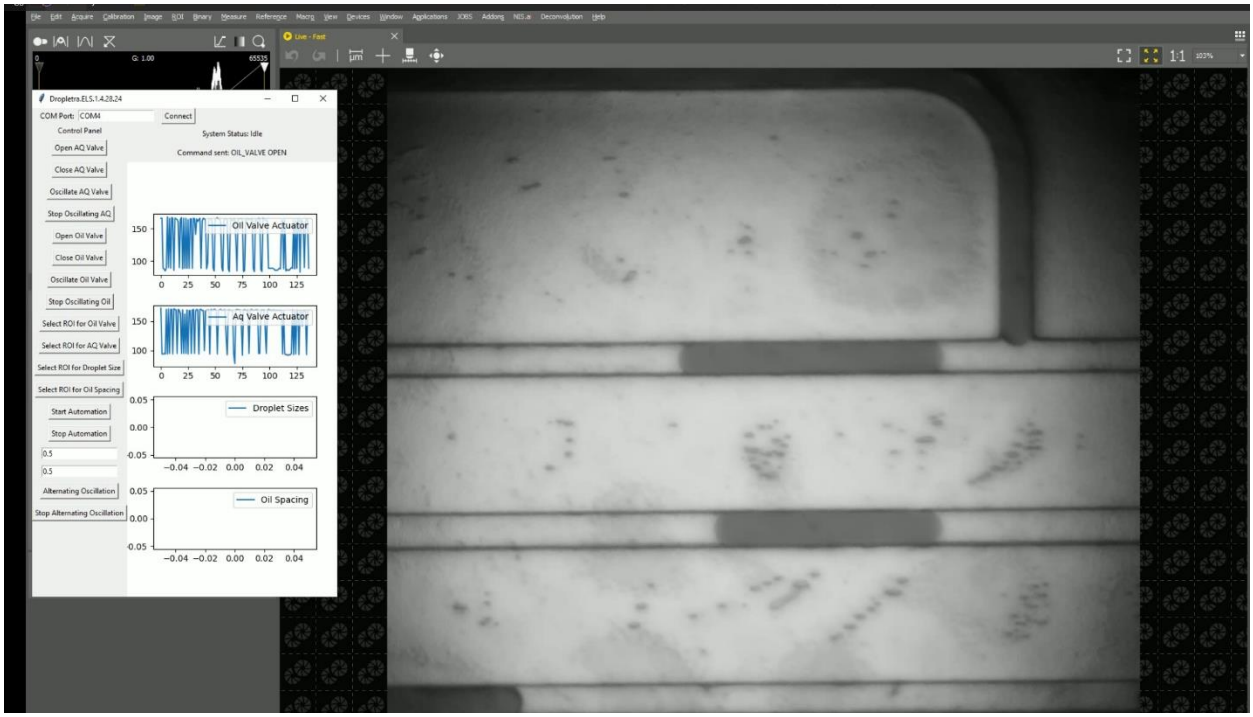

Figure 5.11 Screenshot view of real-time closed-loop control using the developed GUI

visual representation of data allowed for quick identification of any deviations from expected results, facilitating timely adjustments.

Figure 5.11 showcases the user interface of the custom software used to control the microfluidic system, alongside a live feed from the microfluidic device. The software interface displays real-time actuation data for the oil and aqueous valves, providing control over the timing and sequence of droplet generation. The graphical elements include plots of valve actuation states and droplet sizes, illustrating the system's dynamic response to control inputs. This setup allows for precise monitoring and adjustment of droplet and oil segment formation, essential for achieving consistent and reproducible fluidic operations in the device.

Enhanced Precision and Control: The ability to configure and control droplet generation parameters with high precision is crucial for standardizing initial conditions in microfluidic experiments. The system's ability to maintain droplet size within a narrow margin of error demonstrates its effectiveness in achieving consistent experimental setups. This level of control is essential for experiments requiring precise manipulation of biological and chemical samples.

Dynamic Real-Time Adjustments: The real-time control and monitoring capabilities provided by the Real-Time Analysis tab represent a significant advancement. The automated valve controls and closed-loop feedback systems allow the system to adapt dynamically to changes in experimental conditions, ensuring optimal performance and reliability. This adaptability is critical for experiments involving complex fluid dynamics and chemical reactions, where real-time adjustments can significantly impact the outcome[159].

Effective Image Analysis Integration: Integrating computer vision for real-time image analysis enhances the system's ability to monitor and respond to experimental conditions. The ability to

detect and analyze ROIs in real-time allows for automated adjustments that improve experimental precision and efficiency. This feature is particularly valuable in applications such as droplet-based assays and chemical synthesis, where accurate monitoring of droplet characteristics is essential[163].

Comprehensive Data Visualization and Management: Real-time visual feedback and robust data management capabilities ensure that researchers can monitor experiments effectively and document results comprehensively. The plotting canvas provides an intuitive visual representation of key parameters, facilitating quick decision-making and adjustments[164]. Efficient data management supports reproducibility and scalability, essential for advancing microfluidic research and applications.

Broader Implications for Research and Industry: The developed software system not only enhances experimental control and precision but also promotes the broader adoption of microfluidic technologies in various industries. By providing a user-friendly and adaptable platform, the system facilitates innovative applications in biomedical diagnostics,

pharmaceuticals, and environmental engineering. This project underscores the importance of integrating advanced technologies to push the boundaries of what can be achieved in microfluidic research.

The integrated software system developed for microfluidic experiments represents a significant advancement in the field, providing enhanced control, monitoring, and data management capabilities. The system's ability to dynamically adjust to real-time data ensures precise and efficient management of microfluidic processes. This project contributes to the advancement of microfluidic research and its application across various industries, demonstrating the critical role of technology integration in scientific innovation.

5.5 Conclusions

The development of an integrated valve control and monitoring framework with a user-friendly interface has been presented. The framework effectively addresses the challenges associated with precise fluid control, real-time monitoring, and data visualization, which are crucial for the success of various microfluidic applications.

The system demonstrated the capability to precisely control the generation of aqueous droplets in an oil stream by alternating the actuation of oil and aqueous valves. This precise control is essential for applications requiring accurate manipulation of biological and chemical samples.

Real-Time Monitoring and Dynamic Adjustments: The integration of real-time monitoring through a graphical user interface (GUI) allows for immediate assessment and adjustments during experiments. The ability to dynamically adjust valve states based on real-time feedback ensures optimal experimental conditions and enhances the reproducibility and reliability of microfluidic processes.

User-Friendly Interface: The development of a user-friendly interface using Python and PyQt enables researchers to interact seamlessly with the microfluidic system. The interface simplifies the setup, control, and monitoring of experiments, making advanced microfluidic technology accessible to a broader range of users.

The incorporation of computer vision for real-time image analysis enhances the system's ability to detect and respond to changes in experimental conditions. This feature, coupled with robust data visualization tools, provides a comprehensive view of the ongoing processes and facilitates better decision-making and experimental optimization.

In conclusion, the integrated valve control and monitoring framework developed in this project can provide a robust and adaptable platform for advancing microfluidic research and applications.

By addressing key challenges in fluid control, real-time monitoring, and data visualization, this system has the potential to drive significant advancements in biomedical diagnostics, pharmaceutical research, and environmental monitoring, positioning microfluidics as a cornerstone technology in the 21st century.

Chapter 6

Conclusions and Future Works

This dissertation explores the integration of electronics, pneumatics, and computer vision to advance the automation of droplet-based microfluidic systems. Through a series of experiments and developments, we have demonstrated how these interdisciplinary approaches can address the inherent limitations of current microfluidic methodologies, paving the way for innovative applications.

Summary of Findings:

1. **Design and Fabrication of Microfluidic Devices (Chapter 2)**:

In Chapter 2, we focused on the design and fabrication of microfluidic devices, employing polydimethylsiloxane (PDMS) as the primary material due to its favorable properties such as biocompatibility, transparency, and ease of molding. The fabrication process utilized 3D-printed templates, which allowed for precise and customizable microenvironments. This approach not only ensured the reproducibility of the devices but also demonstrated significant versatility in creating complex microfluidic structures tailored to specific experimental needs. The use of 3D-printed templates enabled rapid prototyping and iterative design modifications, facilitating the exploration of various microfluidic applications.

Additionally, we developed a serial communication-based valve control system that significantly advanced the operational capabilities of our microfluidic devices. This system was designed to execute multiple operations simultaneously, thereby enhancing the control over fluidic processes within the microchannels. By integrating a high-resolution pressure sensor into the system, we achieved accurate detection of rapid pressure changes, which is critical for the precise manipulation of fluids at the microscale. The enhanced functionality provided by this sensor allowed for

more responsive and dynamic control of the microfluidic environment, enabling sophisticated experimental setups that require real-time adjustments. Overall, the advancements in device fabrication and control systems established a robust foundation for further research and applications in microfluidics.

2. **Automation Using Computer Programming (Chapter 3)**:

In Chapter 3, we explored the automation of microfluidic droplet generation and manipulation by implementing a 'normally closed' valve system. This system was integrated with computer programming tools, specifically LabVIEW and Arduino, to control and automate the microfluidic processes. The use of LabVIEW provided a graphical interface that facilitated the design and execution of complex control algorithms, while Arduino offered a cost-effective and versatile platform for hardware control, making it accessible for various applications.

The automation system we developed allowed for precise control over the timing and sequence of droplet formation, leveraging the normally closed valves to manage fluid flow with high accuracy. This capability was essential for applications requiring consistent droplet size and spacing, which are critical parameters in many microfluidic experiments. By automating these processes, we significantly reduced manual intervention, thereby minimizing potential errors and enhancing the reproducibility of the experiments.

Furthermore, we designed and validated a multi-step automation process that streamlined the operational workflow. This process involved programming the sequence of valve actuations to achieve specific fluidic outcomes, such as alternating sample and reference droplets or creating complex droplet patterns. The validation of this automation process demonstrated substantial improvements in both operational efficiency and precision, proving the effectiveness of the system in various experimental contexts. This advancement not only simplified the operation of

microfluidic devices but also expanded their potential applications in high-throughput screening, diagnostics, and other fields requiring precise fluid handling.

3. **Pneumatic Automation (Chapter 4)**:

In Chapter 4, we delved into the realm of pneumatic automation for droplet manipulation within microfluidic systems. This approach centered on the use of fundamental pneumatic logic gates, such as NOT, AND, OR, and NAND gates, to control fluid flow without relying heavily on electronic components. By employing these pneumatic gates, we aimed to achieve precise control over droplet operations, such as formation, merging, and sorting, while minimizing the complexity and cost associated with electronic hardware.

The innovative use of pneumatic logic gates provided a new avenue for designing microfluidic systems that are both simpler and more robust. Unlike traditional systems that depend on electronic control for valve actuation, our approach utilized air pressure to manipulate fluid dynamics, offering a cleaner and more sustainable solution. This method also reduced the potential for electrical interference and power supply issues, making the system more reliable and easier to maintain, especially in settings where electronic equipment may be impractical or hazardous.

A key highlight of this chapter was the development of a pneumatic multiplexer, which demonstrated the practical application of pneumatic logic in microfluidic circuits. The multiplexer could control multiple fluid channels with a single pneumatic input, thereby streamlining the design and operation of the microfluidic device. This achievement underscored the feasibility of creating fully pneumatic-controlled microfluidic systems, which hold promise for applications where electronic control is either undesirable or infeasible. The work presented in this chapter showcased the potential for pneumatic automation to revolutionize microfluidic device design, leading to

more efficient, cost-effective, and scalable solutions in various scientific and industrial applications.

4. **Integration of Computer Vision (Chapter 5)**:

In Chapter 5, we explored the integration of computer vision technology with serial communication to achieve real-time feedback and control in microfluidic systems. This innovative approach enabled us to monitor and adjust microfluidic processes dynamically, ensuring precise control over droplet formation and manipulation. By leveraging computer vision, we were able to track droplet characteristics such as size, frequency, and spacing, providing critical data that informed the automated control system.

The implementation of Python-based image analysis played a crucial role in this integration. Using image processing techniques, the system could detect and analyze regions of interest (ROIs) within the microfluidic channels, identifying key features like droplet edges and flow patterns. This real-time analysis allowed the system to make immediate adjustments to valve actuation, optimizing the flow conditions to maintain consistent droplet size and formation rate. This level of control was particularly beneficial for applications requiring high precision and repeatability, such as biochemical assays and single-cell analysis.

The integration of computer vision not only improved the accuracy and efficiency of the microfluidic automation process but also provided a scalable solution for complex microfluidic operations. This chapter demonstrated the potential of combining advanced imaging techniques with automated control systems, paving the way for more sophisticated and adaptable microfluidic devices. The advancements discussed in this chapter highlight the importance of interdisciplinary approaches in enhancing the capabilities of microfluidic technologies, offering new avenues for research and application in fields ranging from biomedical engineering to chemical analysis.

Implications and Future Directions:

The integration of electronics, pneumatics, and computer vision in droplet-based microfluidics represents a significant advancement, paving the way for innovative applications and research. This dissertation has established a robust foundation for future exploration and development in several crucial areas:

1. **Fully Autonomous Systems:** The advancement towards electronic-less, pneumatic-controlled microfluidic devices marks a pivotal shift towards creating more robust and simplified systems. These systems, which rely on fundamental pneumatic logic gates and multiplexers, can significantly reduce the complexity and cost associated with traditional electronic controls. Such developments are particularly promising for applications requiring reliability and minimal maintenance, including biological assays, chemical synthesis, and portable diagnostic tools. The potential for fully autonomous systems opens up possibilities for microfluidics in resource-limited settings and environments where electronic components may be impractical.
2. **Enhanced Precision and Efficiency:** The integration of computer vision algorithms with microfluidic systems has already demonstrated remarkable improvements in precision and efficiency. As these algorithms are further refined and optimized, they promise even greater enhancements. Advanced image analysis techniques can provide more detailed and accurate real-time data, allowing for finer control over droplet formation, manipulation, and sorting. This increased precision is crucial for applications that demand high throughput and accuracy, such as single-cell sequencing, drug screening, and biochemical assays. The continuous feedback loop enabled by computer vision can also help identify and correct any deviations from desired operating conditions, ensuring consistent and reproducible results.

3. **Broader Applications:** The techniques and systems developed through this work have broad implications across multiple fields. In diagnostics, for example, the ability to precisely control droplet environments could lead to more accurate and rapid testing methods. In drug development, microfluidic systems offer a platform for high-throughput screening of potential drug compounds, enabling more efficient identification of candidates. Environmental monitoring is another promising area, where microfluidic devices could be used to detect and quantify pollutants or pathogens in water and air samples. The versatility and scalability of the systems discussed in this dissertation make them adaptable to a wide range of applications, potentially transforming how we approach problems in medicine, environmental science, and industry.

Additional Directions for Future Research:

1. **Scaling-up Flow Control:** Future research should focus on miniaturization and performance scaling of microfluidic systems. Developing efficient flow control for complex networks, including multiplexed microchannels and integrated circuits, will be crucial for advancing the field. This will enable the handling of more sophisticated and large-scale experiments while maintaining precision and control over the microfluidic processes.
2. **Integrated Electronics & Pneumatics:** Seamless integration of electronic and pneumatic control systems is essential for creating versatile microfluidic platforms. Optimizing hybrid systems for precision and robustness can enhance the reliability and functionality of these devices. This integration will allow for more flexible and dynamic control over microfluidic operations, facilitating a wider range of applications and experiments.
3. **Passive Flow Regulation:** The design of passive microvalves and resistors remains a key area for development. Enhancing flow control with reduced system complexity can lead to simpler,

more cost-effective solutions for microfluidic applications. This approach can also improve the reliability and ease of use of microfluidic devices, making them accessible for a broader range of users and applications.

4. **Advanced Computer Vision:** Implementing real-time droplet sorting, merging, and splitting using advanced computer vision techniques will further improve the functionality of microfluidic systems. The use of machine learning algorithms for precision droplet manipulation can lead to more sophisticated and automated control systems, capable of adapting to varying conditions and optimizing performance.

In conclusion, the advancements presented in this dissertation not only enhance the current capabilities of droplet-based microfluidic systems but also set the stage for future innovations. By continuing to integrate new technologies and refining existing ones, the field of microfluidics is poised to make significant contributions to science and technology, offering solutions that are both sophisticated and practical.

References

(1) Shi, N.; Mohibullah, M.; Easley, C. J. Active Flow Control and Dynamic Analysis in Droplet Microfluidics. *Annu. Rev. Anal. Chem.* **2021**, *14* (Volume 14, 2021), 133–153. https://doi.org/10.1146/annurev-anchem-122120-042627.

(2) Bibette, J.; Morse, D. C.; Witten, T. A.; Weitz, D. A. Stability Criteria for Emulsions. *Phys. Rev. Lett.* **1992**, *69* (16), 2439–2442. https://doi.org/10.1103/PhysRevLett.69.2439.

(3) Opalski, A. S.; Kaminski, T. S.; Garstecki, P. Droplet Microfluidics as a Tool for the Generation of Granular Matters and Functional Emulsions. *KONA Powder Part. J.* **2019**, *36*, 50–71. https://doi.org/10.14356/kona.2019004.

(4) *Monodisperse Emulsion Generation via Drop Break Off in a Coflowing Stream | Langmuir*. https://pubs.acs.org/doi/10.1021/la990101e (accessed 2024-06-02).

(5) Thorsen, T.; Roberts, R. W.; Arnold, F. H.; Quake, S. R. Dynamic Pattern Formation in a Vesicle-Generating Microfluidic Device. *Phys. Rev. Lett.* **2001**, *86* (18), 4163–4166. https://doi.org/10.1103/PhysRevLett.86.4163.

(6) Song, H.; Tice, J. D.; Ismagilov, R. F. A Microfluidic System for Controlling Reaction Networks in Time. *Angew. Chem. Int. Ed.* **2003**, *42* (7), 768–772. https://doi.org/10.1002/anie.200390203.

(7) Garstecki, P.; Fuerstman, M. J.; Stone, H. A.; Whitesides, G. M. Formation of Droplets and Bubbles in a Microfluidic T-Junction—Scaling and Mechanism of Break-Up. *Lab. Chip* **2006**, *6* (3), 437–446. https://doi.org/10.1039/B510841A.

(8) Link, D. R.; Anna, S. L.; Weitz, D. A.; Stone, H. A. Geometrically Mediated Breakup of Drops in Microfluidic Devices. *Phys. Rev. Lett.* **2004**, *92* (5), 054503. https://doi.org/10.1103/PhysRevLett.92.054503.

(9) Kumaresan, P.; Yang, C. J.; Cronier, S. A.; Blazej, R. G.; Mathies, R. A. High-Throughput Single Copy DNA Amplification and Cell Analysis in Engineered Nanoliter Droplets. *Anal. Chem.* **2008**, *80* (10), 3522–3529. https://doi.org/10.1021/ac800327d.

(10) Chiu, D. T. Interfacing Droplet Microfluidics with Chemical Separation for Cellular Analysis. *Anal. Bioanal. Chem.* **2010**, *397* (8), 3179–3183. https://doi.org/10.1007/s00216-010-3686-8.

(11) Chiu, D. T.; Lorenz, R. M. Chemistry and Biology in Femtoliter and Picoliter Volume Droplets. *Acc. Chem. Res.* **2009**, *42* (5), 649–658. https://doi.org/10.1021/ar8002464.

(12) Germinario, L. T.; Hebrank, J. H.; Hunter, C. E.; Hunter, J. C.; Li, C.; Maurer, C. W. Droplet Delivery Device for Delivery of Fluids to the Pulmonary System and Methods of Use. US9962507B2, May 8, 2018. https://patents.google.com/patent/US9962507B2/en (accessed 2024-06-02).

(13) Nan, L.; Mao, T.; Shum, H. C. Self-Synchronization of Reinjected Droplets for High-Efficiency Droplet Pairing and Merging. *Microsyst. Nanoeng.* **2023**, *9* (1), 1–12. https://doi.org/10.1038/s41378-023-00502-6.

(14) Yang, T.; Buholzer, K. J.; Sottini, A.; Cao, X.; deMello, A.; Nettels, D.; Schuler, B. Rapid Droplet-Based Mixing for Single-Molecule Spectroscopy. *Nat. Methods* **2023**, *20* (10), 1479–1482. https://doi.org/10.1038/s41592-023-01995-9.

(15) Vallejo, D.; Nikoomanzar, A.; Paegel, B. M.; Chaput, J. C. Fluorescence-Activated Droplet Sorting for Single-Cell Directed Evolution. *ACS Synth. Biol.* **2019**, *8* (6), 1430–1440. https://doi.org/10.1021/acssynbio.9b00103.

(16) Mazutis, L.; Gilbert, J.; Ung, W. L.; Weitz, D. A.; Griffiths, A. D.; Heyman, J. A. Single-Cell Analysis and Sorting Using Droplet-Based Microfluidics. *Nat. Protoc.* **2013**, *8* (5), 870–891. https://doi.org/10.1038/nprot.2013.046.
(17) *Single-cell genome sequencing at ultra-high-throughput with microfluidic droplet barcoding | Nature Biotechnology*. https://www.nature.com/articles/nbt.3880 (accessed 2024-06-03).
(18) Karamitros, C. S.; Morvan, M.; Vigne, A.; Lim, J.; Gruner, P.; Beneyton, T.; Vrignon, J.; Baret, J.-C. Bacterial Expression Systems for Enzymatic Activity in Droplet-Based Microfluidics. *Anal. Chem.* **2020**, *92* (7), 4908–4916. https://doi.org/10.1021/acs.analchem.9b04969.
(19) B. Theberge, A.; Mayot, E.; Harrak, A. E.; Kleinschmidt, F.; S. Huck, W. T.; D. Griffiths, A. Microfluidic Platform for Combinatorial Synthesis in Picolitre Droplets. *Lab. Chip* **2012**, *12* (7), 1320–1326. https://doi.org/10.1039/C2LC21019C.
(20) Shembekar, N.; Chaipan, C.; Utharala, R.; A. Merten, C. Droplet-Based Microfluidics in Drug Discovery, Transcriptomics and High-Throughput Molecular Genetics. *Lab. Chip* **2016**, *16* (8), 1314–1331. https://doi.org/10.1039/C6LC00249H.
(21) Liu, F. X.; Cui, J. Q.; Park, H.; Chan, K. W.; Leung, T.; Tang, B. Z.; Yao, S. Isothermal Background-Free Nucleic Acid Quantification by a One-Pot Cas13a Assay Using Droplet Microfluidics. *Anal. Chem.* **2022**, *94* (15), 5883–5892. https://doi.org/10.1021/acs.analchem.2c00067.
(22) Khajvand, T.; Huang, P.; Li, L.; Zhang, M.; Zhu, F.; Xu, X.; Huang, M.; Yang, C.; Lu, Y.; Zhu, Z. Interfacing Droplet Microfluidics with Antibody Barcodes for Multiplexed Single-Cell Protein Secretion Profiling. *Lab. Chip* **2021**, *21* (24), 4823–4830. https://doi.org/10.1039/D1LC00567G.
(23) Hsu, M. N.; Wei, S.-C.; Guo, S.; Phan, D.-T.; Zhang, Y.; Chen, C.-H. Smart Hydrogel Microfluidics for Single-Cell Multiplexed Secretomic Analysis with High Sensitivity. *Small* **2018**, *14* (49), 1802918. https://doi.org/10.1002/smll.201802918.
(24) Teh, S.-Y.; Lin, R.; Hung, L.-H.; P. Lee, A. Droplet Microfluidics. *Lab. Chip* **2008**, *8* (2), 198–220. https://doi.org/10.1039/B715524G.
(25) *Recent Advances in Droplet Microfluidics | Analytical Chemistry*. https://pubs.acs.org/doi/full/10.1021/acs.analchem.9b05047 (accessed 2024-06-03).
(26) Zhu, Y.; Fang, Q. Analytical Detection Techniques for Droplet Microfluidics—A Review. *Anal. Chim. Acta* **2013**, *787*, 24–35. https://doi.org/10.1016/j.aca.2013.04.064.
(27) N. Baroud, C.; Gallaire, F.; Dangla, R. Dynamics of Microfluidic Droplets. *Lab. Chip* **2010**, *10* (16), 2032–2045. https://doi.org/10.1039/C001191F.
(28) *Passive and active droplet generation with microfluidics: a review - Lab on a Chip (RSC Publishing) DOI:10.1039/C6LC01018K*. https://pubs.rsc.org/en/content/articlehtml/2017/lc/c6lc01018k (accessed 2024-06-03).
(29) Mandsberg, N. K.; Shneidman, A. V.; Jensen, K. H.; Taboryski, R.; Nielsen, L. H.; Aizenberg, J.; Boisen, A. Gradient Droplet Arrays by Acceleration-Mode Dip-Coating. *Adv. Mater. Interfaces* **2022**, *9* (22), 2200667. https://doi.org/10.1002/admi.202200667.
(30) Harriot, J.; Yeh, M.; Pabba, M.; DeVoe, D. L. Programmable Control of Nanoliter Droplet Arrays Using Membrane Displacement Traps. *Adv. Mater. Technol.* **2023**, *8* (21), 2300963. https://doi.org/10.1002/admt.202300963.
(31) *Programmable Control of Multiscale Droplets using V-Valves - Xue - 2023 - Advanced Materials Technologies - Wiley Online Library*. https://onlinelibrary.wiley.com/doi/10.1002/admt.202201553 (accessed 2024-07-31).

(32) Rho, H. S.; Gardeniers, H. Microfluidic Droplet-Storage Array. *Micromachines* **2020**, *11* (6), 608. https://doi.org/10.3390/mi11060608.
(33) *Automated Microfluidic Screening Assay Platform Based on DropLab | Analytical Chemistry*. https://pubs.acs.org/doi/10.1021/ac1020479 (accessed 2024-07-31).
(34) Vandelli, N.; Wroblewski, D.; Velonis, M.; Bifano, T. Development of a MEMS Microvalve Array for Fluid Flow Control. *J. Microelectromechanical Syst.* **1998**, *7* (4), 395–403. https://doi.org/10.1109/84.735347.
(35) *Preface to Special Topic: Selected Papers from the Advances in Microfluidics and Nanofluidics 2014 Conference in Honor of Professor Hsueh-Chia Chang's 60th Birthday | Biomicrofluidics | AIP Publishing*. https://pubs.aip.org/aip/bmf/article/8/5/051901/386117/Preface-to-Special-Topic-Selected-Papers-from-the (accessed 2024-07-31).
(36) Chou, C.-F.; Wei, P.-K.; Chen, Y.-L. Preface to Special Topic: Selected Papers from the Advances in Microfluidics and Nanofluidics 2014 Conference in Honor of Professor Hsueh-Chia Chang's 60th Birthday. *Biomicrofluidics* **2014**, *8* (5), 051901. https://doi.org/10.1063/1.4900715.
(37) H. Grover, W.; C. Ivester, R. H.; C. Jensen, E.; A. Mathies, R. Development and Multiplexed Control of Latching Pneumatic Valves Using Microfluidic Logical Structures. *Lab. Chip* **2006**, *6* (5), 623–631. https://doi.org/10.1039/B518362F.
(38) Padmanabhan, S.; Misteli, T.; DeVoe, D. L. Controlled Droplet Discretization and Manipulation Using Membrane Displacement Traps. *Lab. Chip* **2017**, *17* (21), 3717–3724. https://doi.org/10.1039/C7LC00910K.
(39) Negou, J. T.; Avila, L. A.; Li, X.; Hagos, T. M.; Easley, C. J. Automated Microfluidic Droplet-Based Sample Chopper for Detection of Small Fluorescence Differences Using Lock-In Analysis. *Anal. Chem.* **2017**, *89* (11), 6153–6159. https://doi.org/10.1021/acs.analchem.7b00991.
(40) Deal, K. S.; Easley, C. J. Self-Regulated, Droplet-Based Sample Chopper for Microfluidic Absorbance Detection. *Anal. Chem.* **2012**, *84* (3), 1510–1516. https://doi.org/10.1021/ac202791d.
(41) Shi, N.; Easley, C. J. Programmable µChopper Device with On-Chip Droplet Mergers for Continuous Assay Calibration. *Micromachines* **2020**, *11* (6), 620. https://doi.org/10.3390/mi11060620.
(42) Doonan, S. R.; Bailey, R. C. The K-Channel: A Multi-Functional Architecture for Dynamically Re-Configurable Sample Processing in Droplet Microfluidics. *Anal. Chem.* **2017**, *89* (7), 4091–4099. https://doi.org/10.1021/acs.analchem.6b05041.
(43) Doonan, S. R.; Lin, M.; Bailey, R. C. Droplet CAR-Wash: Continuous Picoliter-Scale Immunocapture and Washing. *Lab. Chip* **2019**, *19* (9), 1589–1598. https://doi.org/10.1039/C9LC00125E.
(44) Shojaeian, M.; Hardt, S. Fast Electric Control of the Droplet Size in a Microfluidic T-Junction Droplet Generator. *Appl. Phys. Lett.* **2018**, *112* (19), 194102. https://doi.org/10.1063/1.5025874.
(45) Teo, A. J. T.; Yan, M.; Dong, J.; Xi, H.-D.; Fu, Y.; Tan, S. H.; Nguyen, N.-T. Controllable Droplet Generation at a Microfluidic T-Junction Using AC Electric Field. *Microfluid. Nanofluidics* **2020**, *24* (3), 21. https://doi.org/10.1007/s10404-020-2327-6.
(46) Raveshi, M. R.; Agnihotri, S. N.; Sesen, M.; Bhardwaj, R.; Neild, A. Selective Droplet Splitting Using Single Layer Microfluidic Valves. *Sens. Actuators B Chem.* **2019**, *292*, 233–240. https://doi.org/10.1016/j.snb.2019.04.115.

(47) Negou, J. T.; Hu, J.; Li, X.; Easley, C. J. Advancement of Analytical Modes in a Multichannel, Microfluidic Droplet-Based Sample Chopper Employing Phase-Locked Detection. *Anal. Methods* **2018**, *10* (28), 3436–3443. https://doi.org/10.1039/C8AY00947C.
(48) Lim, J.; Gruner, P.; Konrad, M.; Baret, J.-C. Micro-Optical Lens Array for Fluorescence Detection in Droplet-Based Microfluidics. *Lab. Chip* **2013**, *13* (8), 1472–1475. https://doi.org/10.1039/C3LC41329B.
(49) Holzner, G.; Du, Y.; Cao, X.; Choo, J.; deMello, A. J.; Stavrakis, S. An Optofluidic System with Integrated Microlens Arrays for Parallel Imaging Flow Cytometry. *Lab. Chip* **2018**, *18* (23), 3631–3637. https://doi.org/10.1039/C8LC00593A.
(50) Choi, C.-H.; Jung, J.-H.; Hwang, T.-S.; Lee, C.-S. In Situ Microfluidic Synthesis of Monodisperse PEG Microspheres. *Macromol. Res.* **2009**, *17* (3), 163–167. https://doi.org/10.1007/BF03218673.
(51) Krutkramelis, K.; Xia, B.; Oakey, J. Monodisperse Polyethylene Glycol Diacrylate Hydrogel Microsphere Formation by Oxygen-Controlled Photopolymerization in a Microfluidic Device. *Lab. Chip* **2016**, *16* (8), 1457–1465. https://doi.org/10.1039/C6LC00254D.
(52) de Rutte, J. M.; Koh, J.; Di Carlo, D. Scalable High-Throughput Production of Modular Microgels for In Situ Assembly of Microporous Tissue Scaffolds. *Adv. Funct. Mater.* **2019**, *29* (25), 1900071. https://doi.org/10.1002/adfm.201900071.
(53) Destgeer, G.; Ouyang, M.; Wu, C.-Y.; Carlo, D. D. Fabrication of 3D Concentric Amphiphilic Microparticles to Form Uniform Nanoliter Reaction Volumes for Amplified Affinity Assays. *Lab. Chip* **2020**, *20* (19), 3503–3514. https://doi.org/10.1039/D0LC00698J.
(54) Price, A. K.; MacConnell, A. B.; Paegel, B. M. hvSABR: Photochemical Dose-Response Bead Screening in Droplets. *Anal. Chem.* **2016**, *88* (5), 2904–2911. https://doi.org/10.1021/acs.analchem.5b04811.
(55) *Microfluidic systems for chemical kinetics that rely on chaotic mixing in droplets | Philosophical Transactions of the Royal Society of London. Series A: Mathematical, Physical and Engineering Sciences*. https://royalsocietypublishing.org/doi/10.1098/rsta.2003.1364 (accessed 2024-07-31).
(56) Rossi, D.; Gargiulo, L.; Valitov, G.; Gavriilidis, A.; Mazzei, L. Experimental Characterization of Axial Dispersion in Coiled Flow Inverters. *Chem. Eng. Res. Des.* **2017**, *120*, 159–170. https://doi.org/10.1016/j.cherd.2017.02.011.
(57) Liu, Y.; Ismagilov, R. F. Dynamics of Coalescence of Plugs with a Hydrophilic Wetting Layer Induced by Flow in a Microfluidic Chemistrode. *Langmuir ACS J. Surf. Colloids* **2009**, *25* (5), 2854–2859. https://doi.org/10.1021/la803518b.
(58) Easley, C. J.; Rocheleau, J. V.; Head, W. S.; Piston, D. W. Quantitative Measurement of Zinc Secretion from Pancreatic Islets with High Temporal Resolution Using Droplet-Based Microfluidics. *Anal. Chem.* **2009**, *81* (21), 9086–9095. https://doi.org/10.1021/ac9017692.
(59) Wang, M.; Roman, G. T.; Perry, M. L.; Kennedy, R. T. Microfluidic Chip for High Efficiency Electrophoretic Analysis of Segmented Flow from a Microdialysis Probe and in Vivo Chemical Monitoring. *Anal. Chem.* **2009**, *81* (21), 9072–9078. https://doi.org/10.1021/ac901731v.
(60) Li, X.; Hu, J.; Easley, C. J. Automated Microfluidic Droplet Sampling with Integrated, Mix-and-Read Immunoassays to Resolve Endocrine Tissue Secretion Dynamics. *Lab. Chip* **2018**, *18* (19), 2926–2935. https://doi.org/10.1039/C8LC00616D.

(61) Hu, J.; Li, X.; Judd, R. L.; Easley, C. J. Rapid Lipolytic Oscillations in Ex Vivo Adipose Tissue Explants Revealed through Microfluidic Droplet Sampling at High Temporal Resolution. *Lab. Chip* **2020**, *20* (8), 1503–1512. https://doi.org/10.1039/D0LC00103A.
(62) Petit-Pierre, G.; Bertsch, A.; Renaud, P. Neural Probe Combining Microelectrodes and a Droplet-Based Microdialysis Collection System for High Temporal Resolution Sampling. *Lab. Chip* **2016**, *16* (5), 917–924. https://doi.org/10.1039/C5LC01544H.
(63) Petit-Pierre, G.; Colin, P.; Laurer, E.; Déglon, J.; Bertsch, A.; Thomas, A.; Schneider, B. L.; Renaud, P. In Vivo Neurochemical Measurements in Cerebral Tissues Using a Droplet-Based Monitoring System. *Nat. Commun.* **2017**, *8* (1), 1239. https://doi.org/10.1038/s41467-017-01419-1.
(64) Ngernsutivorakul, T.; Steyer, D. J.; Valenta, A. C.; Kennedy, R. T. In Vivo Chemical Monitoring at High Spatiotemporal Resolution Using Microfabricated Sampling Probes and Droplet-Based Microfluidics Coupled to Mass Spectrometry. *Anal. Chem.* **2018**, *90* (18), 10943–10950. https://doi.org/10.1021/acs.analchem.8b02468.
(65) Nightingale, A. M.; Leong, C. L.; Burnish, R. A.; Hassan, S.-U.; Zhang, Y.; Clough, G. F.; Boutelle, M. G.; Voegeli, D.; Niu, X. Monitoring Biomolecule Concentrations in Tissue Using a Wearable Droplet Microfluidic-Based Sensor. *Nat. Commun.* **2019**, *10* (1), 2741. https://doi.org/10.1038/s41467-019-10401-y.
(66) Hu, J.; Easley, C. J. Homogeneous Assays of Second Messenger Signaling and Hormone Secretion Using Thermofluorimetric Methods That Minimize Calibration Burden. *Anal. Chem.* **2017**, *89* (16), 8517–8523. https://doi.org/10.1021/acs.analchem.7b02229.
(67) Angelescu, D. E.; Mercier, B.; Siess, D.; Schroeder, R. Microfluidic Capillary Separation and Real-Time Spectroscopic Analysis of Specific Components from Multiphase Mixtures. *Anal. Chem.* **2010**, *82* (6), 2412–2420. https://doi.org/10.1021/ac902698m.
(68) Fidalgo, L. M.; Whyte, G.; Ruotolo, B. T.; Benesch, J. L. P.; Stengel, F.; Abell, C.; Robinson, C. V.; Huck, W. T. S. Coupling Microdroplet Microreactors with Mass Spectrometry: Reading the Contents of Single Droplets Online. *Angew. Chem. Int. Ed.* **2009**, *48* (20), 3665–3668. https://doi.org/10.1002/anie.200806103.
(69) Guetschow, E. D.; Steyer, D. J.; Kennedy, R. T. Subsecond Electrophoretic Separations from Droplet Samples for Screening of Enzyme Modulators. *Anal. Chem.* **2014**, *86* (20), 10373–10379. https://doi.org/10.1021/ac502758h.
(70) Pei, J.; Nie, J.; Kennedy, R. T. Parallel Electrophoretic Analysis of Segmented Samples on Chip for High-Throughput Determination of Enzyme Activities. *Anal. Chem.* **2010**, *82* (22), 9261–9267. https://doi.org/10.1021/ac101755y.
(71) *Delivery of minimally dispersed liquid interfaces for sequential surface chemistry - Lab on a Chip (RSC Publishing)*. https://pubs.rsc.org/en/content/articlelanding/2016/lc/c6lc00473c#! (accessed 2024-06-25).
(72) Feng, S.; Liu, G.; Jiang, L.; Zhu, Y.; Goldys, E. M.; Inglis, D. W. A Microfluidic Needle for Sampling and Delivery of Chemical Signals by Segmented Flows: 21st International Conference on Miniaturized Systems for Chemistry and Life Sciences, MicroTAS 2017. In *The 21st International Conference on Miniaturized Systems for Chemistry and Life Sciences*; Chemical and Biological Microsystems Society, 2017; pp 346–347.
(73) *Mass Activated Droplet Sorting (MADS) Enables High-Throughput Screening of Enzymatic Reactions at Nanoliter Scale - PubMed*. https://pubmed.ncbi.nlm.nih.gov/31868984/ (accessed 2024-06-25).

(74) Trossbach, M.; de Lucas Sanz, M.; Seashore-Ludlow, B.; Joensson, H. N. A Portable, Negative-Pressure Actuated, Dynamically Tunable Microfluidic Droplet Generator. *Micromachines* **2022**, *13* (11), 1823. https://doi.org/10.3390/mi13111823.
(75) Anyaduba, T. D.; Otoo, J. A.; Schlappi, T. S. Picoliter Droplet Generation and Dense Bead-in-Droplet Encapsulation via Microfluidic Devices Fabricated via 3D Printed Molds. *Micromachines* **2022**, *13* (11), 1946. https://doi.org/10.3390/mi13111946.
(76) *ENIAC: The Army-Sponsored Revolution*. https://ftp.arl.army.mil/~mike/comphist/96summary/ (accessed 2024-06-09).
(77) Bacsardi, L.; Imre, S.; Bacsardi, L.; Imre, S. Quantum Based Information Transfer in Satellite Communication. In *Satellite Communications*; IntechOpen, 2010. https://doi.org/10.5772/9999.
(78) Kronzon, I. The Hand-Carried Ultrasound Revolution. *Echocardiography* **2003**, *20* (5), 453–454. https://doi.org/10.1046/j.1540-8175.2003.03081.x.
(79) Riordan, M.; Hoddeson, L. Crystal Fire: The Invention, Development and Impact of the Transistor. *IEEE Solid-State Circuits Soc. Newsl.* **2007**, *12* (2), 24–29. https://doi.org/10.1109/N-SSC.2007.4785574.
(80) Anderson, K. J. Integrating the Circuit. *MRS Bull.* **1991**, *16* (12), 50–50. https://doi.org/10.1557/S0883769400055378.
(81) A Nobel Nod To The Fathers Of Electronics Technology. *Chem. Eng. News Arch.* **2000**, *78* (42), 6. https://doi.org/10.1021/cen-v078n042.p006.
(82) Saxena, A. N. Monolithic Concept and the Inventions of Integrated Circuits by Kilby and Noyce. **2007**, *3*.
(83) Moore, G. E. Cramming More Components onto Integrated Circuits. *Proc. IEEE* **1998**, *86* (1).
(84) Meindl, J. D. Beyond Moore's Law: The Interconnect Era. *Comput. Sci. Eng.* **2003**, *5* (1), 20–24. https://doi.org/10.1109/MCISE.2003.1166548.
(85) Deitel, H. M.; Deitel, B. 2 - The Evolution of Computers. In *Study Guide to Accompany Computer and Data Processing*; Deitel, H. M., Deitel, B., Eds.; Academic Press, 1985; pp 11–22. https://doi.org/10.1016/B978-0-12-209021-9.50005-1.
(86) Shulaker, M. M.; Hills, G.; Patil, N.; Wei, H.; Chen, H.-Y.; Wong, H.-S. P.; Mitra, S. Carbon Nanotube Computer. *Nature* **2013**, *501* (7468), 526–530. https://doi.org/10.1038/nature12502.
(87) Nielsen, M. A.; Chuang, I. L. *Quantum Computation and Quantum Information: 10th Anniversary Edition*. Higher Education from Cambridge University Press. https://doi.org/10.1017/CBO9780511976667.
(88) Joachim, C.; Gimzewski, J. K.; Aviram, A. Electronics Using Hybrid-Molecular and Mono-Molecular Devices. *Nature* **2000**, *408* (6812), 541–548. https://doi.org/10.1038/35046000.
(89) Korivi, N. S.; Jiang, L. A Generic Chip-to-World Fluidic Interconnect System for Microfluidic Devices. In *2007 Thirty-Ninth Southeastern Symposium on System Theory*; 2007; pp 176–180. https://doi.org/10.1109/SSST.2007.352343.
(90) *Shape memory alloy microvalves for a fluidic control system - IOPscience*. https://iopscience.iop.org/article/10.1088/0960-1317/24/2/025001/meta (accessed 2024-06-21).
(91) *Closed-loop feedback control of microbubble diameter from a flow-focusing microfluidic device | Biomicrofluidics | AIP Publishing*. https://pubs.aip.org/aip/bmf/article/14/3/034101/279740/Closed-loop-feedback-control-of-microbubble (accessed 2024-06-21).

(92) *Precise microflow control in lab-on-a-chip and organ-on-a-chip as future applications | IEEE Conference Publication | IEEE Xplore*. https://ieeexplore.ieee.org/document/7452189 (accessed 2024-06-21).
(93) Ezra Tsur, E.; Zimerman, M.; Maor, I.; Elrich, A.; Nahmias, Y. Microfluidic Concentric Gradient Generator Design for High-Throughput Cell-Based Studies. *Front. Bioeng. Biotechnol.* **2017**, *5*, 21. https://doi.org/10.3389/fbioe.2017.00021.
(94) *Bacterial Growth and Adaptation in Microdroplet Chemostats - Jakiela - 2013 - Angewandte Chemie International Edition - Wiley Online Library*. https://onlinelibrary.wiley.com/doi/10.1002/anie.201301524 (accessed 2024-06-25).
(95) Galambos, P.; Benavides, G. L. Electrical and Fluidic Packaging of Surface Micromachined Electromicrofluidic Devices; Mastrangelo, C. H., Becker, H., Eds.; Santa Clara, CA, 2000; pp 186–193. https://doi.org/10.1117/12.395661.
(96) Tipton, K. D.; Rasmussen, B. B.; Miller, S. L.; Wolf, S. E.; Owens-Stovall, S. K.; Petrini, B. E.; Wolfe, R. R. Timing of Amino Acid-Carbohydrate Ingestion Alters Anabolic Response of Muscle to Resistance Exercise. *Am. J. Physiol. Endocrinol. Metab.* **2001**, *281* (2), E197-206. https://doi.org/10.1152/ajpendo.2001.281.2.E197.
(97) Carvell, T.; Burgoyne, P.; Fraser, A. R.; Bridle, H. Categorising Hybrid Material Microfluidic Devices. *Front. Lab Chip Technol.* **2024**, *3*. https://doi.org/10.3389/frlct.2024.1412290.
(98) *IJMS | Free Full-Text | Fabrication and Applications of Microfluidic Devices: A Review*. https://www.mdpi.com/1422-0067/22/4/2011 (accessed 2024-06-25).
(99) Zhang, Y.; Liu, Y. Advances in Integrated Digital Microfluidic Platforms for Point-of-Care Diagnosis: A Review. *Sens. Diagn.* **2022**, *1* (4), 648–672. https://doi.org/10.1039/D2SD00031H.
(100) Zhou, W.; Dou, M.; Timilsina, S. S.; Xu, F.; Li, X. Recent Innovations in Cost-Effective Polymer and Paper Hybrid Microfluidic Devices. *Lab. Chip* **2021**, *21* (14), 2658–2683. https://doi.org/10.1039/D1LC00414J.
(101) Annabestani, M.; Naghavi, N.; Maymandi-Nejad, M. A 3D Analytical Ion Transport Model for Ionic Polymer Metal Composite Actuators in Large Bending Deformations. *Sci. Rep.* **2021**, *11* (1), 6435. https://doi.org/10.1038/s41598-021-85776-4.
(102) Vyawahare, S.; Griffiths, A. D.; Merten, C. A. Miniaturization and Parallelization of Biological and Chemical Assays in Microfluidic Devices. *Chem. Biol.* **2010**, *17* (10), 1052–1065. https://doi.org/10.1016/j.chembiol.2010.09.007.
(103) *A Microfluidic Transistor for Liquid Signal Processing - Consensus*. https://consensus.app/papers/microfluidic-transistor-liquid-signal-processing-gopinathan/1893f20be7e256f6927204227dc18897/?utm_source=chatgpt (accessed 2024-06-25).
(104) Godwin, L. A.; Deal, K. S.; Hoepfner, L. D.; Jackson, L. A.; Easley, C. J. Measurement of Microchannel Fluidic Resistance with a Standard Voltage Meter. *Anal. Chim. Acta* **2013**, *758*, 101–107. https://doi.org/10.1016/j.aca.2012.10.043.
(105) Yoon, S. G.; Chang, S. Microfluidic Capacitive Sensors with Ionic Liquid Electrodes and CNT/PDMS Nanocomposites for Simultaneous Sensing of Pressure and Temperature. *J. Mater. Chem. C* **2017**, *5*, 1910–1919. https://doi.org/10.1039/C6TC03994D.
(106) Ligon, S.; Liska, R.; Stampfl, J.; Gurr, M.; Mülhaupt, R. Polymers for 3D Printing and Customized Additive Manufacturing. *Chem. Rev.* **2017**, *117*, 10212–10290. https://doi.org/10.1021/acs.chemrev.7b00074.
(107) *Additive manufacturing (3D printing): A review of materials, methods, applications and challenges - Consensus*. https://consensus.app/papers/manufacturing-printing-review-materials-

methods-ngo/cb683c1619625583a3c4403ad295922d/?utm_source=chatgpt (accessed 2024-06-25).
(108) Zeng, B.; Cai, Z.; Lalevée, J.; Yang, Q.; Lai, H.; Xiao, P.; Liu, J.; Xing, F. Cytotoxic and Cytocompatible Comparison among Seven Photoinitiators-Triggered Polymers in Different Tissue Cells. *Toxicol. Vitro Int. J. Publ. Assoc. BIBRA* **2021**. https://doi.org/10.1016/j.tiv.2021.105103.
(109) Wolf, M. P.; Salieb-Beugelaar, G. B.; Hunziker, P. PDMS with Designer Functionalities—Properties, Modifications Strategies, and Applications. *Prog. Polym. Sci.* **2018**, *83*, 97–134. https://doi.org/10.1016/j.progpolymsci.2018.06.001.
(110) Gaso, P.; Jandura, D.; Pudis, D. Fabrication of 2D and 3D Photonic Structures Using Laser Lithography. In *20th Slovak-Czech-Polish Optical Conference on Wave and Quantum Aspects of Contemporary Optics*; SPIE, 2016; Vol. 10142, pp 362–366. https://doi.org/10.1117/12.2264450.
(111) Raveendran, R.; Namboothiry, M. A. G. Surface-Treated Poly(Dimethylsiloxane) as a Gate Dielectric in Solution-Processed Organic Field-Effect Transistors. *ACS Omega* **2018**, *3* (9), 11278–11285. https://doi.org/10.1021/acsomega.8b01629.
(112) *PDMS and its Suitability for Analytical Microfluidic Devices | IEEE Conference Publication | IEEE Xplore*. https://ieeexplore.ieee.org/abstract/document/4462299 (accessed 2024-06-25).
(113) Burr, G. W.; Shelby, R. M.; Sidler, S.; di Nolfo, C.; Jang, J.; Boybat, I.; Shenoy, R. S.; Narayanan, P.; Virwani, K.; Giacometti, E. U.; Kurdi, B. N.; Hwang, H. Experimental Demonstration and Tolerancing of a Large-Scale Neural Network (165 000 Synapses) Using Phase-Change Memory as the Synaptic Weight Element. *IEEE Trans. Electron Devices* **2015**, *62* (11), 3498–3507. https://doi.org/10.1109/TED.2015.2439635.
(114) Nge, P. N.; Rogers, C. I.; Woolley, A. T. Advances in Microfluidic Materials, Functions, Integration, and Applications. *Chem. Rev.* **2013**, *113* (4), 2550–2583. https://doi.org/10.1021/cr300337x.
(115) Duffy, D. C.; McDonald, J. C.; Schueller, O. J.; Whitesides, G. M. Rapid Prototyping of Microfluidic Systems in Poly(Dimethylsiloxane). *Anal. Chem.* **1998**, *70* (23), 4974–4984. https://doi.org/10.1021/ac980656z.
(116) McDonald, J. C.; Whitesides, G. M. Poly(Dimethylsiloxane) as a Material for Fabricating Microfluidic Devices. *Acc. Chem. Res.* **2002**, *35* (7), 491–499. https://doi.org/10.1021/ar010110q.
(117) Waheed, S.; M. Cabot, J.; P. Macdonald, N.; Lewis, T.; M. Guijt, R.; Paull, B.; C. Breadmore, M. 3D Printed Microfluidic Devices: Enablers and Barriers. *Lab. Chip* **2016**, *16* (11), 1993–2013. https://doi.org/10.1039/C6LC00284F.
(118) Urrios, A.; Parra-Cabrera, C.; Bhattacharjee, N.; Gonzalez-Suarez, A. M.; Rigat-Brugarolas, L. G.; Nallapatti, U.; Samitier, J.; DeForest, C. A.; Posas, F.; Garcia-Cordero, J. L.; Folch, A. 3D-Printing of Transparent Bio-Microfluidic Devices in PEG-DA. *Lab. Chip* **2016**, *16* (12), 2287–2294. https://doi.org/10.1039/c6lc00153j.
(119) *PDMS Curing Inhibition on 3D-Printed Molds: Why? Also, How to Avoid It? | Analytical Chemistry*. https://pubs.acs.org/doi/full/10.1021/acs.analchem.0c04944 (accessed 2024-06-25).
(120) de Almeida Monteiro Melo Ferraz, M.; Nagashima, J. B.; Venzac, B.; Le Gac, S.; Songsasen, N. 3D Printed Mold Leachates in PDMS Microfluidic Devices. *Sci. Rep.* **2020**, *10* (1), 994. https://doi.org/10.1038/s41598-020-57816-y.

(121) Niculescu, A.-G.; Chircov, C.; Bîrcă, A. C.; Grumezescu, A. M. Fabrication and Applications of Microfluidic Devices: A Review. *Int. J. Mol. Sci.* **2021**, *22* (4), 2011. https://doi.org/10.3390/ijms22042011.
(122) *The relationship between the Young's modulus and dry etching rate of polydimethylsiloxane (PDMS) | Biomedical Microdevices*. https://link.springer.com/article/10.1007/s10544-019-0379-8 (accessed 2024-06-25).
(123) *Micromachines | Free Full-Text | 3D Printed Unibody Lab-on-a-Chip: Features Survey and Check-Valves Integration*. https://www.mdpi.com/2072-666X/6/4/437 (accessed 2024-06-25).
(124) *Inexpensive and rapid fabrication of PDMS microfluidic devices for biological testing applications using low cost commercially available 3D printers - IOPscience*. https://iopscience.iop.org/article/10.1088/1361-6439/acf2a7/meta (accessed 2024-06-25).
(125) Babatain, W.; Bhattacharjee, S.; Hussain, A. M.; Hussain, M. M. Acceleration Sensors: Sensing Mechanisms, Emerging Fabrication Strategies, Materials, and Applications. *ACS Appl. Electron. Mater.* **2021**, *3* (2), 504–531. https://doi.org/10.1021/acsaelm.0c00746.
(126) Paguirigan, A. L.; Beebe, D. J. Microfluidics Meet Cell Biology: Bridging the Gap by Validation and Application of Microscale Techniques for Cell Biological Assays. *BioEssays* **2008**, *30* (9), 811–821. https://doi.org/10.1002/bies.20804.
(127) *Biosensors | Free Full-Text | Surface Modification Techniques for Endothelial Cell Seeding in PDMS Microfluidic Devices*. https://www.mdpi.com/2079-6374/10/11/182 (accessed 2024-06-25).
(128) *MacSphere: MERGING OMNIPHOBIC LUBRICANT-INFUSED COATINGS WITH DIFFERENT MICROFLUIDIC MODALITIES TO ENHANCE DEVICE FABRICATION AND FUNCTIONALITY*. https://macsphere.mcmaster.ca/handle/11375/23024 (accessed 2024-06-25).
(129) *PDMS lab-on-a-chip fabrication using 3D printed templates - Lab on a Chip (RSC Publishing) DOI:10.1039/C3LC50956G*. https://pubs.rsc.org/en/content/articlehtml/2013/lc/c3lc50956g (accessed 2024-06-25).
(130) Naderi, A.; Bhattacharjee, N.; Folch, A. Digital Manufacturing for Microfluidics. *Annu. Rev. Biomed. Eng.* **2019**, *21* (Volume 21, 2019), 325–364. https://doi.org/10.1146/annurev-bioeng-092618-020341.
(131) *Centrifugal Casting of Microfluidic Components With PDMS | J. Micro Nano-Manuf. | ASME Digital Collection*. https://asmedigitalcollection.asme.org/micronanomanufacturing/article/1/2/021001/380381/Centrifugal-Casting-of-Microfluidic-Components (accessed 2024-06-25).
(132) *Passive micropumping in microfluidics for point-of-care testing - PubMed*. https://pubmed.ncbi.nlm.nih.gov/32509049/ (accessed 2024-06-25).
(133) *Preprogrammed capillarity to passively control system-level sequential and parallel microfluidic flows - Lab on a Chip (RSC Publishing) DOI:10.1039/C3LC50187F*. https://pubs.rsc.org/en/content/articlehtml/2013/lc/c3lc50187f (accessed 2024-06-25).
(134) *Siphon-driven microfluidic passive pump with a yarn flow resistance controller - Lab on a Chip (RSC Publishing)*. https://pubs.rsc.org/en/content/articlelanding/2014/lc/c4lc00510d (accessed 2024-06-25).
(135) *Microfluidic Passive Valve with Ultra-Low Threshold Pressure for High-Throughput Liquid Delivery - PMC*. https://www.ncbi.nlm.nih.gov/pmc/articles/PMC6952951/ (accessed 2024-06-25).

(136) *Micromachines | Free Full-Text | Microfluidic Passive Flow Regulatory Device with an Integrated Check Valve for Enhanced Flow Control*. https://www.mdpi.com/2072-666X/10/10/653 (accessed 2024-06-25).
(137) *Active microfluidic transport in two-dimensional handlebodies - Soft Matter (RSC Publishing) DOI:10.1039/D0SM00610F*. https://pubs.rsc.org/en/content/articlehtml/2020/sm/d0sm00610f (accessed 2024-06-25).
(138) *Modeling and experimental verification of the flow characteristics of an active controlled microfluidic valve with annular boundary - Chun-Peng Pan, Dai-Hua Wang, 2016*. https://journals.sagepub.com/doi/full/10.1177/1045389X15624801 (accessed 2024-06-25).
(139) *Active porous transition towards spatiotemporal control of molecular flow in a crystal membrane | Nature Communications*. https://www.nature.com/articles/ncomms9934 (accessed 2024-06-25).
(140) *Integratable magnetic shape memory micropump for high-pressure, precision microfluidic applications | Microfluidics and Nanofluidics*. https://link.springer.com/article/10.1007/s10404-018-2058-0 (accessed 2024-06-25).
(141) *Biosensors | Free Full-Text | Novel Pumping Methods for Microfluidic Devices: A Comprehensive Review*. https://www.mdpi.com/2079-6374/12/11/956 (accessed 2024-06-25).
(142) *Mechanically programmed valving technology and the active flow switching application in centrifugal microfluidics - ScienceDirect*. https://www.sciencedirect.com/science/article/pii/S0925400517320981 (accessed 2024-06-25).
(143) *PDMS Selective Bonding for the Fabrication of Biocompatible All Polymer NC Microvalves | IEEE Journals & Magazine | IEEE Xplore*. https://ieeexplore.ieee.org/abstract/document/6549182 (accessed 2024-06-25).
(144) *Normally Closed Microfluidic Valves with Microstructured Valve Seats: A Strategy for Industrial Manufacturing of Thermoplastic Microfluidics with Microvalves | IEEE Conference Publication | IEEE Xplore*. https://ieeexplore.ieee.org/abstract/document/9056136 (accessed 2024-06-25).
(145) Takehara, H.; Jiang, C.; Uto, K.; Ebara, M.; Aoyagi, T.; Ichiki, T. Novel Microfluidic Valve Technology Based on Shape Memory Effect of Poly(ε-Caprolactone). *Appl. Phys. Express* **2013**, *6* (3), 037201. https://doi.org/10.7567/APEX.6.037201.
(146) *Droplet-based μChopper device with a 3D-printed pneumatic valving layer and a simple photometer for absorbance based fructosamine quantification in human serum - PubMed*. https://pubmed.ncbi.nlm.nih.gov/37605899/ (accessed 2024-06-25).
(147) *Pneumatic Pressure Control: An Open-Source Droplet Microfluidic System - Consensus*. https://consensus.app/papers/pressure-control-opensource-droplet-microfluidic-system-gao/a9d38cd25faa515d8d8c4c07f9412172/?utm_source=chatgpt (accessed 2024-06-25).
(148) *Integrated pneumatic micro-pumps for high-throughput droplet-based microfluidics - Consensus*. https://consensus.app/papers/integrated-micropumps-highthroughput-microfluidics-choi/44c58cf6bb6a5eca9a7029900600e6a0/?utm_source=chatgpt (accessed 2024-06-25).
(149) *Measuring rapid enzymatic kinetics by electrochemical method in droplet-based microfluidic devices with pneumatic valves. - Consensus*. https://consensus.app/papers/measuring-kinetics-method-dropletbased-devices-valves-han/a257880f9add5b158ec319273bf7750d/?utm_source=chatgpt (accessed 2024-06-25).
(150) *Selective Formation and Removal of Liquid Microlenses at Predetermined Locations Within Microfluidics Through Pneumatic Control - Consensus*.

https://consensus.app/papers/formation-removal-liquid-microlenses-predetermined-dong/3cb493e284b75c81abe456f4cadfba79/?utm_source=chatgpt (accessed 2024-06-25).
(151) *Development and multiplexed control of latching pneumatic valves using microfluidic logical structures. - Consensus*. https://consensus.app/papers/development-multiplexed-control-latching-valves-using-grover/8fc852ff2ae45108a0f596fed4049093/?utm_source=chatgpt (accessed 2024-06-25).
(152) *Open-Source Pressure Controller Based on Compact Electro-Pneumatic Regulators for Droplet Microfluidics Applications - Consensus*. https://consensus.app/papers/opensource-pressure-controller-based-compact-filatov/27f6fdab09df5398870841044b98a2f2/?utm_source=chatgpt (accessed 2024-06-25).
(153) *Semi-autonomous liquid handling via on-chip pneumatic digital logic. - Consensus*. https://consensus.app/papers/liquid-handling-digital-logic-nguyen/21e6be4c058f54348be6e40d51289b24/?utm_source=chatgpt (accessed 2024-06-25).
(154) *Pneumatic computers for embedded control of microfluidics | Science Advances*. https://www.science.org/doi/10.1126/sciadv.adg0201 (accessed 2024-06-21).
(155) *High-density fabrication of normally closed microfluidic valves by patterned deactivation of oxidized polydimethylsiloxane - Lab on a Chip (RSC Publishing)*. https://pubs.rsc.org/en/content/articlelanding/2011/lc/c0lc00112k (accessed 2024-06-21).
(156) Preston, D. J.; Jiang, H. J.; Sanchez, V.; Rothemund, P.; Rawson, J.; Nemitz, M. P.; Lee, W.-K.; Suo, Z.; Walsh, C. J.; Whitesides, G. M. A Soft Ring Oscillator. *Sci. Robot.* **2019**, *4* (31), eaaw5496. https://doi.org/10.1126/scirobotics.aaw5496.
(157) *Microfluidic pneumatic logic circuits and digital pneumatic microprocessors for integrated microfluidic systems - Lab on a Chip (RSC Publishing)*. https://pubs.rsc.org/en/content/articlelanding/2009/lc/b904354c (accessed 2024-06-21).
(158) Whitesides, G. M. The Origins and the Future of Microfluidics. *Nature* **2006**, *442* (7101), 368–373. https://doi.org/10.1038/nature05058.
(159) Squires, T. M.; Quake, S. R. Microfluidics: Fluid Physics at the Nanoliter Scale. *Rev. Mod. Phys.* **2005**, *77* (3), 977–1026. https://doi.org/10.1103/RevModPhys.77.977.
(160) *QUARK MATTER IN MASSIVE COMPACT STARS - IOPscience*. https://iopscience.iop.org/article/10.1088/2041-8205/740/1/L14/meta (accessed 2024-06-25).
(161) *Lab-on-a-chip: microfluidics in drug discovery | Nature Reviews Drug Discovery*. https://www.nature.com/articles/nrd1985 (accessed 2024-06-25).
(162) *Microfluidic Lab-on-a-Chip Platforms: Requirements, Characteristics and Applications | SpringerLink*. https://link.springer.com/chapter/10.1007/978-90-481-9029-4_17 (accessed 2024-06-25).
(163) Bradski, G.; Kaehler, A. *Learning OpenCV: Computer Vision with the OpenCV Library*; O'Reilly Media, Inc., 2008.
(164) Hunter, J. D. Matplotlib: A 2D Graphics Environment.

Appendix I
Python Scripts

Script 2.1: Python code for surface roughness analysis of a microfluidic device image. The code converts the image to grayscale, applies a Gaussian filter to reduce noise, and then uses the Sobel operator to detect edges. The roughness metrics, including standard deviation, mean, and maximum of the gradient magnitudes, are calculated and printed. The results are displayed as the original image, the Gaussian-blurred image, and the Sobel gradient magnitude image.

```
import cv2
import numpy as np
import matplotlib.pyplot as plt

def calculate_roughness_metrics(image):
    # Convert image to grayscale
    gray = cv2.cvtColor(image, cv2.COLOR_BGR2GRAY)

    # Apply Gaussian filter
    gaussian_blurred = cv2.GaussianBlur(gray, (5, 5), 0)

    # Apply Sobel operator
    sobelx = cv2.Sobel(gaussian_blurred, cv2.CV_64F, 1, 0, ksize=3)
    sobely = cv2.Sobel(gaussian_blurred, cv2.CV_64F, 0, 1, ksize=3)

    # Calculate gradient magnitude
    sobel_magnitude = np.sqrt(sobelx**2 + sobely**2)

    # Calculate roughness metrics
    std_dev = np.std(sobel_magnitude)
    mean = np.mean(sobel_magnitude)
    maximum = np.max(sobel_magnitude)

    return std_dev, mean, maximum

# Load the image
image_path = 'path_to_image'  # Replace with the path to your image
image = cv2.imread(image_path)

# Check if the image is loaded properly
if image is None:
    raise FileNotFoundError(f"Image not found at {image_path}")
```

```
# Calculate roughness metrics for the whole image
metrics = calculate_roughness_metrics(image)

# Print the results
print("Surface Roughness Metrics for the Whole Image:")
print(f"Standard Deviation: {metrics[0]:.2f}")
print(f"Mean: {metrics[1]:.2f}")
print(f"Maximum: {metrics[2]:.2f}")

# Plot the results
fig, ax = plt.subplots(1, 3, figsize=(18, 5))

# Original Image
ax[0].imshow(cv2.cvtColor(image, cv2.COLOR_BGR2RGB))
ax[0].set_title('Original Image')
ax[0].axis('off')

# Gaussian Blurred Image
gray = cv2.cvtColor(image, cv2.COLOR_BGR2GRAY)
gaussian_blurred = cv2.GaussianBlur(gray, (5, 5), 0)
ax[1].imshow(gaussian_blurred, cmap='gray')
ax[1].set_title('Gaussian Blurred')
ax[1].axis('off')

# Sobel Magnitude
sobelx = cv2.Sobel(gaussian_blurred, cv2.CV_64F, 1, 0, ksize=3)
sobely = cv2.Sobel(gaussian_blurred, cv2.CV_64F, 0, 1, ksize=3)
sobel_magnitude = np.sqrt(sobelx**2 + sobely**2)
ax[2].imshow(sobel_magnitude, cmap='gray')
ax[2].set_title('Sobel Magnitude')
ax[2].axis('off')

plt.show()
```

Script 6.2: Python Tkinter application for controlling a droplet-based microfluidic system. This script creates a GUI for manual and automated control of oil and aqueous valves using an Arduino. Features include real-time plotting of actuator intensities, droplet sizes, and oil spacing, as well as options to oscillate valves and save experiment data. The GUI allows selection of regions of interest (ROIs) for accurate measurement and control and supports serial communication with the Arduino for executing commands.

```python
import tkinter as tk
from tkinter import simpledialog, messagebox, filedialog, Toplevel, Label, Entry, Button
import threading
import serial
import time
import cv2
import numpy as np
import pyautogui
import csv
from datetime import datetime
from matplotlib.figure import Figure
import matplotlib.pyplot as plt
from matplotlib.backends.backend_tkagg import FigureCanvasTkAgg

class ValveControlApp(tk.Tk):
    def __init__(self):
        super().__init__()
        self.title('Dropletra.ELS.1.4.28.24')
        self.geometry('500x800')
        self.com_port = tk.StringVar(value='COM4')  # Default COM port
        self.init_ui()
        self.arduino = None
        self.running = False
        self.record_video = None
        self.csv_file = None
        self.video_writer = None
        self.aq_intensities = []
        self.oil_intensities = []
        self.droplet_sizes = []
        self.oil_sizes = []

    def connect_to_arduino(self):
        try:
            self.arduino = serial.Serial(self.com_port.get(), 9600, timeout=1)
            time.sleep(2)  # Ensure the connection is established
            messagebox.showinfo("Connection", "Connected to Arduino on " + self.com_port.get())
        except Exception as e:
            messagebox.showerror("Connection Failed", str(e))

    def init_ui(self):
        config_frame = tk.Frame(self)
        config_frame.pack(side=tk.TOP, fill=tk.X)

        com_label = Label(config_frame, text="COM Port:")
        com_label.pack(side=tk.LEFT, padx=(10, 2))
        com_entry = Entry(config_frame, textvariable=self.com_port)
        com_entry.pack(side=tk.LEFT, padx=(2, 10))
        connect_button = Button(config_frame, text="Connect", command=self.connect_to_arduino)
        connect_button.pack(side=tk.LEFT, padx=(2, 10))

```

```
# Manual control buttons column
manual_frame = tk.Frame(self)
manual_frame.pack(side=tk.LEFT, anchor = tk.W, fill=tk.BOTH, expand=True)
tk.Label(manual_frame, text="Control Panel").pack()
tk.Button(manual_frame, text="Open AQ Valve", command=lambda: self.send_command("AQ_VALVE OPEN\n")).pack(pady=5)
tk.Button(manual_frame, text="Close AQ Valve", command=lambda: self.send_command("AQ_VALVE CLOSE\n")).pack(pady=5)
tk.Button(manual_frame, text="Oscillate AQ Valve", command=self.start_oscillation_aq).pack(pady=5)
tk.Button(manual_frame, text="Stop Oscillating AQ", command=self.stop_oscillation_aq).pack(pady=5)
tk.Button(manual_frame, text="Open Oil Valve", command=lambda: self.send_command("OIL_VALVE OPEN\n")).pack(pady=5)
tk.Button(manual_frame, text="Close Oil Valve", command=lambda: self.send_command("OIL_VALVE CLOSE\n")).pack(pady=5)
tk.Button(manual_frame, text="Oscillate Oil Valve", command=self.start_oscillation_oil).pack(pady=5)
tk.Button(manual_frame, text="Stop Oscillating Oil", command=self.stop_oscillation_oil).pack(pady=5)
tk.Button(manual_frame, text="Select ROI for Oil Valve", command=lambda: self.select_roi('aq')).pack(pady=5)
tk.Button(manual_frame, text="Select ROI for AQ Valve", command=lambda: self.select_roi('oil')).pack(pady=5)
tk.Button(manual_frame, text="Select ROI for Droplet Size", command=lambda: self.select_roi('droplet')).pack(pady=5)
tk.Button(manual_frame, text="Select ROI for Oil Spacing", command=lambda: self.select_roi('oilsize')).pack(pady=5)
tk.Button(manual_frame, text="Start Automation", command=self.start_automation).pack(pady=5)
tk.Button(manual_frame, text="Stop Automation", command=self.stop_automation).pack(pady=5)
self.aq_oscillation_time = tk.DoubleVar(value=0.5)
self.oil_oscillation_time = tk.DoubleVar(value=0.5)
tk.Entry(manual_frame, textvariable=self.aq_oscillation_time).pack(pady=5)
tk.Entry(manual_frame, textvariable=self.oil_oscillation_time).pack(pady=5)
tk.Button(manual_frame, text="Alternating Oscillation", command=self.start_alternating_oscillation).pack(pady=5)
tk.Button(manual_frame, text="Stop Alternating Oscillation", command=self.stop_alternating_oscillation).pack(pady=5)
self.status_label = tk.Label(self, text="System Status: Idle")
self.status_label.pack(pady=5)
self.status_label = tk.Label(self, text="Copyright (c) 2024 Easley Lab Softwares. All rights reserved.")
self.status_label.pack(pady=5)

# Real-time plotting setup
plot_frame = tk.Frame(self)
plot_frame.pack(side=tk.RIGHT, anchor=tk.E, fill=tk.BOTH, expand=True)

# Create a figure with three subplots
self.fig, (self.ax_aq, self.ax_oil, self.ax_dropsize, self.ax_oilsize) = plt.subplots(4, 1)  # 3 rows, 1 column
self.fig.subplots_adjust(hspace=0.5)  # Adjust space between plots

# Create a single canvas for the figure and pack it
self.canvas = FigureCanvasTkAgg(self.fig, master=plot_frame)
self.canvas.get_tk_widget().pack(side=tk.TOP, fill=tk.BOTH, expand=True)

# Example of initial plot settings
self.ax_aq.set_title('Oil Valve Actuator')
self.ax_aq.set_ylabel('Intensity')
self.ax_aq.set_xlabel('Time (sec)')

self.ax_oil.set_title('Aq Valve Actuator')
self.ax_oil.set_ylabel('Intensity')
self.ax_oil.set_xlabel('Time (sec)')
```

```
        self.ax_dropsize.set_title('Droplet Size')
        self.ax_dropsize.set_ylabel('Length (micrometer)')
        self.ax_dropsize.set_xlabel('Time (sec)')

        self.ax_oilsize.set_title('Oil Spacing')
        self.ax_oilsize.set_ylabel('Length (micrometer)')
        self.ax_oilsize.set_xlabel('Time (sec)')

        # Draw the initial plot
        self.canvas.draw()

    def send_command(self, command):
        if self.arduino and self.arduino.is_open:
            self.arduino.write(command.encode())
            self.status_label.config(text=f"Command sent: {command.strip()}")
            self.last_command = command.strip()  # Store the last command sent
            time.sleep(0.1)
        else:
            messagebox.showerror("Error", "Arduino is not connected.")

    def start_oscillation_aq(self):
        self.oscillating_aq = True
        threading.Thread(target=self.oscillate_valve, args=("AQ_VALVE", self.aq_oscillation_time.get()), daemon=True).start()

    def stop_oscillation_aq(self):
        self.oscillating_aq = False

    def start_oscillation_oil(self):
        self.oscillating_oil = True
        threading.Thread(target=self.oscillate_valve, args=("OIL_VALVE", self.oil_oscillation_time.get()), daemon=True).start()

    def stop_oscillation_oil(self):
        self.oscillating_oil = False

    def oscillate_valve(self, valve_type, period):
        while getattr(self, f"oscillating_{valve_type.split('_')[0].lower()}"):
            self.send_command(f"{valve_type} OPEN\n")
            time.sleep(period)
            self.send_command(f"{valve_type} CLOSE\n")
            time.sleep(period)

    def start_alternating_oscillation(self):
        self.alternating = True
        threading.Thread(target=self.alternate_valves, daemon=True).start()

    def stop_alternating_oscillation(self):
        self.alternating = False

    def alternate_valves(self):
        while self.alternating:
```

```
            self.send_command("AQ_VALVE OPEN\n")
            time.sleep(self.aq_oscillation_time.get())
            self.send_command("AQ_VALVE CLOSE\n")
            self.send_command("OIL_VALVE OPEN\n")
            time.sleep(self.oil_oscillation_time.get())
            self.send_command("OIL_VALVE CLOSE\n")

    def select_roi(self, valve):
        # User clicks on the screen to select the ROI
        image = pyautogui.screenshot()
        image = cv2.cvtColor(np.array(image), cv2.COLOR_RGB2BGR)
        cv2.imshow("Select ROI", image)
        cv2.setMouseCallback("Select ROI", self.click_and_crop, valve)
        cv2.waitKey(0)
        cv2.destroyAllWindows()

    def click_and_crop(self, event, x, y, flags, param):
        if event == cv2.EVENT_LBUTTONDOWN:
            if param == 'aq':
                self.roi_aq = (x, y, 1, 1)
                print(f"AQ ROI set at: {self.roi_aq}")
            elif param == 'oil':
                self.roi_oil = (x, y, 1, 1)
                print(f"Oil ROI set at: {self.roi_oil}")
            elif param == 'droplet':
                self.roi_droplet = (x, y, 1, 1)
                print(f"droplet ROI set at: {self.roi_droplet}")
            elif param == 'oilsize':
                self.roi_oilsize = (x, y, 1, 1)
                print(f"Oil ROI set at: {self.roi_oilsize}")
            cv2.destroyWindow("Select ROI")

    def start_automation(self):
        save_experiment = messagebox.askyesno("Save Experiment", "Do you want to save the experiment data?")
        if save_experiment:
            video_filename = filedialog.asksaveasfilename(defaultextension=".avi", filetypes=[("AVI video", "*.avi")])
            csv_filename = filedialog.asksaveasfilename(defaultextension=".csv", filetypes=[("CSV file", "*.csv")])
            self.setup_video_writer(video_filename)
            self.setup_csv_writer(csv_filename)
        self.running = True
        threading.Thread(target=self.automation_logic, daemon=True).start()
        self.status_label.config(text="Automation Started")

    def setup_video_writer(self, filename):
        screen_region = pyautogui.size()  # Get screen size
        fourcc = cv2.VideoWriter_fourcc(*'XVID')  # Video codec
        self.video_writer = cv2.VideoWriter(filename, fourcc, 20.0, (screen_region.width, screen_region.height))

    def setup_csv_writer(self, filename):
        self.csv_file = open(filename, mode='w', newline='')
```

```
        self.csv_writer = csv.writer(self.csv_file)
        self.csv_writer.writerow(["Time", "AQ Intensity", "Droplet Size", "Oil Intensity", "Oil Size", "Valve State"])

    def automation_logic(self):
        while self.running:
            screenshot = pyautogui.screenshot()
            frame = np.array(screenshot)
            gray_frame = cv2.cvtColor(frame, cv2.COLOR_BGR2GRAY)
            aq_intensity = np.mean(gray_frame[self.roi_aq[1]:self.roi_aq[1]+1, self.roi_aq[0]:self.roi_aq[0]+1])
            oil_intensity = np.mean(gray_frame[self.roi_oil[1]:self.roi_oil[1]+1, self.roi_oil[0]:self.roi_oil[0]+1])
           # Threshold to identify droplets and oil
            _, droplet_mask = cv2.threshold(gray_frame[self.roi_droplet[1]:self.roi_droplet[1]+1, self.roi_droplet[0]:self.roi_droplet[0]+1], 50, 255, cv2.THRESH_BINARY_INV)
            _, oil_mask = cv2.threshold(gray_frame[self.roi_oilsize[1]:self.roi_oilsize[1]+1, self.roi_oilsize[0]:self.roi_oilsize[0]+1], 50, 255, cv2.THRESH_BINARY_INV)
           # Calculate droplet and oil sizes
            droplet_sizes = self.calculate_sizes(droplet_mask)
            oil_sizes = self.calculate_sizes(oil_mask)
            self.aq_intensities.append(aq_intensity)
            self.oil_intensities.append(oil_intensity)
            self.droplet_sizes.append(droplet_sizes)
            self.oil_sizes.append(oil_sizes)
            self.update_plots()

            if aq_intensity < 150:
                self.send_command("AQ_VALVE CLOSE\n")
                self.send_command("OIL_VALVE OPEN\n")
            if oil_intensity < 150:
                self.send_command("AQ_VALVE OPEN\n")
                self.send_command("OIL_VALVE CLOSE\n")

            if self.video_writer:
                self.video_writer.write(cv2.cvtColor(frame, cv2.COLOR_RGB2BGR))

            if self.csv_file:
                now = datetime.now().strftime("%Y-%m-%d %H:%M:%S")
                self.csv_writer.writerow([now, aq_intensity, droplet_sizes, oil_intensity, oil_sizes, self.last_command])
            time.sleep(0.1)

    def calculate_sizes(self, mask):
            if mask.ndim > 1:
                mask = mask.flatten()  # Ensure mask is 1D for simplicity
                transitions = np.diff(mask.astype(int))  # Find changes from 0 to 1 or 1 to 0
                starts = np.where(transitions == 1)[0]  # Start of a droplet/oil
                ends = np.where(transitions == -1)[0]  # End of a droplet/oil
            if starts.size > 0 and ends.size > 0 and ends[0] < starts[0]:
                ends = ends[1:]  # Adjust ends if it starts before the first start
                sizes = ends - starts  # Calculate sizes
                return sizes.tolist()  # Return as a list


    def update_plots(self):
```

```
        self.after(0, self._update_plots)

    def _update_plots(self):

        self.ax_aq.clear()
        self.ax_aq.plot(self.aq_intensities, label='OIl Valve Actuator')
        self.ax_aq.legend(loc='upper right')

        self.ax_oil.clear()
        self.ax_oil.plot(self.oil_intensities, label='Aq Valve Actuator')
        self.ax_oil.legend(loc='upper right')

        self.ax_dropsize.clear()
        self.ax_dropsize.plot(self.droplet_sizes, label='Droplet Sizes')
        self.ax_dropsize.legend(loc='upper right')

        self.ax_oilsize.clear()
        self.ax_oilsize.plot(self.oil_sizes, label='Oil Spacing')
        self.ax_oilsize.legend(loc='upper right')

        self.canvas.draw()


    def stop_automation(self):
        self.running = False
        self.status_label.config(text="Automation Stopped")
        if self.video_writer:
            self.video_writer.release()
            self.video_writer = None
        if self.csv_file:
            self.csv_file.close()
            self.csv_file = None

    def on_closing(self):
        if messagebox.askokcancel("Quit", "Do you want to quit?"):
            if self.arduino.is_open:
                self.arduino.close()
        self.destroy()

if __name__ == "__main__":
    app = ValveControlApp()
    app.protocol("WM_DELETE_WINDOW", app.on_closing)
    app.mainloop()
```

Appendix II
Arduino Scripts

Script 5.1 Arduino code for controlling oil and aqueous valves. This script initializes digital pins connected to relays controlling the oil and aqueous valves. Through serial communication, it reads commands to open or close these valves, ensuring both are initially closed on startup. The loop continuously checks for incoming serial commands to toggle the valve states and sends confirmation messages back via the serial port.

```
const int oilValvePin = 27;  // Pin connected to the oil valve control (relay)
const int aqValvePin = 31;   // Pin connected to the aqueous valve control (relay)

void setup() {
  // Initialize the digital pins as outputs.
  pinMode(oilValvePin, OUTPUT);
  pinMode(aqValvePin, OUTPUT);

  // Start serial communication at 9600 bps.
  Serial.begin(9600);

  // Ensure both valves are closed initially.
  digitalWrite(oilValvePin, LOW);
  digitalWrite(aqValvePin, LOW);
}

void loop() {
  // Check if data is available to read from the serial port.
  if (Serial.available() > 0) {
    // Read the incoming string until a newline is received.
    String command = Serial.readStringUntil('\n');

    // Handle the command for the oil valve.
    if (command == "OIL_VALVE OPEN") {
      digitalWrite(oilValvePin, HIGH);
      Serial.println("Oil valve opened");
    } else if (command == "OIL_VALVE CLOSE") {
      digitalWrite(oilValvePin, LOW);
      Serial.println("Oil valve closed");
    }

    // Handle the command for the aqueous valve.
    if (command == "AQ_VALVE OPEN") {
      digitalWrite(aqValvePin, HIGH);
      Serial.println("Aqueous valve opened");
    } else if (command == "AQ_VALVE CLOSE") {
      digitalWrite(aqValvePin, LOW);
      Serial.println("Aqueous valve closed");
    }
  }
}
```